Journal Pre-proof

Variant-specific vaccination induces systems immune responses and potent *in vivo* protection against SARS-CoV-2

Lei Peng, Paul A. Renauer, Arya Ökten, Zhenhao Fang, Jonathan J. Park, Xiaoyu Zhou, Qianqian Lin, Matthew B. Dong, Renata Filler, Qiancheng Xiong, Paul Clark, Chenxiang Lin, Craig B. Wilen, Sidi Chen

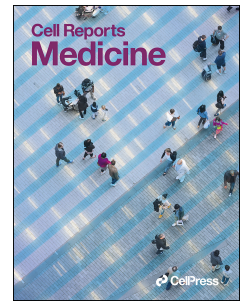Please cite this article as: Peng, L., Renauer, P.A., Ökten, A., Fang, Z., Park, J.J., Zhou, X., Lin, Q., Dong, M.B., Filler, R., Xiong, Q., Clark, P., Lin, C., Wilen, C.B., Chen, S., Variant-specific vaccination induces systems immune responses and potent *in vivo* protection against SARS-CoV-2, *Cell Reports Medicine* (2022), doi: https://doi.org/10.1016/j.xcrm.2022.100634.

This is a PDF file of an article that has undergone enhancements after acceptance, such as the addition of a cover page and metadata, and formatting for readability, but it is not yet the definitive version of record. This version will undergo additional copyediting, typesetting and review before it is published in its final form, but we are providing this version to give early visibility of the article. Please note that, during the production process, errors may be discovered which could affect the content, and all legal disclaimers that apply to the journal pertain.
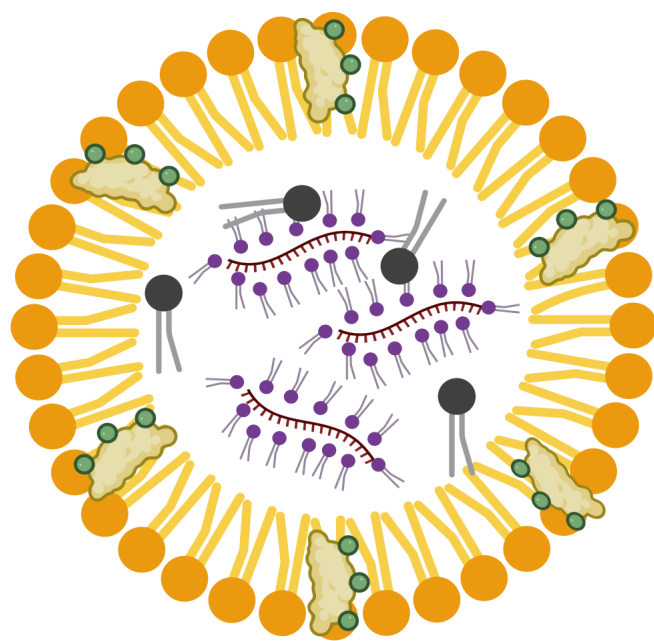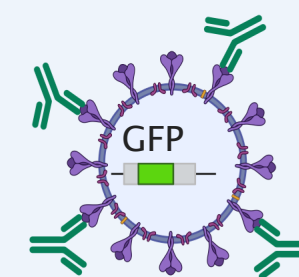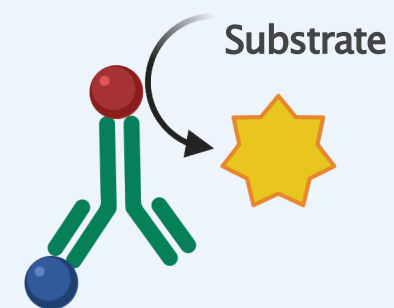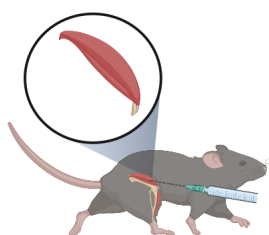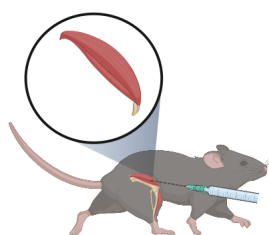
1

Variant-specific vaccination induces systems immune responses

and potent *in vivo* protection against SARS-CoV-2

4
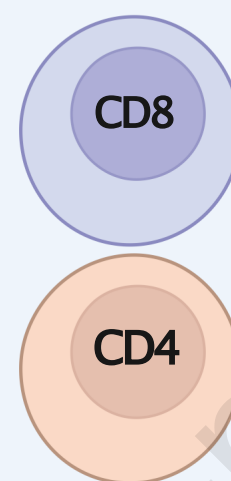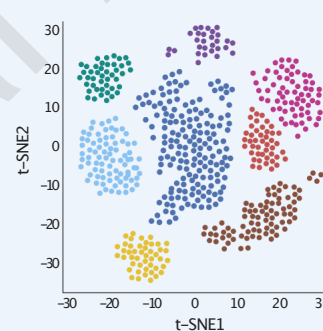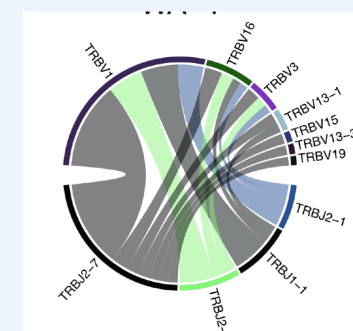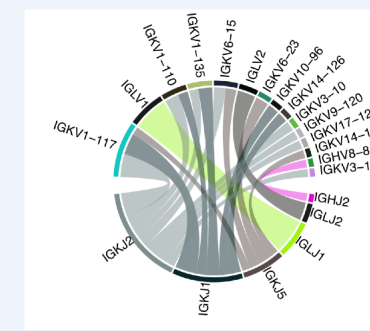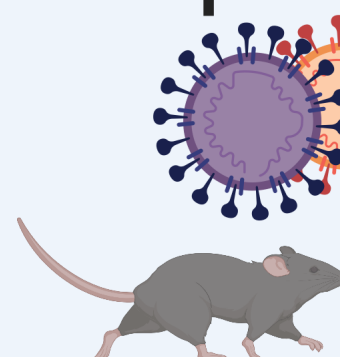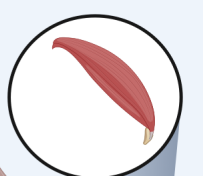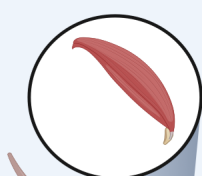
Authors

Lei Peng [1,2,3,*], Paul A. Renauer [1,2,3,4,*], Arya Ökten [5,6,*], Zhenhao Fang [1,2,3,*], Jonathan J. Park [1,2,3,7,*], Xiaoyu Zhou [1,2,3,*], Qianqian Lin [1,2,3], Matthew B. Dong [1,2,3,5,7,8], Renata Filler [5,6], Qiancheng Xiong [9,11], Paul Clark [1,2,3], Chenxiang Lin [9,10,11], Craig B. Wilen [5,6,@], and Sidi Chen [1,2,3,4,7,8,9,10,11,12,13,14,@,#]

Affiliations

1. Department of Genetics, Yale University School of Medicine, New Haven, CT, USA
2. System Biology Institute, Yale University, West Haven, CT, USA
3. Center for Cancer Systems Biology, Yale University, West Haven, CT, USA
4. Molecular Cell Biology, Genetics, and Development Program, Yale University, New Haven, CT, USA
5. Department of Immunobiology, Yale University, New Haven, CT, USA
6. Department of Laboratory Medicine, Yale University, New Haven, CT, USA
7. M.D.-Ph.D. Program, Yale University, West Haven, CT, USA
8. Immunobiology Program, Yale University, New Haven, CT, USA
9. Department of Cell Biology, Yale University, New Haven, CT, USA
10. Department of Biomedical Engineering, Yale University, New Haven, CT, USA
11. Nanobiology Institute, Yale University, New Haven, CT, USA
12. Yale Comprehensive Cancer Center, Yale University School of Medicine, New Haven, CT, USA
13. Yale Stem Cell Center, Yale University School of Medicine, New Haven, CT, USA
14. Yale Center for Biomedical Data Science, Yale University School of Medicine, New Haven, CT, USA

* These authors contributed equally.

@ Senior authors:
    SC (sidi.chen@yale.edu); CBW (craig.wilen@yale.edu)

Lead contact:
    SC (sidi.chen@yale.edu)
    +1-203-737-3825 (office)
    +1-203-737-4952 (lab)

1 **Abstract**

2 Lipid-nanoparticle (LNP)-mRNA vaccines offer protection against COVID-19. However, multiple variant

3 lineages caused widespread breakthrough infections. Here, we generate LNP-mRNAs specifically encoding

4 wildtype (WT), B.1.351 and B.1.617 SARS-CoV-2 spikes, and systematically study their immune responses.

5 All three LNP-mRNAs induced potent antibody and T cell responses in animal models. However, differences

6 in neutralization activity have been observed between variants. All three vaccines offer potent protection

7 against in vivo challenges of authentic viruses of WA-1, Beta and Delta variant. Single cell transcriptomics

8 of WT- and variant-specific LNP-mRNA vaccinated animals reveal a systematic landscape of immune cell

9 populations and global gene expression. Variant-specific vaccination induces a systemic increase of reactive

10 CD8 T cells and altered gene expression programs in B and T lymphocytes. BCR-seq and TCR-seq unveil

11 repertoire diversity and clonal expansions in vaccinated animals. These data provide assessment of efficacy

12 and direct systems immune profiling of variant-specific LNP-mRNA vaccination *in vivo*.

13

14 **Keywords**

1 **Introduction**

2 Severe acute respiratory syndrome coronavirus (SARS-CoV-2), the pathogen of coronavirus disease 2019

3 (COVID-19), has caused the ongoing global pandemic [1]. Although lipid nanoparticle (LNP) - mRNA based

4 vaccines such as BNT162b2 (Pfizer-BioNTech) and mRNA-1273 (Moderna) have demonstrated high efficacy

5 against COVID-19, breakthrough infections have been widely reported in fully vaccinated individuals[2,3 4-8].

6 Moreover, the virus continues to mutate and multiple dangerous variant lineages have evolved, such as B.1.1.7,

7 B.1.351, and, more recently B.1.617 [9,10]. The B.1.1.7 lineage (Alpha variant, or "UK variant") has an increased

8 rate of transmission and higher mortality [11]. The B.1.351 lineage (Beta variant, or "South Africa variant") has

9 an increased rate of transmission, resistance to antibody therapeutics, and reduced vaccine efficacy [12-14]. The

10 lineage B.1.617 ("Indian variant" lineage, including B.1.617.1 "Kappa variant", B.1.617.2 "Delta variant" and

11 B.1.617.3) has recently emerged, spread rapidly, and become dominant in multiple regions in the world [15,16].

12 The on-going surge of infections in the US is predominantly caused by the Delta variant, originating from the

13 B.1.617 lineage that has >1,000 fold higher viral load in infected individuals [17,18]. The B.1.617 lineage has an

14 increased rate of transmission, showing reduced serum antibody reactivity in vaccinated individuals, and

15 exhibits resistance to antibody therapeutics [19-23]. These variants often spread faster than the ancestral "wildtype"

16 (WT) virus (also noted as Wuhan-1 or WA-1, with identical spike sequences), cause more severe disease, are

17 more likely to escape certain host immune response, cause disproportionally higher numbers of breakthrough

18 infections despite the status of full vaccination [14,24-27], and have been designated by WHO and CDC as "variants

19 of concern" (VoCs) [28]. Regarding their effects on vaccine efficacy, B.1.351, for example, has been known to

20 reduce the efficacy of the Pfizer-BioNTech vaccine from >90% to near 70%[27]. The Delta variant has also

21 resulted in significant reduction of vaccine efficacy especially for individuals who received only a single dose

22 [26], and has caused wide-spread breakthrough infections despite the status of full vaccination[29].

23

24 It has been widely hypothesized that the next-generation of COVID-19 vaccines can be designed to directly

25 target these variants ("variant-specific vaccines"). However, to date, there has been no literature report on any

26 approved or clinical stage variant-specific vaccine. Moreover, the immune responses, specificity, cross-

27 reactivity, and host cell gene expression landscapes upon vaccination have to be rigorously tested for such

28 variant-specific vaccines to be developed. To directly assess the immunogenicity of potential variant-specific

29 SARS-CoV-2 vaccination, we generated LNP-mRNA vaccine candidates that encode the B.1.351 and B.1.617

30 spikes, along with the WT spike. With these variant-specific LNP-mRNAs, we characterized the immune

31 responses they induce in animals against homologous (cognate) and heterologous spike antigens and SARS-

32 CoV-2 pseudoviruses. To better understand the systematic immune responses induced by variant-specific

33 SARS-CoV-2 spike mRNA-LNP vaccination, we analyzed the combined single-cell transcriptomes and

1 lymphocyte antigen receptor repertoires of mice immunized with B.1.351 and B.1.617 spike mRNA-LNP

2 vaccine candidates.

3

4 **Results**

5 **Design, generation and physical characterization of variant-specific SARS-CoV-2 spike LNP-mRNAs**

6 We designed and generated nucleotide-modified mRNAs separately encoding full-length SARS-CoV-2 WT,

7 B.1.351 and B.1.617 spikes. The HexaPro mutations[30] were introduced and the furin cleavage site[31] was

8 replaced with a GSAS sequence to stabilize the prefusion state and preserve integrity of spike S1 and S2

9 subunits (**Figure 1A-1B**). The protein expression and receptor binding ability of modified spike mRNA were

10 confirmed by *in vitro* cell transfection and flow cytometry where the spike binding to the human ACE2-Fc

11 fusion protein was detected by PE-anti-Fc antibody (**Figure 1C**). We encapsulated the spike mRNA with LNP,

12 and evaluated their size and homogeneity by dynamic light scattering (DLS) and transmission electron

13 microscopy (TEM) (**Figure 1D**). The WT (WA-1), B.1.351 and B.1.617 mRNA LNPs have mean diameters

14 of 80.7 ± 6.9nm, 66.4 ± 5.3 nm and 72.2 ± 5.8 nm with a monodispersed size distribution as determined by

15 DLS and polydispersity indices of 0.08, 0.13 and 0.08, respectively (**Figure 1E-F**). The immunogenicity of

16 the LNP-mRNA was assessed in C57BL/6Ncr mice by two intramuscular injections (doses) of 1 µg or 10 µg

17 LNP-encapsulated mRNA, separated by 3 weeks (prime and boost, respectively) (**Figure 1G**). Serum samples

18 were collected two weeks after the prime and boost, and then subjected to ELISA and neutralization assays to

19 evaluate the antibody response. These mice were sacrificed 40 days post vaccination, and the spleen, lymph

20 nodes and blood cells were collected for downstream assays, including single cell transcriptomics sequencing

21 (scRNA-seq), bulk and single cell BCR sequencing (BCR-seq) and TCR sequencing (TCR-seq), as well as

22 flow cytometry. All procedures were standardized across all groups.

23

24 **Immune responses induced by WT-LNP-mRNA vaccination in mice**

25 WT-LNP-mRNA (WA-1-LNP-mRNA) induced dose-dependent binding antibody responses against spike

26 ECD (Ectodomain of spike protein) and RBD of SARS-CoV-2 WT, B.1.351 and B.1.617 variants after prime

27 and boost (**Figure 1H-I**). Compared to the post-prime immune response, orders of magnitudes increase in

28 immune response were observed after the boost injection, suggesting that the second dose significantly boosted

29 B cell immunity to SARS-CoV-2 antigens (**Figure 1H-I**). Using a pseudovirus neutralization assay that has

30 been widely reported to be consistent with authentic virus results [32,33], the serum samples from mice receiving

31 WT-LNP-mRNA vaccination also showed potent neutralization activity against all three variants, again with

32 a strong prime-boost effect (**Figure 1J**). However, the neutralization ability of WT-LNP-mRNA vaccinated

33 sera was found to be several fold lower against either B.1.351 or B.1.617 as compared to the cognate WT

1 pseudovirus (**Figure 1J**). These observations are consistent with the series of reports showing dramatic

2 reduction in neutralization of B.1.351 and B.1.617 variants by vaccinated individuals' sera, convalescent sera,

3 and therapeutic antibodies [12,13,23,34].

4

5 To evaluate the T cell response to the spike peptides, the splenocytes were isolated from mouse spleens 40

6 days post vaccination and the antigen-specific CD4$^+$ and CD8$^+$ T cell response to S peptide pools were

7 determined by intracellular cytokine staining (**Figure S 2**). WT-LNP-mRNA, at both low and high doses,

8 induced reactive CD8$^+$ T cells producing interferon γ (IFN-γ, IFNg), tumor necrosis factor α (TNF-α, TNFα),

9 and interleukin 2 (IL-2) (**Figure 1K**), at levels consistent with previously reported studies[31,35]. WT-LNP-

10 mRNA at both doses also induced reactive CD4$^+$ T cells that produce IFN-γ$^+$, but little for TNF-α, IL-2, IL-4

11 or IL-5 (**Figure 1L; Figure S 2B**). As technical quality controls, there is no difference in cytokine production

12 between vaccinated groups and the PBS group when cells were treated with vehicle (no peptide) or

13 PMA/ionomycin (**Figure S 2C-D**). These results suggest that WT-LNP-mRNA vaccines can induce potent

14 spike protein specific CD4 and CD8 T cell responses.

15

16 **Binding and neutralizing antibody responses of B.1.617-LNP-mRNA and B.1.351-LNP-mRNA**

17 Both B.1.617-LNP-mRNA and B.1.351-LNP-mRNA induced dose-dependent binding antibody responses

18 against spike ECD and RBD of SARS-CoV-2 WT, B.1.351 and B.1.617 variants (**Figure 2A-2B**). The strong

19 boost effect in ELISA was also observed for these two variant-specific LNP-mRNAs (**Figure 2A-2B**). The

20 dose-dependence effect was observed in both B.1.617-LNP-mRNA and B.1.351-LNP-mRNA groups across

21 three types of ELISA antigens of both RBD and ECD, although the dose effect was less prominent in the post-

22 boost samples, where both doses showed high titers at potential saturation level (**Figure 2A-2B; Figure S 1A-

23 B**). Relatively speaking, higher antibody responses was often observed with ECD antigen, suggesting an

24 immunogenic domain other than RBD contributed to the additional response to spike ECD (**Figure 2A-2B;

25 Figure S 1A-B**). Overall, the binding intensity as measured by serum titer between RBD and ECD strongly

26 correlates with each other across all vaccination groups (**Figure S 1C**).

27

28 We then examined pseudovirus-neutralizing antibody response. Both B.1.617-LNP-mRNA and B.1.351-LNP-

29 mRNA elicited potent neutralizing antibodies, of which response mirrored the trend of post-prime and post-

30 boost response reported in ELISA (**Figure 2C**). The initial level of neutralization was at $10^2 - 10^3$ level of

31 reciprocal IC50 after priming for most groups (**Figure 2C**). Consistent with findings in ELISA, an

32 approximately two orders of magnitude increase in neutralization titer by boost was observed across all groups

33 (for both vaccine candidates and for all three pseudovirus types) in the low dose (1 µg) setting, and there was

1 an approximately one order of magnitude increase in the high dose (10 µg) setting (**Figure 2C**). The dose

2 effect of serum neutralization activity for both B.1.617-LNP-mRNA and B.1.351-LNP-mRNA was observed

3 at priming for most groups, but negligible post boost (i.e. both 1 µg and 10 µg dose groups reach reciprocal

4 IC50 titer of 10^4 level after boost) (**Figure 2C**). Both B.1.617-LNP-mRNA and B.1.351-LNP-mRNA

5 effectively neutralize pseudoviruses of all three SARS-CoV-2 pseudoviruses post boost at titers of 10^4 level

6 (**Figure 2C**). Interestingly, B.1.351-LNP-mRNA vaccinated animals neutralize pseudoviruses of all three

7 SARS-CoV-2 at similar levels post boost at both doses (**Figure 2C**); while B.1.617-LNP-mRNA vaccinated

8 animals showed significantly higher titer against its cognate B.1.617 pseudovirus (by several folds). Compared

9 to WT LNP-mRNA, B.1.617 LNP-mRNA displayed significantly higher post-boost binding and neutralizing

10 antibody titers against its cognate antigen, B.1.617 variant (**Figure 2D-2E**). The B.1.351, on the other hand,

11 showed higher post-boost binding, but not neutralization titers against B.1.351 antigen. Overall, across all

12 vaccination groups, the neutralization activity strongly correlates with binding intensity for ECD binding

13 (**Figure 2E**), which also holds true for RBD binding (**Figure S 1D**). Comparison of WT-LNP-mRNA, B.1.617-

14 LNP-mRNA and B.1.351-LNP-mRNA for their effects in ELISA and neutralization titers corroborated with

15 the observations above (**Figure S 1E-G**).

16

17 **B.1.617-LNP-mRNA and B.1.351-LNP-mRNA elicited strong systemic T cell response against SARS-**

18 **CoV-2 spike**

19 Similarly, to evaluate the T cell response to the spike peptides, the splenocytes were isolated from mouse

20 spleens 40 days post vaccination and the antigen-specific CD4$^+$ and CD8$^+$ T cell responses to S peptide pools

21 were determined by intracellular cytokine staining (**Figure S 2E-G**). Positive control PMA/ionomycin

22 treatment group and negative control no peptide group were both validated (**Figure S 2F-G**). Both B.1.617-

23 LNP-mRNA and B.1.351-LNP-mRNA, at low and high doses, induced potent reactive CD8$^+$ T cell responses

24 in terms of cellular production of IFN-γ, TNF-α, and IL-2 (**Figure 3A-3C**). Both LNP-mRNAs at both doses

25 also induced reactive CD4$^+$ T cells that produce IFN-γ, but only minimally for TNF-α, and had no effect on

26 IL-2, IL-4 or IL-5 (**Figure 3D; Figure S 2E**). Multi-channel flow analysis showed that both B.1.617-LNP-

27 mRNA and B.1.351-LNP-mRNA, at both low and high doses, induced polyfunctional CD8$^+$ T cells

28 subpopulation that simultaneously produce two cytokines, such as IFN-γ$^+$;TNF-α$^+$, IFN-γ$^+$;IL-2, or TNF-

29 α$^+$;IL-2$^+$ CD8$^+$ T cells (**Figure 3E-G**). Both LNP-mRNAs at both doses also induced polyfunctional CD4$^+$ T

30 cells that produce IFN-γ and TNF-α at the same time (**Figure 3H**).

31

32 **WT- and variant-specific- LNP-mRNA vaccinations offer strong protection against authentic SARS-**

33 **CoV-2 ancestral and VoC viruses *in vivo***

1   To further evaluated the protective potency of WT-LNP-mRNA, B.1.617-LNP-mRNA and B.1.351-LNP-

2   mRNA against the challenge of authentic SARS-CoV-2 ancestral virus (WA-1) and VoC viruses (Beta and

3   Delta), we perform *in vivo* vaccination and infection experiments in a biosafety level 3 (BSL3) setting. We

4   first immunized K18-hACE2 mice with two doses of WT-LNP-mRNA, B.1.617-LNP-mRNA and B.1.351-

5   LNP-mRNA, a prime (day 0) and a boost (day 21) (**Figure 4A**). One week after boost, we randomly divided

6   these three types of LNP-mRNA vaccinated mice into three subgroups each (**Figure 4B**) and challenged K18-

7   hACE2 mice with 10^3 plaque forming units (PFUs), a dose that's 10x of half lethal dose (10x LD50), of

8   SARS-CoV-2 WA-1 virus (**Figure 4B**).

9

10 As a result, virtually all mice in the placebo group developed severe disease due to viral challenge, and

11 consistently decreased body weight, for all three viruses (**Figure 4C-D**). Despite differences of severity

12 between viruses, in the placebo treated group, the majority of animals succumbed from the disease by day 10

13 post infection, with 80% death in WA-1 virus group, 100% death in Beta virus group and 60% in Delta virus

14 group, respectively (**Figure 4C-D**). In sharp contrast, all mice receiving any of the three vaccine (WT-LNP-

15 mRNA, B.1.617-LNP-mRNA or B.1.351-LNP-mRNA) were free of severe disease symptoms, largely

16 maintained their body weight throughout the duration of the study, and all (100%) survived from SARS-CoV-

17 2 infection in the time course of experiment (**Figure 4C-D**). These data demonstrated that all three LNP-

18 mRNAs, including both WT- and variant-specific- LNP-mRNA vaccinations, can protect the animals from

19 lethal SARS-CoV-2 challenges.

20

21 **Single cell immune repertoire mapping of WT- and variant-specific- LNP-mRNA vaccinated animals**

22 In order to gain insights on the global composition and transcriptional landscape of the immune cells, we

23 performed single cell transcriptomics (scRNA-seq) on the spleen samples of 24 animals from all three

24 vaccination groups (WT/WA-1-LNP-mRNA, B.1.351-LNP-mRNA, and B.1.617-LNP-mRNA, both 1 µg and

25 10 µg dose groups), plus a control group (PBS treated). Gene expression profiling was performed in a total of

26 141,729 single cells, as projected on a Uniform Manifold Approximation and Projection (UMAP) (**Figure 5A**).

27 Cells were clustered by generating a shared nearest neighbors (SNN) graph, and optimizing the modularity

28 using the Louvain algorithm with multilevel refinement algorithm with an empirically chosen resolution, based

29 on the best spatial separation of major immune populations cells via *Cd3d*, *Cd19*, *Ncr1*, *Itgam*, *Itgax*, and *Sdc1*

30 expression via UMAP visualization (**Figure 5B**). The clusters were then labeled based on the expression of

31 different immune cell markers (**Figures S3-S6, Dataset S1**). For better resolution of complex cell types, B

32 cells, T cells and dendritic cells (DCs) (*Cd45+Cd19+, Cd45+Cd3d+*, and *Cd45+Itgax+* clusters, respectively)

33 were separately subset, rescaled, visualized in low dimensional UMAP space, clustered, and populations were

1 identified using the method above (**Figure 5F; Figures S4-S6**). Labeled cell types were tested for homogeneity

2 by performing Wilcoxon rank sum testing of scaled data and assessing discreet hierarchical clustering of

3 populations using the top 10 DEGs in each cell type compared to all others (**Figure 5C**). Using these methods,

4 we identified 32 populations of immune cells, including 7 B cell, 13 T cell, and 4 DC subsets, as well as

5 endothelial cells and a population *of Cd19+CD3d+* cells, labeled as B cell-T cell doublets, based on similar

6 observations of *Cd19+Cd3+* splenocytes doublets via flow cytometry. Comparisons between different

7 vaccination groups showed vaccine-specific shifts in immune population proportions. Of note, macrophage

8 (Mφ) populations were significantly increased in B.1.351-LNP-mRNA and B.1.617-LNP-mRNA, but

9 decreased in WT/WA-1-LNP-mRNA groups, relative to the PBS control group (**Figure 5D**). Most notably, all

10 three variant groups had significantly increased levels of activated cytotoxic T cells (Tc1) and significantly

11 decreased follicular (Fo) B cells compared to the PBS control group (**Figure 5G**). The shift from Fo B cells

12 appears to be accompanied by increases in activated germinal center (GC) B cells for B.1.351-LNP-mRNA

13 and B.1.617-LNP-mRNA groups and B1 cells for the WT/WA-1-LNP-mRNA group, although to non-

14 significant extents (**Figure 5G**). Together, these immune shifts in macrophages, T cells, and B cells are

15 consistent with an increased immune response.

16

17 **Gene expression signatures of B cell and T cell populations of B.1.617-LNP-mRNA and B.1.351-LNP-**

18 **mRNA vaccinated animals**

19 Because B and T cells are the cornerstones of adaptive immunity against SARS-CoV-2, we further investigated

20 the B cell sub-populations and T cell sub-populations, respectively. Specifically, we performed differential

21 expression analyses in activated B cells (Activated and GC B cells), activated CD4 T cells, and activated CD8

22 T cells across vaccination groups. In each comparison, we accounted for the complexities amongst

23 experimental conditions, heterogeneous immune cell populations, and inconsistent transcriptional sampling

24 between cells using scRNA-seq technologies by fitting the data to generalized linear models and assessing

25 how each vaccine variant influences each activated cell type, relative to the PBS treatment. The top upregulated

26 genes in activated B cells represent transcription and translation machineries, which are consistent between

27 WT/WA-1-, B.1.351- and B.1.617- specific LNP-mRNA vaccination groups (**Figure 6A**). This strong

28 signature was also observed in T cells (**Figure 6D**), consistent with the phenomenon of active lymphocyte

29 activation upon vaccination [36-38]. Next, we identified vaccine-specific pathway changes in each cell type using

30 a pathway analysis, in which significant gene set enrichment analysis results are aggregated into "supra-

31 pathway" clusters to highlight unique pathways amongst highly redundant gene ontologies. Our results show

32 upregulation of transcription/translation-related pathways in B cells and CD8 T cells from all three vaccination

33 groups (**Figures 6B, C, E, F**), while the variant vaccination groups showed significantly enhanced effector

1   functions in CD8 T cells, including leukocyte differentiation and cellular extravasation in the B.1.351 group

2   and cell killing in the B.1.617 group (**Figures 6E-F**). We next investigated how the B.1.351-LNP-mRNA and

3   B.1.617-LNP-mRNA variant vaccines compared to WT/WA-1-LNP-mRNA. Results from differential

4   analyses showed broad differences in immune response and cellular metabolism pathways across each cell

5   type, in either comparison (**Figures S8 and S9**). These data characterize the immune responses generated from

6   each variant vaccine and how these compare to the WT/WA-1 vaccination. In particular, these results provide

7   evidence for a broadly altered immune populations and transcriptomic signatures upon vaccination, including

8   activation of B cell and CD8 T cell subsets, as well as enhanced effector function in CD8 T cells. The

9   differential analyses between variant-specific vaccination and WT vaccination also showed differences in the

10 gene expression in B and T cells.

11

12 **TCR and BCR diversity mapping of B.1.617-LNP-mRNA and B.1.351-LNP-mRNA vaccinated animals**

13 To reveal the B and T cell clonal diversity and influence by vaccination, we performed VDJ repertoire mapping

14 and clonal analyses of B cell and T cell populations of WA-1-LNP-mRNA, B.1.351-LNP-mRNA and B.1.617-

15 LNP-mRNA vaccinated animals. We performed both single cell BCR sequencing (scBCR-seq) and single cell

16 TCR sequencing (scTCR-seq) on the spleen samples of all groups (6 vaccination groups and a PBS group, n

17 = 24 mice total). We sequenced a total of 154,203 single B cells and 77,699 single T cells. Clonal composition

18 showed the BCR repertoire in the single cell BCR-seq dataset, revealing a trend towards decreased clonal

19 diversity in variant-specific vaccine treated animals, a signal of clonal expansion (**Figure 7A-B, e; Figure

20 S10A**). The clonal composition of single cell TCR showed a similar decrease in clonal diversity (**Figure 7C-

21 D, e; Figure S10B**). This phenomenon is consistent with the clonal expansion of stimulated lymphocytes upon

22 vaccination.

23

24 To further validate the observations, we also performed bulk BCR-seq and bulk TCR-seq for all these mice on

25 additional tissue samples, including spleen, peripheral blood cells and lymph node (LN). The bulk BCR-seq

26 and TCR-seq data revealed systematic clonality maps of *IGH, IGK, IGL, TRA*, and *TRB* repertoires from the

27 spleen, blood, and LN samples of the variant-specific LNP-mRNA vaccinated along with PBS treated animals

28 (**Figure 7F; Figures S11A and S12A**). Analyses of *IGK, IGL, TRA*, and *TRB* repertoires showed trends of

29 decreasing unique clonotype numbers in B.1.351-LNP-mRNA and B.1.617-LNP-mRNA vs PBS peripheral

30 blood samples (**Figures S11B and S12B**), concomitant with an increased proportion of hyperexpanded

31 clonotypes (> 1% total clones) (**Figures S11C and S12C**). There is also an increased percent of the repertoire

32 occupied by the top 10 and top 50 most abundant *IGK, TRA*, and *TRB* clonotypes in the blood, significantly in

33 *TRA* chains of 10 µg variant vaccinated and 1 µg B.1.351 vaccinated samples (**Figure 7G**). Lastly, true

1   diversity estimates of TRA and TRB chains were significantly decreased in the blood samples of all 1µg

2   B.1.351 and both 10µg variant vaccinated samples, relative to PBS controls (**Figure 7H**). these combined data

3   unveiled BCR and TCR repertoire clonality, diversity and respective shifts in variant-specific LNP-mRNA

4   vaccinated animals as compared to placebo-treated. In addition, these results are consistent with the

5   observation of decreased clonal diversity from single cell VDJ profiling, which together suggest a clonal

6   expansion of B cells and more notably, T cells.

7

Discussion

9   Although efficacious COVID-19 mRNA vaccines have been deployed globally, the rapid spread of SARS-

10 CoV-2 VoCs with higher contagiousness as well as resistance to therapies and vaccines demands evaluation

11 of next-generation COVID-19 vaccines specifically targeting these evolving VoCs. Mounting evidence has

12 suggested that the B.1.351 and B.1.617 lineage variants of SARS-CoV-2 possesses much stronger immune

13 escape capability than the original wildtype virus [13,23]. The lower neutralizing titers in fully vaccinated patients

14 were found associated with breakthrough infections [4]. It has been speculated that the waning immunity from

15 early vaccination and emergence of more virulent SARS-CoV-2 variants may lead to reduction in vaccine

16 protection and increase of breakthrough infections[6,39]. It has been reported that mRNA vaccines' efficacy

17 against B.1.351 and B.1.617.2 dropped significantly[27,40]. Moreover, for individuals receiving only a single

18 dose of vaccine, the protective efficacy can be dramatically lower [41]. It is worth noting that efficacy value and

19 definition may vary from study to study[42,43], which were conducted in different regions and populations. All

20 these factors prompted us to evaluate the next-generation mRNA vaccine candidates encoding the B.1.351 and

21 B.1.617 spike as antigens.

22

23 While the findings of differential antibody responses of vaccination against cognate vs. heterologous antigens

24 is in line with the effect of dampening immunity by variants for WT vaccines in human study, however, prior

25 studies were done using WT vaccines against VoCs, not variant-specific vaccines, which are entirely different

26 drug compositions. Currently there is limited published work or immunological data on variant-specific

27 vaccines. Our study directly produced, characterized, and systematically profiled the immunity of variant-

28 specific vaccines. It's critical to learn their potential protective benefits against wildtype or variants of SARS-

29 CoV-2. In fact, this becomes increasingly important due to the continuous rise of new variants of concern. In

30 reaction to the VoCs, major vaccine producers are actively developing variant-specific vaccines and test their

31 effect in clinical trials (e.g. Pfizer/BioNTech and Moderna), highlighting the clinical relevance.

32

1   Our study characterized the titers and cross-reactivity of sera from mice vaccinated with WT- / WA-1-,

2   B.1.351- or B.1.617-LNP-mRNAs to all three WT, B.1.351 and B.1.617 spike antigens, pseudoviruses and

3   authentic viruses. In agreement with findings in patients' sera, we found that the neutralizing titers of WT

4   vaccine sera were several folds lower against the two variants of concerns than against WT pseudovirus.

5   Interestingly, the B.1.617-LNP-mRNA vaccinated sera also showed particularly strong neutralization activity

6   against its cognate B.1.617 pseudovirus, while the B.1.351-LNP-mRNA showed similar neutralization activity

7   against all three pseudoviruses. It is worth noting that all three forms of vaccine candidates can induce potent

8   B and T cell responses to WT as well as the two VoCs' spikes. The *in vivo* challenge experiments showed that

9   all three vaccine candidates, i.e. WT/WA-1-, B.1.351- and B.1.617- LNP-mRNAs offer strong protection

10   against all three authentic viruses (WA-1, Beta and Delta) in mice.

11

12   The T cell-biased immune response is important for antiviral immunity and thereby the efficacy and safety of

13   viral vaccines [44]. To evaluate the Th1 and Th2 immune response by the variant vaccines, we performed

14   intracellular staining of Th1 and Th2 cytokines in splenocytes. After stimulation with peptide pools covering

15   the entire S protein, the splenocytes from three mRNA vaccine groups produced more hallmark Th1 cytokine

16   IFN-γ in both $CD4^+$ and $CD8^+$ T cells than those from PBS group. Our flow cytometry data suggested that the

17   two variant vaccine candidates induced strong Th1-biased immune responses, just like the WT vaccine, of

18   which Th1 response had been observed by previous studies in animal models [31,35].

19

20   Single cell sequencing is a powerful technology for immune and gene expression profiling, which has been

21   utilized for mapping immune responses to COVID-19 infection [45,46]. In order to gain insights on the

22   transcriptional landscape of the immune cells, and clonal repertoire changes specifically in B and T cells, we

23   performed single cell transcriptomics, as well as BCR and TCR repertoire sequencing. The single cell

24   transcriptomics data revealed a systematic landscape of immune cell populations in B.1.351-LNP-mRNA and

25   B.1.617-LNP-mRNA vaccinated animals. We mapped out the repertoires and associated global gene

26   expression status of the immune populations including B cells, T cells, and innate immune cells. From the

27   overall splenocyte population, we observed a distinct and significant increase in the CD8 T cell, activated B

28   cell, and macrophage cell populations in vaccinated animals. Interestingly, differential expression between

29   vaccinated and placebo-treated animals showed a strong signature of increased expression of transcriptional

30   and translational machinery in both B and T cells. While the actual mechanism awaits future studies, these

31   phenomena are potentially reflective of the active proliferation and immune responses in these lymphocytes.

32

1 BCR and TCR sequencing are efficient tools for mapping of clonal repertoire diversity, which has been rapidly

2 utilized for sequencing COVID-19 patients [46,47]. BCR-seq and TCR-seq unveiled the diversity and clonality

3 and respective shifts in variant-specific LNP-mRNA inoculated animals as compared to placebo-treated. The

4 decrease in VDJ clonal diversity, along with clonal expansion of a small number of clones, are observed in

5 vaccinated animals as compared to placebo group. Vaccinated animals from both B.1.351-LNP-mRNA and

6 B.1.617-LNP-mRNA groups have clonal TCR expansion, especially pronounced in peripheral blood samples.

7 The induction of diverse and expanding clones is a signature of vaccine induced protective immunity [38]. The

8 goal of this experiment is to profile the global repertoire of BCR and TCR, rather than just the antigen-specific

9 cells. Alternatively, antigen-specific sorting will zoom into the picture of those clones that are reactive to the

10 spike antigen, but may miss other antigenic or bystander clones. The population of B or plasma cells contain

11 antigen-specific clones in the vaccinated animals, as suggested by positive ELISA, neutralization and

12 protection data. While outside the scope of this study, it is of future interest to further dissect the clonal

13 expanded populations of B cells or plasma cell for antigen-specific responses, for example, whether they are

14 monoclonal, oligoclonal, polyclonal and whether there are increased mutations for GC selection. In addition,

15 the T cell clonal evolution is complex as it involves responses to both structural proteins (S, M, N, E) and non-

16 structural proteins (NSPs). We performed the unsorted single cell and bulk BCR/TCR-seq analysis using the

17 entire populations from the samples to charter a comprehensive landscape of the BCR/TCR repertoires in the

18 WT- and variant-specific vaccinated animals.

19

20 In summary, our study provided direct assessment of *in vivo* immune responses to vaccination using LNP-

21 mRNAs encoding specific SARS-CoV-2 variant spikes in pre-clinical animal models. The single cell and bulk

22 VDJ repertoire mapping also provided unbiased datasets and robust systems immunology of SARS-CoV-2

23 vaccination by LNP-mRNA specifically encoding B.1.351 and B.1.617 spikes. Last but not least, all three

24 vaccine candidates, including WT-LNP-mRNA, B.1.351-LNP-mRNA, and B.1.617-LNP-mRNA showed full

25 protective potency for mice against the challenge of authentic SARS-CoV-2 viruses, not only the ancestral

26 WA-01, but also two variants of concern, Beta and Delta. These original data may offer valuable insights for

27 the development of the next-generation COVID-19 vaccines against the SARS-CoV-2 pathogen and especially

28 its emerging variants of concern [21].

29

30 **Limitation of the Study**

31 We note a few limitations of our study. 1) The characterized VoC-specific vaccine candidates target the WT

32 and the two variants dominant in 2020-2021, while new VoCs continue to emerge and evolve. Investigation

33 of vaccine candidates targeting emerging variants are warranted. 2) Although commonly used, the animal

1 model in this study is mouse, which has certain species specific immune response different from human. Non-
2 human primate and clinical studies are necessary to further advance the development of variant-specific
3 vaccines. 3) In our experimental setting, mice were challenged shortly after boost. However, in real world
4 setting, individuals might face viral exposure at various time points before, during, or after vaccination. The
5 efficacy and safety of the variant-specific vaccine candidates need to be rigorously tested in future translational
6 and clinical studies.

7

8

1 **Acknowledgments**

7

8 **Funding**

14

15 **Declaration of Interest:**

16 A patent application has been filed by Yale University related to the data described here (inventors: SC, LP,

17 ZF, JP, XZ, MD). Yale University has committed to rapidly executable nonexclusive royalty-free licenses to

18 intellectual property rights for the purpose of making and distributing products to prevent, diagnose, and treat

19 COVID-19 infection during the pandemic and for a short period thereafter. SC is a scientific Founder of

20 EvolveImmune Tx and Cellinfinity Bio, unrelated to this study. The remaining authors declare no competing

21 interests.

22

23 **Author Contributions:**

24 LP*: Developed vaccination systems, performed majority of experiments, manuscript prep

25 PAR*: Developed NGS pipelines, performed majority of NGS analyses, manuscript prep

26 AÖ*: Performed BL3 in vivo challenge experiment

27 ZF*: Prepared LNPs, performed ELISAs, participated in animal experiments, manuscript prep

28 JJP*: Developed NGS pipelines, performed initial NGS analyses, manuscript prep

29 XZ*: Developed vaccination immune assays, performed flow experiments

30 QL, MBD, QX: assisted experiments or assay setup

31 RF, PC: assisted experimental logistics

32 CL: provided TEM resources

33 CBW: Design and supervised BL3 work, manuscript prep, funding

34 SC: Conceptualization, overall design and supervision, manuscript prep, funding

1

2 **STAR Methods**

3

4 KEY RESOURCES TABLE

5 Key resources table is provided as a separate supplementary file.

6

7 RESOURCE AVAILABILITY

8 Lead contact

9 Further information and requests for resources and reagents should be directed to and will be fulfilled by the

10 Lead Contact, Sidi Chen (sidi.chen@yale.edu).

11

12 Materials Availability Statement

13 All unique/stable reagents generated in this study are available from the lead contact. Certain materials such

14 as vaccine candidates will be shared with a completed Materials Transfer Agreement.

15

16 Data and Code Availability

17 All data generated or analyzed during this study are included in this article, supplementary information, and

18 source data files. Specifically, source data and statistics for non-high-throughput experiments are provided in

19 a supplementary table excel file. Processed data and statistics for NGS experiments are provided in Data S1.

20 The raw NGS data have been deposited at SRA and are publicly available. Additional Supplemental flow

21 cytometry raw data are available from Mendeley Data at http://dx.doi.org/ 10.17632/2m6hvhhmr4.1.

22 The original codes of data analysis are available from the lead contact upon reasonable request.

23 Any additional information required to reanalyze the data reported in this paper is available from the lead

24 contact upon request.

25

26

27 EXPERIMENTAL MODEL AND SUBJECT DETAILS

28

29 **Institutional approval**

30 This study has received institutional regulatory approval. All recombinant DNA (rDNA) and biosafety work

31 were performed under the guidelines of Yale Environment, Health and Safety (EHS) Committee with approved

32 protocols (Chen-15-45, 18-45, 20-18, 20-26). All animal work was performed under the guidelines of Yale

33 University Institutional Animal Care and Use Committee (IACUC) with approved protocols (Chen-2018-

34 20068; Chen-2020-20358; Wilen 2021-20198).

1

Animals

2

3 *M. musculus* (mice), 6-8 weeks old females of C57BL/6Ncr were purchased from Charles River. *M. musculus*

4 (mice), 6-8 weeks old females of K18-hACE2 mice (B6.Cg-Tg(K18-ACE2)2Prlmn/J) were purchased from

5 Jackson Laboratory and used for immunogenicity study. Animals were housed in individually ventilated cages

6 in a dedicated vivarium with clean food, water, and bedding. Animals are housed with a maximum of 5 mice

7 per cage, at regular ambient room temperature (65-75°F, or 18-23°C), 40-60% humidity, and a 14 h:10 h light

8 cycle. All experiments utilize randomized littermate controls.

9

Cell Lines

10

11 HEK293T (ATCC) and 293T-hACE2 (gifted from Dr Bieniasz' lab) cell lines were cultured in complete

12 growth medium, Dulbecco's modified Eagle's medium (DMEM; Thermo fisher) supplemented with 10% Fetal

13 bovine serum (FBS, Hyclone),1% penicillin-streptomycin (Gibco) (D10 media for short). Cells were typically

14 passaged every 1-2 days at a split ratio of 1:2 or 1:4 when the confluency reached at 80%.

15

In vivo **efficacy testing against challenges of authentic SARS-CoV-2 and variant viruses**

16

17 The protective efficacy of SARS-CoV-2 WT and variant mRNA-LNP against replication-competent SARS-

18 CoV-2 virus and variant virus were evaluated in vivo. These experiments were performed in an animal BSL3

19 (ABSL3) facility. Replication competent SARS-CoV-2 (USA-WA1/2020) virus and the Beta variant (B.1.351)

20 were produced in VeroE6-ACE2-TMPRSS2 cells. The Delta variant (B.1.617.2) was produced in WT Vero

21 E6 cells. Titers for all three viruses were determined by plaque assay using WT Vero E6.

22

23 8-week old littermate controlled female K18-hACE2 mice (B6.Cg-Tg(K18-ACE2)2Prlmn/J) were purchased

24 from the Jackson Laboratory. Mice were randomly distributed into groups, received 10 μg of WT-LNP mRNA,

25 B.1.351-LNP-mRNA or B.1.617-LNP-mRNA via the intramuscular route on day 0 (Prime) and day 21 (Boost).

26 One week after boost, the LNP-mRNA vaccinated, and control mice were subdivided into three groups

27 randomly, then sedated with isoflurane. SARS-CoV-2 isolated USA-WA1/2020, Beta variant, or Delta variant

28 was inoculated intranasally at a dose of 10^3 PFU/mouse (determined using WT Vero E6) in 50 ul of DPBS.

29 Survival, body conditions, and weights of mice were monitored daily for 10 consecutive days.

30

31

32 METHOD DETAILS

33

1 **Plasmid construction**

2 The DNA sequences of B.1.351 and B.1.617 SARS-CoV-2 spikes for the mRNA transcription and pseudovirus

3 assay were synthesized as gBlocks (IDT) and cloned by Gibson Assembly (NEB) into pcDNA3.1 plasmids.

4 To improve expression and retain prefusion conformation, six prolines (HexaPro variant, 6P) were introduced

5 to the SARS-CoV-2 spike sequence in the mRNA transcription plasmids. The plasmids for the pseudotyped

6 virus assay including pHIV$_{NL}$GagPol and pCCNanoLuc2AEGFP are gifts from Dr. Bieniasz' lab[48]. The C-

7 terminal 19 amino acids were deleted in the SARS-CoV-2 spike sequence for the pseudovirus assay.

8

9 **Cell culture**

10 HEK293T (ATCC) and 293T-hACE2 (gifted from Dr Bieniasz' lab) cell lines were cultured in complete

11 growth medium, Dulbecco's modified Eagle's medium (DMEM; Thermo fisher) supplemented with 10% Fetal

12 bovine serum (FBS, Hyclone),1% penicillin-streptomycin (Gibco) (D10 media for short). Cells were typically

13 passaged every 1-2 days at a split ratio of 1:2 or 1:4 when the confluency reached at 80%.

14

15 **mRNA production by in vitro transcription and vaccine formulation**

16 A sequence-optimized mRNA encoding B.1.351 variant (6 P) or B.1.617 variant (6P) protein was synthesized

17 *in vitro* using an HiscribeTM T7 ARCA mRNA Kit (with tailing) (NEB), with 50% replacement of uridine by

18 N1-methyl-pseudouridine. A linearized DNA template containing the B.1.351 variant (6 P) or B.1.617 variant

19 (6P) open reading frame flanked by 5′ untranslated region (UTR) and 3′ UTR sequences and was terminated

20 by an encoded polyA tail was used as template. The above DNA templates were obtained from circulated

21 plasmids pVP22b (B.1351 variant (6P)) and pVP29b (B.1.617 variant (6P)). pVP22b and pVP29b plasmids

22 were linearized with BbsI restriction enzyme digestion and cleaned up with gel purification.

23

24 Tthe mRNA was synthesized and purified by following the manufacturer's instructions and kept frozen at -

25 80 °C until further use. The mRNA was encapsulated in a lipid nanoparticle (Genvoy-ILM^{TM}, Precision

26 Nanosystem) using the NanoAssemblr® Ignite™ machine (Precision Nanosystems). All procedures are

27 following the guidance of manufacturers. In brief, Genvoy-ILM^{TM}, containing 50% PNI ionizable lipid,10%

28 DSPC, 37.5% cholesterol, 2.5% PNI stabilizer, were mixed with mRNA in acetate buffer, pH 5.0, at a ratio of

29 6:1 (Genvoy-ILM^{TM}: mRNA). The mixture was neutralized with Tris-Cl pH 7.5, sucrose was added as a

30 cryoprotectant. The final solution was sterile filtered and stored frozen at -80 °C until further use. The particle

31 size of mRNA-LNP was determined by DLS machine (DynaPro NanoStar, Wyatt, WDPN-06). The

32 encapsulation and mRNA concentration were measured by using Quant-iT™ RiboGreen™ RNA Assay Kit

33 (Thermofisher).

1

Negative-stain TEM

5 μl of the sample was deposited on a glow-discharged formvar/carbon-coated copper grid (Electron Microscopy Sciences, catalog number FCF400-Cu-50), incubated for 1 min and blotted away. The grid was washed briefly with 2% (w/v) uranyl formate (Electron Microscopy Sciences, catalog number 22450) and stained for 1 min with the same uranyl formate buffer. Images were acquired using a JEOL JEM-1400 Plus microscope with an acceleration voltage of 80 kV and a bottom-mount 4k × 3k charge-coupled device camera (Advanced Microscopy Technologies, AMT).

In vitro mRNA expression

HEK293T cells were electroporated with mRNA encoding B.1351 variant (6P) or B.1.617 variant (6P) proteins using Neon™ Transfection System 10 μL Kit following the standard protocol provided by manufacturer. After 12 h, the cells were collected and resuspended in MACS buffer (D-PBS with 2 mM EDTA and 0.5% BSA). To detect surface-protein expression, the cells were stained with 10 μg/mL ACE2–Fc chimera (Genescript, Z03484) in MACS buffer for 30 min on ice. Thereafter, cells were washed twice in MACS buffer and incubated with PE–anti-human FC antibody (Biolegend, M1310G05) in MACS buffer for 30 min on ice. Live/Dead aqua fixable stain (Invitrogen) were used to assess viability. Data acquisition was performed on BD FACSAria II Cell Sorter (BD). Analysis was performed using FlowJo software.

Mice immunization and sample collection

A standard two-dose schedule given 21 days apart was adopted [49]. 1 μg or 10 μg LNP-mRNA were diluted in 1X PBS and inoculated into mice intramuscularly for prime and boost. Control mice received PBS. Two weeks post-prime (day14) and two weeks post-boost (day 35), sera were collected from experimental mice and utilized for following ELISA and neutralization assay of pseudovirus. Forty days (day 40) after prime, mice were euthanized for endpoint data collection. Splenocytes were collected for T cell stimulation and cytokine analysis, and single cell profiling. Lymphocytes were separately collected from mouse blood, spleen and draining lymph nodes and applied for Bulk BCR and TCR profiling.

Cell isolation from animals

For every mouse treated with either LNP-mRNA or PBS. Blood, spleens and draining lymph nodes were separately collected. Spleen and lymph node were homogenized gently and filtered with a 100 μm cell strainer (BD Falcon, Heidelberg, Germany). The cell suspension was centrifuged for 5 min with 400 g at 4 °C. Erythrocytes were lysed briefly using ACK lysis buffer (Lonza) with 1mL per spleen for 1~2 mins before

1   adding 10 mL PBS containing 2% FBS to restore iso-osmolarity. The single-cell suspensions were filtered

2   through a 40 μm cell strainer (BD Falcon, Heidelberg, Germany).

3

4   **Flow Cytometry**

5   Spleens from three mice in LNP mRNA vaccine groups and four mice in PBS group were collected five days

6   post boost. Mononuclear single-cell suspensions from whole mouse spleens were generated using the above

7   method. 0.5 million splenocytes were resuspended with 200μl into RPMI1640 supplemented with 10% FBS,

8   1% penicillin–streptomycin antibiotic, Glutamax and 2mM 2-mercaptoethonal, anti-mouse CD28 antibody

9   (Biolegend, Clone 37.51) and seed into 96- well plate for overnight. The splenocytes were incubated for 6 hr

10   at 37°C in vitro with BrefeldinA (Biolegend) under three conditions: no peptide, PMA/Ionomycin, and

11   PepTivator® SARS-CoV-2 Prot_S Complete peptide pool (Miltenyi Biotec, 15 mers with 11 amino acid

12   overlap) covering the entire SARS-CoV-2 S protein. Peptide pools were used at a final concentration of 200

13   ng/ml. Following stimulation, cells were washed with PBS before surface staining with LIVE/DEAD Fixable

14   Dead Cell Stain (Invitrogen, 1:1000) and a surface stain cocktail containing the following antibodies: CD3

15   PE/Cy7 (Biolegend, Clone 17A2,1:200), CD8a BV421(Biolegend, Clone QA17A07, 1:200), CD4 FITC

16   (Biolegend, Clone GK1.5,1:200) in MACS buffer (D-PBS with 2 mM EDTA and 0.5% BSA) on ice for 20

17   min, cells were washed with MACS buffer then fixed and permeabilized using the BD Cytofix/Cytoperm

18   fixation/permeabilization solution kit according to the manufacturer's instructions. Cells were washed in

19   perm/wash solution for 5 min, and stained by intracellular staining for 30 min at 4 °C using a cocktail of the

20   following antibodies: IFN-γ PE (Biolegend, Clone W18272D,1:500), TNF Percp-Cy5.5(Biolegend, Clone

21   MP6-XT22, 1:500), IL2 BV510 (Biolegend, Clone JES6-5H4, 1:500), IL4 BV605 (Biolegend, Clone

22   11B11,1:500), IL5 APC(Biolegend, Clone TRFK5,1:500) in MACS buffer. Finally, cells were washed in

23   MACS for twice and resuspended in MACS buffer before running on BD FACSAria II Cell Sorter (BD).

24   Analysis was performed using FlowJo software according to the gating strategy outlined in a Supplemental

25   Figure. Polyfunctional T cells were analyzed by examination of cellular populations expressing multiple

26   markers.

27

28   **ELISA**

29   The 384-well ELISA plates were coated with 3 μg/ml of antigens overnight at 4 degree. The antigen panel

30   used in the ELISA assay includes SARS-CoV-2 spike S1+S2 ECD and RBD of 2019-nCoV (SINO, ECD

31   40589-V08B1 and RBD 40592-V08B), Indian variant B.1.617 (SINO, ECD 40589-V08B12 and RBD 40592-

32   V08H88), South African variant (SINO, ECD 40589-V08B07 and RBD 40592-V08H85) and. spike RBD of

33   wild-type, South African variant and Indian variant. Plates were washed with PBS plus 0.5% Tween 20 (PBST)

1 three times using the 50TS microplate washer (Fisher Scientific, NC0611021) and blocked with 0.5% BSA in

2 PBST at room temperature for one hour. Plasma was serially diluted twofold or fourfold starting at a 1:2000

3 dilution. Samples were added to the coated plates and incubate at room temperature for one hour, followed by

4 washes with PBST five times. Anti-mouse secondary antibody was diluted to 1:2500 in blocking buffer and

5 incubated at room temperature for one hour. Plates were washed five times and developed with

6 tetramethylbenzidine substrate (Biolegend, 421101). The reaction was stopped with 1 M phosphoric acid, and

7 OD at 450 nm was determined by multimode microplate reader (PerkinElmer EnVision 2105). The binding

8 response (OD450) were plotted against the dilution factor in log10 scale to display the dilution-dependent

9 response. The area under curve of the dilution-dependent response (Log10 AUC) was calculated to evaluate

10 the potency of the serum antibody binding to spike antigens.

11

12 **SARS-CoV-2 pseudovirus reporter and neutralization assays**

13 HIV-1 based SARS-CoV-2 WT, B.1.351 variant, and B.1.617 variant pseudotyped virions were generated

14 using respective spike sequences and applied in neutralization assays. Plasmid expressing a C-terminally

15 truncated SARS-CoV-2 S protein (pSARS-CoV-2Δ19) was from Dr Bieniasz' lab. Plasmids expressing a C-

16 terminally truncated SARS-CoV-2 B.1.351 variant S protein (B.1.351 variant-Δ19) and SARS-CoV-2 B.1.617

17 variant S protein (B.1.617 variant-Δ19) were generated as above. The three plasmids-based HIV-1

18 pseudotyped virus system were utilized to generate (HIV-1/NanoLuc2AEGFP)-SARS-CoV-2 particles, (HIV-

19 1/NanoLuc2AEGFP)-B.1.351 variant particles, and B.1.617 variant particles. The reporter vector,

20 pCCNanoLuc2AEGFP, and HIV-1 structural/regulatory proteins (pHIVNLGagPol) expression plasmid were

21 gifts from Dr Bieniasz's lab. Briefly, 293T cells were seeded in 150 mm plates, and transfected with 21 µg

22 pHIVNLGagPol, 21 µg pCCNanoLuc2AEGFP, and 7.5 µg of a SARS-CoV-2 SΔ19 or B.1.351 variant-Δ19

23 or SARS-CoV-2 SA SΔ19 plasmid, utilizing 198 µl PEI. At 48 h after transfection, the 20-ml supernatant was

24 harvested and filtered through a 0.45-µm filter, and concentrated before aliquoted and frozen in -80°C.

25

26 The pseudovirus neutralization assays were performed on 293T-hACE2 cell. One day before, 293T-hACE2

27 cells were plated in a 96 well plate, 0.01×10^6 cells per well. The following day, serial dilution serum plasma,

28 collected from PBS or LNP-mRNA vaccine immunized mice and started from 1:100 (5-fold serial dilution

29 using complete growth medium), 55 µL aliquots were mixed with the same volume of SARS-CoV-2 WT,

30 B.1.351 variant, and B.1.617 variant pseudovirus. The mixture was incubated for 1 hr at 37 °C incubator,

31 supplied with 5% CO_2. Then 100 µL of the mixtures were added into 96-well plates with 293T-hACE2 cells.

32 Plates were incubated at 37°C supplied with 5% CO_2. 48 hr later, 293T-hACE2 cells were collected and the

33 GFP+ cells were analyzed with Attune NxT Acoustic Focusing Cytometer (Thermo Fisher). The 50%

1   inhibitory concentration (IC50) was calculated with a four-parameter logistic regression using GraphPad Prism

2   (GraphPad Software Inc.).

3

4   Bulk BCR and TCR sequencing

5   Lymphocytes from blood, draining lymph node, spleen of each mRNA-LNP vaccinated and control mice were

6   collected as described above for mouse immunization and sample collection. mRNA of lymphocytes from

7   three tissues were extracted using a commercial RNeasy® Plus Mini Kit (Qiagen). Following bulk BCR and

8   TCR are prepared using SMARTer Mouse BCR IgG H/K/L Profiling Kit and SMARTer Mouse TCR a/b

9   profiling kit separately (Takara). Based on the extracted mRNA amount of each sample, the input RNA

10   amounts for bulk BCR libraries were as follows: lymphocytes from blood (100 ng), lymphocytes from lymph

11   node (1000 ng), and lymphocytes from spleen (1000 ng). The input RNA amounts for bulk TCR libraries were

12   as follows: lymphocytes from blood (100 ng), lymphocytes from lymph node (500 ng), and lymphocytes from

13   spleen (500 ng). All procedures followed the standard protocol of the manufacture. The pooled library was

14   sequenced using MiSeq (Illumina) with 2*300 read length.

15

16   Single cell profiling

17   Splenocytes were collected from mRNA-LNP vaccinated and control mice were collected as described above

18   for mouse immunization and sample collection, and normalized to 1000 cells/μL. Standard volumes of cell

19   suspension were loaded to achieve targeted cell recovery to 10000 cells. The samples were subjected to 14

20   cycles of cDNA amplification. Following this, gene expression (GEX), TCR-enriched and BCR-enriched

21   libraries were prepared according to the manufacturer's protocol (10x Genomics). All libraries were sequenced

22   using a NovaSeq 6000 (Illumina) with 2*150 read length.

23

24

25   Single cell transcriptomics data analysis for immune repertoire profiling

26   Single cell gene expression data were pre-processed with a standard Cell Ranger v6.0.1 (10x Genomics)

27   pipeline, aligning reads to the mm10 mouse reference transcriptome. Data set integration and cell population

28   analyses were then performed using the Seurat v4.0.5 package for the R statistical programming language [50].

29   Specifically, each data set was filtered (cells with 200-2500 RNA features and < 5% mitochondrial RNA), log-

30   normalized, scaled then integrated using the method by Stuart et al., using PBS vaccination samples as the

31   reference group (reciprocal-PCA method, 2000 anchors, k = 20) [51]. The integrated data was rescaled, centered,

32   then visualized in low-dimensional space by uniform manifold approximation and projection (UMAP) [52], using

33   the first 15 dimensions from a principal components analysis (PCA), chosen based on the elbow plot method.

1 Cells were clustered by generating a shared nearest neighbors (SNN) graph (k = 20, first 15 PCA dimensions)

2 and optimizing modularity using the Louvain algorithm with multilevel refinement algorithm and an

3 empirically chosen resolution, based on the best spatial separation of major immune populations cells via *Cd3d*,

4 *Cd19*, *Ncr1*, *Itgam*, *Itgax*, and *Sdc1* expression on UMAP visualization. The clusters were then labeled using

5 the expression patterns of immune cell markers (**Dataset S1**), based on (a) the proportion of cells within each

6 cluster that express the markers (>10% of cells with scaled expression > 1) and (b) the cluster-averaged scaled

7 expression > 0 (Figures 5B, S3-6). For better resolution of complex cell types, B cells, T cells and dendritic

8 cells (DCs) (*Cd45+Cd19+, Cd45+Cd3d+,* and *Cd45+Itgax+* clusters, respectively) were separately subset,

9 rescaled, visualized in low dimensional UMAP space, clustered, and populations were identified using the

10 method above. Labeled cell types were tested for homogeneity by performing Wilcoxon rank sum testing of

11 scaled data and assessing discreet hierarchical clustering of populations using the top 10 DEGs in each cell

12 type compared to all others.

13

14 Differential expression analyses compared the effect of different variant vaccines on activated B cells

15 (Activated and germinal center B cells), activated CD4 T cells (Th1, Th2, Treg, Th17, Tfh, and exhausted CD4

16 T cells), and activated CD8 T cells (Tc1, Tcm, and exhausted CD8 T cells) using a modified edgeR analysis

17 pipeline. Briefly, low-expression genes (< 5 % detection across cells) were excluded, TMM-wsp size factors

18 were calculated, data were fit to a gamma-Poisson generalized linear model (~ scaled cell detection rate + WA-

19 1 + B.1.351 + B.1.617 + vaccine concentration + cell type) (Dataset S1), and the fitted data were assessed by

20 quasi-likelihood F tests [53,54]. Model fitting and DE was performed using the glmGamPoi package for R [55], and

21 the following vaccination statuses were used as the coefficient equal to zero under the null hypothesis: (1)

22 WA-1, (2) B.1.351, (3) B.1.617, (4) B.1.351 - WA-1, or (5) B.1.617 - WA-1.

23

24 Downstream analyses were performed using differentially expressed genes (DEGs) with an FDR-adjusted p

25 value < 0.01 and a log fold-change (log-FC) > 0.5 or < -0.5 for upregulated and downregulated genes,

26 respectively. First, DEGs were sorted by significance and analyzed by the gProfiler2 R package with biological

27 process gene ontology (GO) terms for mus musculus, against known genes as the analysis domain [56,57].

28 Analysis results were filtered to include those with an adjusted p value (gProfiler gSCS method) < 0.01, GO

29 terms <= 600 genes, and terms that included > 4 DEGs. If there were more than 3 filtered terms, results were

30 clustered into "supra-pathways" by constructing an undirected network graph with (1) edges weighted by

31 filtered pathway similarity coefficients (coefficient = Jaccard + Overlap of genes between GO terms;

32 coefficients > 0.375), (2) a layout calculated via Fruchterman-Reingold algorithm, and (3) terms clustered by

33 the Leiden algorithm (modularity function, 1000 iterations, resolution = 0.8), all of which using the iGraph,

1 network, and sna R packages. The clustered pathways were labeled by the most significant pathway from each

2 cluster.

3

VDJ sequencing data analysis

5 Bulk VDJ sequencing data had adapters trimmed by Trimmomatic v0.39 in single-end mode, clipping Illumina

6 TruSeq adapters with default settings and filtering reads with an average quality score < 30 [58]. Clonotypes

7 were called using MiXCR v2.1.5 with the recommended settings for 5' RACE (RNA alignment to V gene

8 transcripts with P region) [59]. Single-cell sequencing data was processed using the Cellranger v5.0.1 (10x

9 Genomics) pipeline and aligned to the mm10 VDJ reference. The MiXCR clonotype output or Cell Ranger

10 AIRR-formated output (bulk and single cell VDJ analyses, respectively) were used as inputs to Immunarch

11 v0.6.6 R package for calculating summary statistics, diversity metrics, and repertoire overlaps.

12

Standard Statistical analysis

14 The statistical methods are described in figure legends and/or supplementary Excel tables. The statistical

15 significance was labeled as follows: n.s., not significant; * $p < 0.05$; ** $p < 0.01$; *** $p < 0.001$; **** $p <$

16 0.0001. Prism (GraphPad Software) and RStudio were used for these analyses. Additional information can be

17 found in the Nature Research Reporting Summary.

18

Replication, randomization, blinding and reagent validations

20 Replicate experiments have been performed for all key data shown in this study.

21 Biological or technical replicate samples were randomized where appropriate. In animal experiments, mice

22 were randomized by littermates.

23 Experiments were not blinded.

24 NGS data processing were blinded using metadata. Subsequent analyses were not blinded.

25 Commercial antibodies were validated by the vendors, and re-validated in house as appropriate. Custom

26 antibodies were validated by specific antibody - antigen interaction assays, such as ELISA. Isotype controls

27 were used for antibody validations.

28 Cell lines were authenticated by original vendors, and re-validated in lab as appropriate.

29 All cell lines tested negative for mycoplasma.

30

31

1   **Supplemental Data items**

2

3   **Data S1. A zip file that contains the following excels:**

4   1. Compiled single cell gene expression data (Figure 5-6)

5   2. Compiled single cell gene differential expression data (Figure 5-6)

6   3. Compiled single cell BCR and TCR sequencing data (Figure 7)

7   4. Compiled bulk BCR sequencing data (Figure 7)

8   5. Compiled bulk TCR sequencing data (Figure 7)

9   **Related to Figures 5, 6, 7**

10

11   **Source data and statistics.**

12   An excel file that contains source data and statistics of non-NGS experiments

13   "VarVac original data and statistics non-NGS 20220420.xlsx"

14   **Related to Figures 1, 2, 3, 4**

15

16

1 **Figure Legends**

2 **Figure 1 | Overview of the primary experimental design, and the B and T cell responses induced by WT-**

3 **LNP-mRNA vaccination against SARS-CoV-2 WT, B.1.351 and B.1.617 spikes in mice.**

4 **A**, Schematic of the designs of three variant-specific LNP-mRNA vaccine candidates. Functional elements

5 were shown in the spike mRNA and translated protein of SARS-CoV-2 WT, B.1.351 and B.1.617 spikes,

6 including protein domains, HexaPro and variant-specific mutations.

7 **B**, 3D structure highlighting certain variant-specific mutations in B.1.351 and B.1.617 spikes. Distribution of

8 mutations of B.1.351 and B.1.617 were shown in the structure of SARS-CoV-2 (PDB: 6VSB). Mutations of

9 B.1.351 and B.1.617 were shown as spheres, except for those in the unstructured loop regions. Certain

10 mutations were not visible in the structure as they fall into floppy regions of spike.

11 **C**, Graphical representation of B.1.351-LNP-mRNA complex and B.1.617-LNP-mRNA complex formation.

12 The spike mRNAs of B.1.351 and B.1.617 were

13 encapsulated by LNP via NanoAssemblr Ignite. The size and encapsulation rate of the mRNA-LNP complex

14 were measured by dynamic light scatter (DLS) and Ribogreen assay, respectively.

15 **D**, After electroporated into 293FT cells, *In vitro* expression of B.1.351-spike or B.1.617-spike mRNA were

16 detected by flowcytometry using the human ACE2-Fc fusion protein and PE-anti-Fc antibody.

17 **E-F**, DLS (**e**) and TEM (**f**) of size and monodispersity characterization of LNP-mRNAs.

18 **G**, Schematic of overall design of primary experiments. Six- to 8-week-old C57BL/6Ncr mice (B.1.351-LNP-

19 mRNA (top) and B.1.617-LNP-mRNA**,** n = 6 mice per group; WT-LNP-mRNA, n = 4 mice; PBS, n = 9)

20 received 1 or 10 μg of WT-LNP mRNA, B.1.351-LNP-mRNA or B.1.617-LNP-mRNA via the intramuscular

21 route on day 0 (Prime) and day 21 (Boost). Blood was collected twice, two weeks post prime and boost. The

22 binding and pseudovirus-neutralizing antibody responses induced by LNP-mRNA were evaluated by ELISA

23 and neutralization assay. Mice were euthanized at day 40. The spleen, lymph node and blood samples were

24 collected to analyze immune responses in by flow cytometry, bulk BCR and TCR profiling and single cell

25 profiling.

26 **H-I,** Serum ELISA titers of WT-LNP mRNA vaccinated animals (n = 4). Serum antibody titer as area under

27 curve (AUC) of $\log_{10}$-transformed curve ($1og_{10}$ AUC) to spike RBDs (**h**) and ECDs (**i**) of SARS-CoV-2 WT,

28 B.1.351 and B.1.617. Two-way ANOVA with Tukey's multiple comparisons test was used to assess statistical

29 significance.

30 **J,** Serum neutralization titers of WT-LNP mRNA vaccinated animals (n = 4). Cross neutralization of SARS-

31 CoV-2 WT, B.1.351 or B.1.617 pseudovirus infection of ACE2-overexpressed 293T cells. Two-way ANOVA

32 with Tukey's multiple comparisons test was used to assess statistical significance.

1 **K-L**, T cell response of WT-LNP mRNA vaccinated animals (n = 4). CD8$^+$ (**k**) and CD4$^+$ (**l**) T cell responses

2 were measured by intracellular cytokine staining 6 hours after addition of BFA. The unpaired parametric t test

3 was used to evaluate the statistical significance.

4 **Notes:**

5 In this figure:

6 Each dot represents data from one mouse.

7 Data are shown as mean ± s.e.m. plus individual data points in dot plots.

8 Statistical significance labels: n.s., not significant; * p < 0.05; ** p < 0.01; *** p < 0.001; **** p < 0.0001

9 Source data and additional statistics for experiments are provided in a supplemental excel file.

10 **See also: Figure(s) S1, S2**

11

12 **Figure 2 | B.1.351-LNP-mRNA and B.1.617-LNP-mRNA elicit robust binding and pseudovirus-**

13 **neutralizing antibody response against all three variants in mice**

14 **A,** Serum ELISA titers of animals vaccinated by B.1.351-LNP-mRNA (top) and B.1.617-LNP-mRNA

15 (bottom), against RBD from three different spikes (WT, B.1.351, and B.1.617) of SARS-CoV-2 (n = 6).

16 **B,** Serum ELISA titers of animals vaccinated by B.1.351-LNP-mRNA (top) and B.1.617-LNP-mRNA

17 (bottom), against ECD from three different spikes (WT, B.1.351, and B.1.617) of SARS-CoV-2 (n = 6).

18 **C,** Serum neutralization titers of animals vaccinated by B.1.351-LNP-mRNA (top) and B.1.617-LNP-mRNA

19 (bottom), against three pseudoviruses (WT, B.1.351, and B.1.617) of SARS-CoV-2 (n = 6).

20 **D-E,** Direct comparison of serum ELISA (D) and neutralization (E) titers of animals boosted by WT, B.1.351-

21 LNP-mRNA and B.1.617-LNP-mRNA, against WT, B.1.351, and B.1.617 spikes or pseudoviruses of SARS-

22 CoV-2.

23 **F**, Heatmap of neutralization titers of animals vaccinated by all three LNP-mRNAs, against three

24 pseudoviruses (WT, B.1.351, and B.1.617) of SARS-CoV-2.

25 **G**, Correlation X-Y scatterplots of ELISA and neutralization titers between ELISA ECD log10AUC vs

26 neutralization log10IC50 for all vaccine groups

27 **Notes:**

28 In this figure:

29 Each dot represents data from one mouse.

30 Data are shown as mean ± s.e.m. plus individual data points in dot plots.

31 Statistical significance labels: n.s., not significant; * p < 0.05; ** p < 0.01; *** p < 0.001; **** p < 0.0001

32 Source data and additional statistics for experiments are provided in a supplemental excel file.

33 **See also: Figure(s) S1**

1

Figure 3 | B.1.351-LNP-mRNA and B.1.617-LNP-mRNA induced S protein-specific T cell response

A-C Percentage of CD8$^+$ T cells expressing IFN-γ (**a**), TNFα (**b**), and IL-2 (**c**), in response to stimulation of S peptide pools (n=3). Left panels, representative flow plots; right panels, dot-bar plots for statistics of the left panels.

D, Percentage of CD4$^+$ T cells expressing IFN-γ in response to stimulation of S peptide pools (n = 3). Left panels, representative flow plots; right panels, dot-bar plots for statistics of the left panels.

E-H, B.1.351-LNP-mRNA and B.1.617-LNP-mRNA induced S protein-specific polyfunctional CD8 and CD4 T cells

E-G, Percentage of CD8$^+$ T cells expressing both IFN-γ and TNFα (**E**), both IFN-γ and IL-2(**F**), TNFα and IL-2 (**G**), in response to stimulation of S peptide pools (n = 3). Left panels, representative flow plots; right panels, dot-bar plots for statistics of the left panels.

H, Percentage of CD4$^+$ T cells expressing both IFN-γ and TNFα in response to stimulation of S peptide pools (n = 3). Left panels, representative flow plots; right panels, dot-bar plots for statistics of the left panels.

Notes:

In this figure:

Each dot represents data from one mouse.

Data are shown as mean ± s.e.m. plus individual data points in dot plots.

Statistical significance labels: n.s., not significant; * $p < 0.05$; ** $p < 0.01$; *** $p < 0.001$; **** $p < 0.0001$

Source data and additional statistics for experiments are provided in a supplemental excel file.

See also: Figure(s) S2

Figure 4 | B.1.351-LNP-mRNA and B.1.617-LNP-mRNA showed *in vivo* protect efficacy against the challenge of replication competent authentic SARS-CoV-2 and variant viruses

A, Schematic of authentic virus challenge experiments on mRNA-LNP vaccinated mice. hACE2-K18 mice were separated randomly and received 10 μg of WT-LNP mRNA, B.1.351-LNP-mRNA or B.1.617-LNP-mRNA via the intramuscular route on day 0 (Prime) and day 21 (Boost). One week after boost (day28), the mRNA-LNP vaccinated, and control mice were distributed into three groups and challenged with WA-1, beta, and delta authentic live virus. Survival, body conditions, and weights of mice were monitored daily for 10 consecutive days.

B, A numeric summary of the number of hACE2-K18 mice that vaccinated with WT-LNP mRNA, B.1.351-LNP-mRNA or B.1.617-LNP-mRNA and challenged with three different authentic virus WA01, Beta (B.1.351) and Delta (B.1.617.2).

1 **C**, Body weight curves of WT-LNP mRNA, B.1.351-LNP-mRNA, B.1.617-LNP-mRNA vaccinated, and

2 control hACE2 transgenic mice under lethal challenges with different authentic virus WA-01 (Left), Beta

3 (Middle), and Delta (Right).

4 **D**, Survival curves of WT-LNP mRNA, B.1.351-LNP-mRNA or B.1.617-LNP-mRNA vaccinated, and control

5 hACE2 transgenic mice under lethal challenges with different authentic virus WA-01 (Left), Beta (Middle),

6 and Delta (Right).

7 **Notes:**

8 In this figure:

9 Each dot represents data from one mouse.

10 Data are shown as mean ± s.e.m. plus individual data points in dot plots.

11 Statistical significance labels: n.s., not significant; * p < 0.05; ** p < 0.01; *** p < 0.001; **** p < 0.0001

12 Source data and additional statistics for experiments are provided in a supplemental excel file.

13

14 **Figure 5 | Single cell transcriptomics of variant-specific LNP-mRNA vaccinated animals**

15 **A,** UMAP visualizations of all 141,729 cells pooled across samples and conditions. Cells are color-labeled by

16 vaccine, concentration, and unsupervised clustering in each panel, top to bottom. Clusters are labeled by cell

17 types that were assigned, based on the expression of cell type-specific markers.

18 **B,** UMAP heatmaps of the expression of major cell type-specific markers across all cells.

19 **C,** Heatmap of differentially expressed genes (DEGs) across indicated cell types. Differential expression

20 analyses were performed using Wilcoxon rank sum test for each cell type vs all other cells, and the heatmap

21 includes the 10 DEGs from each analysis (absolute log2-FC > 4, q < 0.01).

22 **D,** Boxplots of overall cell type proportions compared across vaccine groups (n = 6 for each). Comparisons

23 were performed using a 2-way ANOVA test, accounting for vaccine and cell type as covariates, with Dunnet's

24 post-hoc analysis for multiple comparisons against PBS as the control. Data were analyzed together, but

25 displayed separately for clarity.

26 **E,** Stacked bar chart of cell proportions between different vaccination groups (n = 6 for each).

27 **F,** UMAP visualization of T cell and B cell sub-populations across all samples and conditions. Sub-clusters

28 are labeled by cell types, assigned by the expression of cell type-specific markers.

29 **G,** Boxplots of B and T subset proportions compared across vaccine groups (n = 6 for each). Comparisons

30 were performed using a 2-way ANOVA test, accounting for vaccine and cell type as covariates, with Dunnet's

31 post-hoc analysis for multiple comparisons against PBS as the control. Data were analyzed together, but

32 displayed separately for clarity.

33 **Notes:**

1 In this figure, panels **D** and **G**:

2 Each dot represents data from one mouse.

3 The high dose (n = 3 each) and low dose (n = 3 each) groups for each vaccine were merged (n = 6 total) in

4 single cell data analysis, same thereafter.

5 Statistical significance labels: n.s., not significant; * $p < 0.05$; ** $p < 0.01$; *** $p < 0.001$; **** $p < 0.0001$
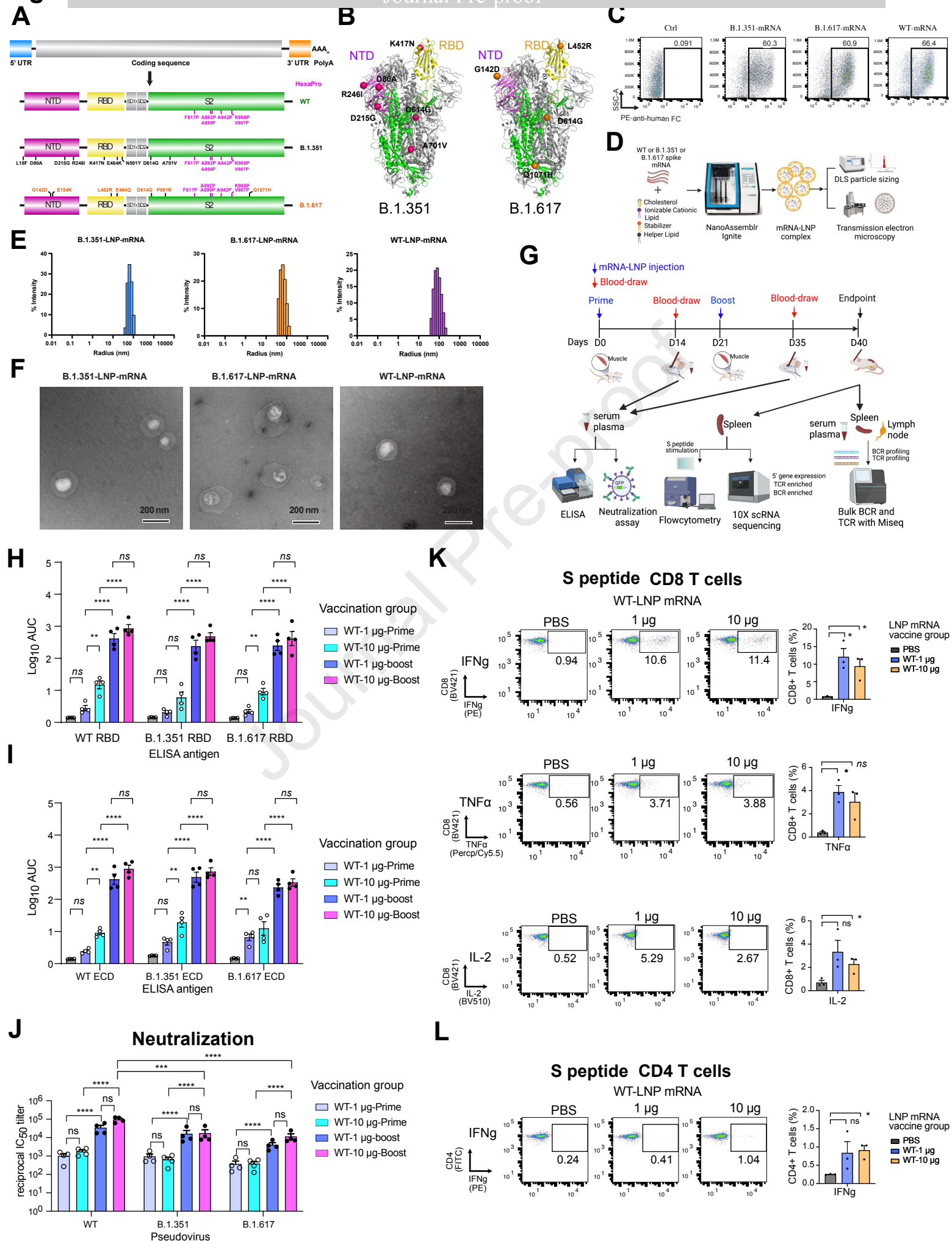
6 **See also: Figures S3-6**

7

8 **Figure 6 | Single cell analysis of activated B cell and CD8 T cell populations with gene expression**

9 **signatures of variant-specific LNP-mRNA vaccinated animals**

10 **A,** Volcano plots of differential expression (DE) analyses for each vaccination group vs PBS in B cells.

11 Analyses were performed using quasi-likelihood F tests of scRNA-seq data fitted with gamma-Poisson

12 generalized linear models.

13 **B,** Network plots of clustered terms from pathway analyses of upregulated genes in the indicated in B cell DE

14 analysis. Pathway enrichment analyses were performed by gProfiler2, and significantly enriched pathways

15 were clustered with Leiden algorithm. Pathway clusters (supra-pathways) are labeled by their most significant

16 member term along with its enrichment q value. The top five supra-pathways are shown for each plot.

17 **C,** Expression heatmaps of DE genes from selected upregulated supra-pathways in B cell DE analysis. Single-

18 cell expression values were scaled then averaged across vaccination groups.

19 **D,** Volcano plots of differential expression (DE) analyses for each vaccination group vs PBS in CD8 T cells.

20 Analyses were performed using quasi-likelihood F tests of scRNA-seq data fitted with gamma-Poisson

21 generalized linear models.

22 **E,** Network plots of clustered terms from pathway analyses of upregulated genes in the indicated in CD8 T

23 cell DE analysis. Pathway enrichment analyses were performed by gProfiler2, and significantly enriched

24 pathways were clustered with Leiden algorithm. Pathway clusters (supra-pathways) are labeled by their most

25 significant member term along with its enrichment q value. The top five supra-pathways are shown for each

26 plot.

27 **F,** Expression heatmaps of DE genes from selected upregulated supra-pathways in CD8 T cell DE analysis.

28 Single-cell expression values were scaled then averaged across vaccination groups.

29 **See also: Figures S7-9**

30

31 **Figure 7 | VDJ repertoire and clonal analyses of B cell and T cell populations from variant-specific LNP-**

32 **mRNA vaccinated animals**

1   **A,** Clonal composition bar plot depicting proportion of the BCR repertoire occupied by the clones of a given

2   size for all samples in the single cell BCR-seq dataset.

3   **B,** Bar plot of Chao1 indices for each condition for repertoires in the single cell BCR-seq dataset (n = 6 for

4   each group).

5   **C,** Clonal composition bar plot depicting proportion of the TCR repertoire occupied by the clones of a given

6   size for all samples in the single cell TCR-seq dataset.

7   **D,** Bar plot of unique clonotypes for each for repertoires in the single cell TCR-seq.

8   **E,** Circos plots of V-J clonotype distribution for single cell BCR-seq dataset (left panel) and single cell TCR-

9   seq dataset (right panel). The 20 most abundant V-J combinations are shown for pooled vaccination group.

10   **F,** Clonal composition bar plot depicting proportion of the BCR repertoire occupied by the clones of a given

11   size for all samples in the bulk BCR-seq dataset (left panel) and bulk TCR-seq dataset (right panel).

12   **G,** Bar plots depicting relative abundances of IGH, IGK, IGL, TRA, TRB, and TRD clonotypes within specific

13   frequency ranges in the bulk BCR/TCR-seq data from different tissues of different vaccination groups.

14   Relative abundances are presented for individual and grouped samples in **e** and **f**, respectively.

15   **H,** Bar plots of the effective clone numbers (true diversity estimates) for selected BCR and TCR chain

16   repertoires in the bulk TCR-seq dataset across vaccination and tissue groups.

17   **Notes:**

18   For the single-cell BCR/TCR-seq datasets, n = 6 samples for the PBS, and n=3 for WA-1 1ug, WA-1 10 µg,

19   B.1.351 1 µg, B.1.351, B.1.617 1ug, and B.1.617 10 µg groups. For the bulk BCR/TCR-seq datasets, n = 4

20   PBS samples, and n=3 for B.1.351 1ug, B.1.351, B.1.617 1ug, and B.1.617 10 µg groups.

21   Statistics for **F** and **G** performed using two-way ANOVA tests with Dunnet's multiple comparison test.

22   Statistical significance labels: n.s., not significant; * $p < 0.05$; ** $p < 0.01$; *** $p < 0.001$; **** $p < 0.0001$

23   **See also: Figure S10-12**

24

25

References

1. Dong, E., Du, H., and Gardner, L. (2020). An interactive web-based dashboard to track COVID-19 in real time. Lancet Infect Dis *20*, 533-534. 10.1016/S1473-3099(20)30120-1.

2. Hacisuleyman, E., Hale, C., Saito, Y., Blachere, N.E., Bergh, M., Conlon, E.G., Schaefer-Babajew, D.J., DaSilva, J., Muecksch, F., Gaebler, C., et al. (2021). Vaccine Breakthrough Infections with SARS-CoV-2 Variants. N Engl J Med *384*, 2212-2218. 10.1056/NEJMoa2105000.

3. Kustin, T., Harel, N., Finkel, U., Perchik, S., Harari, S., Tahor, M., Caspi, I., Levy, R., Leshchinsky, M., Ken Dror, S., et al. (2021). Evidence for increased breakthrough rates of SARS-CoV-2 variants of concern in BNT162b2-mRNA-vaccinated individuals. Nat Med. 10.1038/s41591-021-01413-7.

4. Bergwerk, M., Gonen, T., Lustig, Y., Amit, S., Lipsitch, M., Cohen, C., Mandelboim, M., Gal Levin, E., Rubin, C., Indenbaum, V., et al. (2021). Covid-19 Breakthrough Infections in Vaccinated Health Care Workers. N Engl J Med. 10.1056/NEJMoa2109072.

5. Tyagi, K., Ghosh, A., Nair, D., Dutta, K., Singh Bhandari, P., Ahmed Ansari, I., and Misra, A. (2021). Breakthrough COVID19 infections after vaccinations in healthcare and other workers in a chronic care medical facility in New Delhi, India. Diabetes Metab Syndr *15*, 1007-1008. 10.1016/j.dsx.2021.05.001.

6. Callaway, E. (2021). COVID vaccine boosters: the most important questions. Nature *596*, 178-180. 10.1038/d41586-021-02158-6.

7. Mizrahi, B., Lotan, R., Kalkstein, N., Peretz, A., Perez, G., Ben-Tov, A., Chodick, G., Gazit, T., and Patalon, T. (2021). Correlation of SARS-CoV-2 Breakthrough Infections to Time-from-vaccine; Preliminary Study. MedRxiv. https://doi.org/10.1101/2021.07.29.21261317.

8. Stephen J. Thomas, E.D.M.J., Nicholas Kitchin, Judith Absalon, Alejandra Gurtman, Stephen Lockhart, John L. Perez, Gonzalo Pérez Marc, Fernando P. Polack, Cristiano Zerbini, Ruth Bailey, Kena A. Swanson, Xia Xu, Satrajit Roychoudhury, Kenneth Koury, Salim Bouguermouh, Warren V. Kalina, David Cooper, Robert W. Frenck Jr., Laura L. Hammitt, Özlem Türeci, Haylene Nell, Axel Schaefer, Serhat Ünal, Qi Yang, Paul Liberator, Dina B. Tresnan, Susan Mather, Philip R. Dormitzer, Uğur Şahin, William C. Gruber, Kathrin U. Jansen (2021). Six Month Safety and Efficacy of the BNT162b2 mRNA COVID-19 Vaccine. MedRxiv. https://doi.org/10.1101/2021.07.28.21261159.

9. Taylor, P.C., Adams, A.C., Hufford, M.M., de la Torre, I., Winthrop, K., and Gottlieb, R.L. (2021). Neutralizing monoclonal antibodies for treatment of COVID-19. Nat Rev Immunol. 10.1038/s41577-021-00542-x.

10. Liu, Z., VanBlargan, L.A., Bloyet, L.M., Rothlauf, P.W., Chen, R.E., Stumpf, S., Zhao, H., Errico, J.M., Theel, E.S., Liebeskind, M.J., et al. (2021). Identification of SARS-CoV-2 spike mutations that attenuate monoclonal and serum antibody neutralization. Cell Host Microbe *29*, 477-488 e474. 10.1016/j.chom.2021.01.014.

11. Davies, N.G., Abbott, S., Barnard, R.C., Jarvis, C.I., Kucharski, A.J., Munday, J.D., Pearson, C.A.B., Russell, T.W., Tully, D.C., Washburne, A.D., et al. (2021). Estimated transmissibility and impact of SARS-CoV-2 lineage B.1.1.7 in England. Science *372*. 10.1126/science.abg3055.

12. Zhou, D., Dejnirattisai, W., Supasa, P., Liu, C., Mentzer, A.J., Ginn, H.M., Zhao, Y., Duyvesteyn, H.M.E., Tuekprakhon, A., Nutalai, R., et al. (2021). Evidence of escape of SARS-CoV-2 variant B.1.351 from natural and vaccine-induced sera. Cell *184*, 2348-2361 e2346. 10.1016/j.cell.2021.02.037.

13. Wang, P., Nair, M.S., Liu, L., Iketani, S., Luo, Y., Guo, Y., Wang, M., Yu, J., Zhang, B., Kwong, P.D., et al. (2021). Antibody resistance of SARS-CoV-2 variants B.1.351 and B.1.1.7. Nature *593*, 130-135. 10.1038/s41586-021-03398-2.
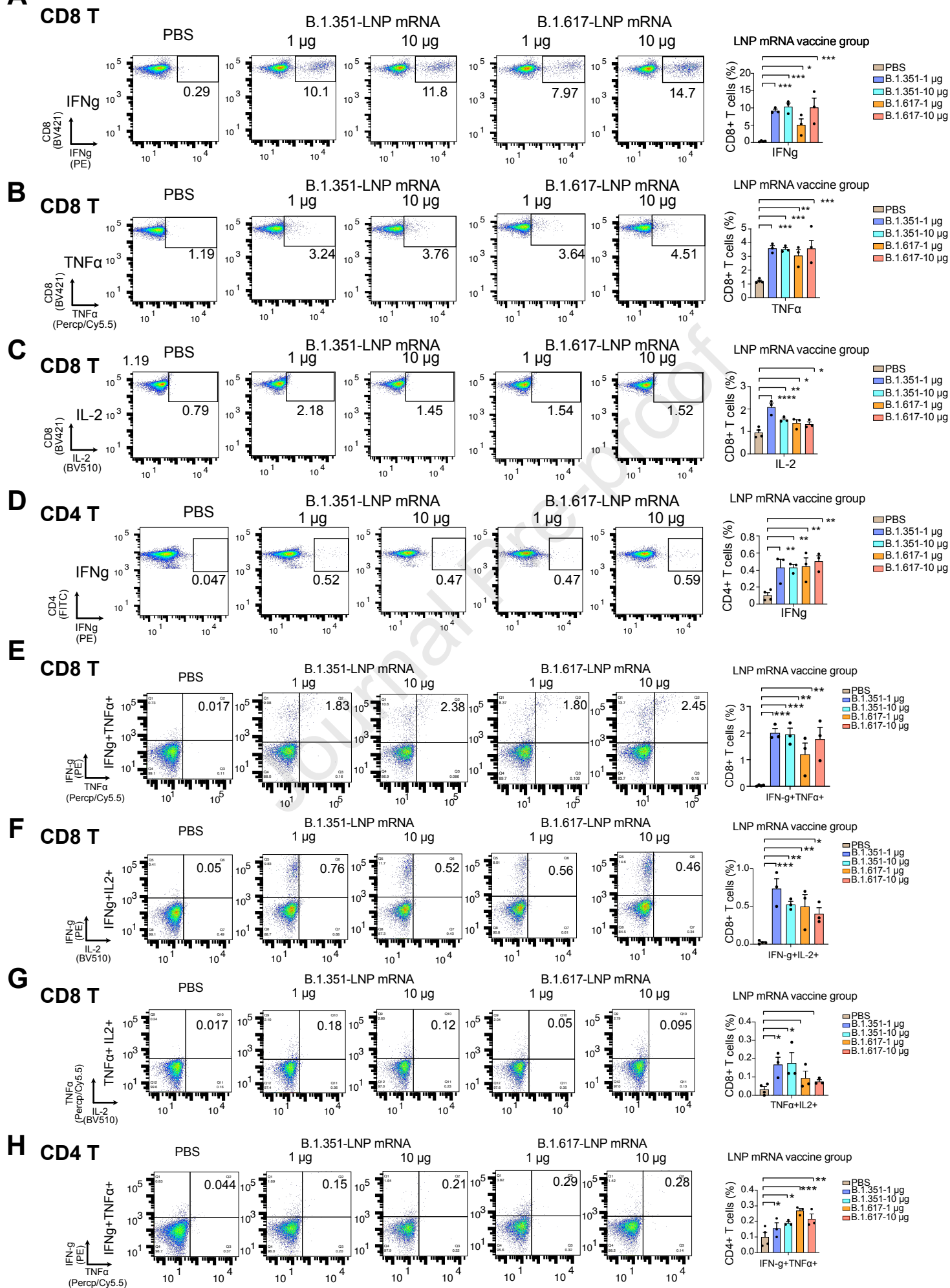
14. Tegally, H., Wilkinson, E., Giovanetti, M., Iranzadeh, A., Fonseca, V., Giandhari, J., Doolabh, D., Pillay, S., San, E.J., Msomi, N., et al. (2021). Detection of a SARS-CoV-2 variant of concern in South Africa. Nature *592*, 438-443. 10.1038/s41586-021-03402-9.

15. Rambaut, A., Holmes, E.C., O'Toole, A., Hill, V., McCrone, J.T., Ruis, C., du Plessis, L., and Pybus, O.G. (2021). Addendum: A dynamic nomenclature proposal for SARS-CoV-2 lineages to assist genomic epidemiology. Nat Microbiol *6*, 415. 10.1038/s41564-021-00872-5.

16. Rambaut, A., Holmes, E.C., O'Toole, A., Hill, V., McCrone, J.T., Ruis, C., du Plessis, L., and Pybus, O.G. (2020). A dynamic nomenclature proposal for SARS-CoV-2 lineages to assist genomic epidemiology. Nat Microbiol *5*, 1403-1407. 10.1038/s41564-020-0770-5.

17. Reardon, S. (2021). How the Delta variant achieves its ultrafast spread. Nature. 10.1038/d41586-021-01986-w.

18. Baisheng Li, A.D., Kuibiao Li, Yao Hu, Zhencui Li, Qianling Xiong, Zhe Liu, Qianfang Guo, Lirong Zou, Huan Zhang, Meng Zhang, Fangzhu Ouyang, Juan Su, Wenzhe Su, Jing Xu, Huifang Lin, Jing Sun, Jinju Peng, Huiming Jiang, Pingping Zhou, Ting Hu, Min Luo, Yingtao Zhang, Huanying Zheng, Jianpeng Xiao, Tao Liu, Rongfei Che, Hanri Zeng, Zhonghua Zheng, Yushi Huang, Jianxiang Yu, Lina Yi, Jie Wu, Jingdiao Chen, Haojie Zhong, Xiaoling Deng, Min Kang, Oliver G. Pybus, Matthew Hall, Katrina A. Lythgoe, Yan Li, Jun Yuan, Jianfeng He, Jing Lu (2021). Viral infection and transmission in a large, well-traced outbreak caused by the SARS-CoV-2 Delta variant. MedRxiv. https://doi.org/10.1101/2021.07.07.21260122.

19. Yadav, P.D., Sapkal, G.N., Abraham, P., Ella, R., Deshpande, G., Patil, D.Y., Nyayanit, D.A., Gupta, N., Sahay, R.R., Shete, A.M., et al. (2021). Neutralization of variant under investigation B.1.617 with sera of BBV152 vaccinees. Clin Infect Dis. 10.1093/cid/ciab411.

20. Wall, E.C., Wu, M., Harvey, R., Kelly, G., Warchal, S., Sawyer, C., Daniels, R., Hobson, P., Hatipoglu, E., Ngai, Y., et al. (2021). Neutralising antibody activity against SARS-CoV-2 VOCs B.1.617.2 and B.1.351 by BNT162b2 vaccination. Lancet *397*, 2331-2333. 10.1016/S0140-6736(21)01290-3.

21. Singh, J., Rahman, S.A., Ehtesham, N.Z., Hira, S., and Hasnain, S.E. (2021). SARS-CoV-2 variants of concern are emerging in India. Nat Med *27*, 1131-1133. 10.1038/s41591-021-01397-4.

22. Tada, T., Zhou, H., Dcosta, B.M., Samanovic, M.I., Mulligan, M., and Landau, N.R. (2021). The Spike Proteins of SARS-CoV-2 B.1.617 and B.1.618 Variants Identified in India Provide Partial Resistance to Vaccine-elicited and Therapeutic Monoclonal Antibodies. bioRxiv. https://doi.org/10.1101/2021.05.14.444076.

23. Planas, D., Veyer, D., Baidaliuk, A., Staropoli, I., Guivel-Benhassine, F., Rajah, M.M., Planchais, C., Porrot, F., Robillard, N., Puech, J., et al. (2021). Reduced sensitivity of SARS-CoV-2 variant Delta to antibody neutralization. Nature. 10.1038/s41586-021-03777-9.

24. Zhou, D., Dejnirattisai, W., Supasa, P., Liu, C., Mentzer, A.J., Ginn, H.M., Zhao, Y., Duyvesteyn, H.M.E., Tuekprakhon, A., Nutalai, R., et al. (2021). Evidence of escape of SARS-CoV-2 variant B.1.351 from natural and vaccine-induced sera. Cell. 10.1016/j.cell.2021.02.037.

25. Wang, P., Nair, M.S., Liu, L., Iketani, S., Luo, Y., Guo, Y., Wang, M., Yu, J., Zhang, B., Kwong, P.D., et al. (2021). Antibody resistance of SARS-CoV-2 variants B.1.351 and B.1.1.7. Nature. 10.1038/s41586-021-03398-2.
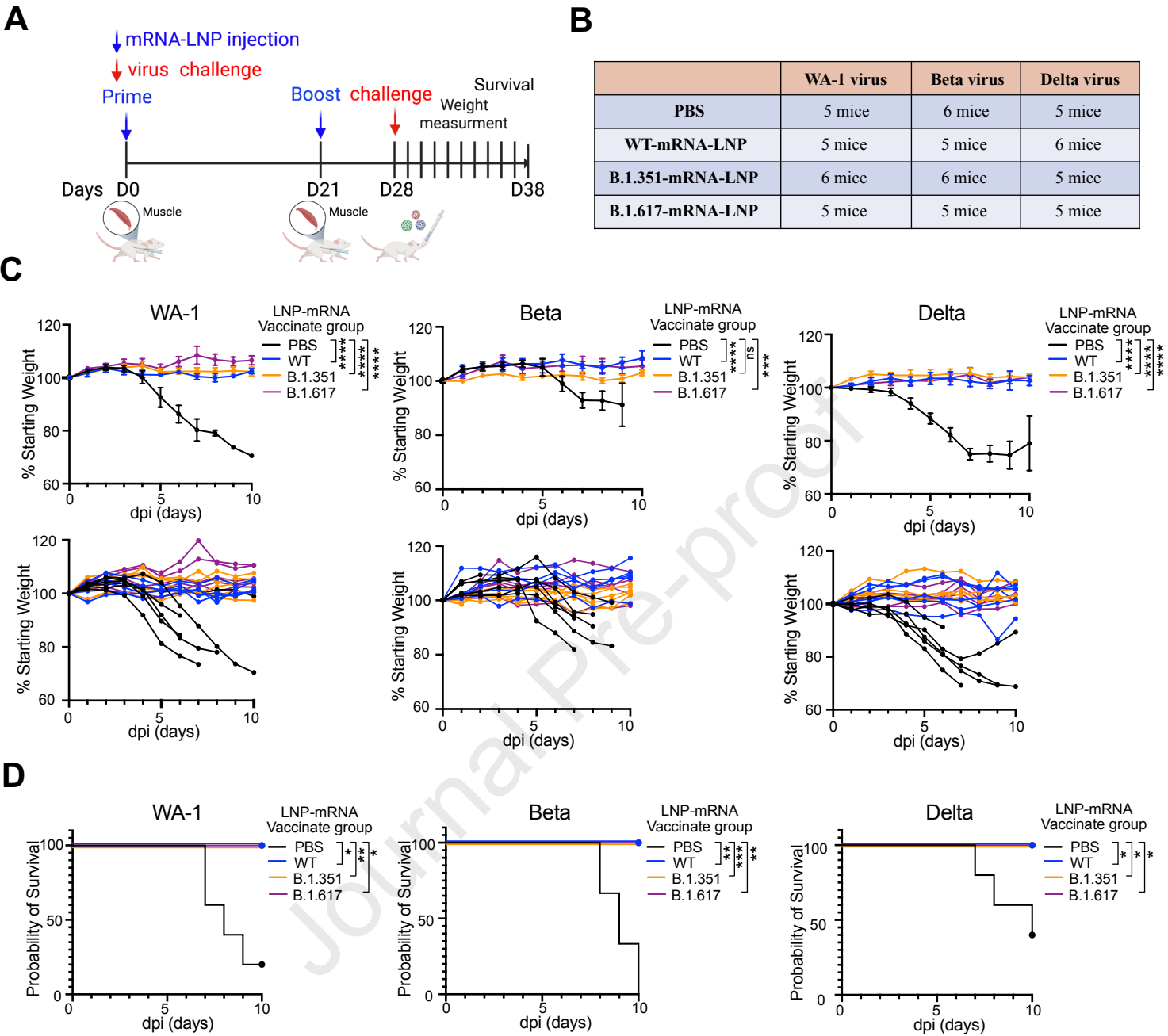
26. Lopez Bernal, J., Andrews, N., Gower, C., Gallagher, E., Simmons, R., Thelwall, S., Stowe, J., Tessier, E., Groves, N., Dabrera, G., et al. (2021). Effectiveness of Covid-19 Vaccines against the B.1.617.2 (Delta) Variant. N Engl J Med. 10.1056/NEJMoa2108891.

27. Abu-Raddad, L.J., Chemaitelly, H., Butt, A.A., and National Study Group for, C.-V. (2021). Effectiveness of the BNT162b2 Covid-19 Vaccine against the B.1.1.7 and B.1.351 Variants. N Engl J Med *385*, 187-189. 10.1056/NEJMc2104974.

28. Taylor, P.C., Adams, A.C., Hufford, M.M., de la Torre, I., Winthrop, K., and Gottlieb, R.L. (2021). Neutralizing monoclonal antibodies for treatment of COVID-19. Nat Rev Immunol *21*, 382-393. 10.1038/s41577-021-00542-x.

29. Brown, C.M., Vostok, J., Johnson, H., Burns, M., Gharpure, R., Sami, S., Sabo, R.T., Hall, N., Foreman, A., Schubert, P.L., et al. (2021). Outbreak of SARS-CoV-2 Infections, Including COVID-19 Vaccine Breakthrough Infections, Associated with Large Public Gatherings - Barnstable County, Massachusetts, July 2021. MMWR Morb Mortal Wkly Rep *70*, 1059-1062. 10.15585/mmwr.mm7031e2.

30. Wrapp, D., Wang, N., Corbett, K.S., Goldsmith, J.A., Hsieh, C.L., Abiona, O., Graham, B.S., and McLellan, J.S. (2020). Cryo-EM structure of the 2019-nCoV spike in the prefusion conformation. Science *367*, 1260-1263. 10.1126/science.abb2507.

31. Laczko, D., Hogan, M.J., Toulmin, S.A., Hicks, P., Lederer, K., Gaudette, B.T., Castano, D., Amanat, F., Muramatsu, H., Oguin, T.H., 3rd, et al. (2020). A Single Immunization with Nucleoside-Modified mRNA Vaccines Elicits Strong Cellular and Humoral Immune Responses against SARS-CoV-2 in Mice. Immunity *53*, 724-732 e727. 10.1016/j.immuni.2020.07.019.

32. Schmidt, F., Weisblum, Y., Muecksch, F., Hoffmann, H.H., Michailidis, E., Lorenzi, J.C.C., Mendoza, P., Rutkowska, M., Bednarski, E., Gaebler, C., et al. (2020). Measuring SARS-CoV-2 neutralizing antibody activity using pseudotyped and chimeric viruses. J Exp Med *217*. 10.1084/jem.20201181.

33. Chen, R.E., Winkler, E.S., Case, J.B., Aziati, I.D., Bricker, T.L., Joshi, A., Darling, T.L., Ying, B., Errico, J.M., Shrihari, S., et al. (2021). In vivo monoclonal antibody efficacy against SARS-CoV-2 variant strains. Nature *596*, 103-108. 10.1038/s41586-021-03720-y.

34. Edara, V.V., Pinsky, B.A., Suthar, M.S., Lai, L., Davis-Gardner, M.E., Floyd, K., Flowers, M.W., Wrammert, J., Hussaini, L., Ciric, C.R., et al. (2021). Infection and Vaccine-Induced Neutralizing-Antibody Responses to the SARS-CoV-2 B.1.617 Variants. N Engl J Med *385*, 664-666. 10.1056/NEJMc2107799.

35. Corbett, K.S., Edwards, D.K., Leist, S.R., Abiona, O.M., Boyoglu-Barnum, S., Gillespie, R.A., Himansu, S., Schafer, A., Ziwawo, C.T., DiPiazza, A.T., et al. (2020). SARS-CoV-2 mRNA vaccine design enabled by prototype pathogen preparedness. Nature *586*, 567-571. 10.1038/s41586-020-2622-0.

36. Teijaro, J.R., and Farber, D.L. (2021). COVID-19 vaccines: modes of immune activation and future challenges. Nat Rev Immunol *21*, 195-197. 10.1038/s41577-021-00526-x.

37. Jeyanathan, M., Afkhami, S., Smaill, F., Miller, M.S., Lichty, B.D., and Xing, Z. (2020). Immunological considerations for COVID-19 vaccine strategies. Nat Rev Immunol *20*, 615-632. 10.1038/s41577-020-00434-6.

38. Clem, A.S. (2011). Fundamentals of vaccine immunology. J Glob Infect Dis *3*, 73-78. 10.4103/0974-777X.77299.

39. Pegu, A., O'Connell, S., Schmidt, S.D., O'Dell, S., Talana, C.A., Lai, L., Albert, J., Anderson, E., Bennett, H., Corbett, K.S., et al. (2021). Durability of mRNA-1273 vaccine-induced antibodies against SARS-CoV-2 variants. Science. 10.1126/science.abj4176.

40. Lopez Bernal, J., Andrews, N., Gower, C., Gallagher, E., Simmons, R., Thelwall, S., Stowe, J., Tessier, E., Groves, N., Dabrera, G., et al. (2021). Effectiveness of Covid-19 Vaccines against the B.1.617.2 (Delta) Variant. N Engl J Med *385*, 585-594. 10.1056/NEJMoa2108891.

41. Iacobucci, G. (2021). Covid-19: Single vaccine dose is 33% effective against variant from India, data show. Bmj-Brit Med J *373*. ARTN n1346
10.1136/bmj.n1346.

42. Charmet, T., Schaeffer, L., Grant, R., Galmiche, S., Cheny, O., Von Platen, C., Maurizot, A., Rogoff, A., Omar, F., David, C., et al. (2021). Impact of original, B.1.1.7, and B.1.351/P.1 SARS-CoV-2 lineages on vaccine effectiveness of two doses of COVID-19 mRNA vaccines: Results from a nationwide case-control study in France. Lancet Reg Health Eur *8*, 100171. 10.1016/j.lanepe.2021.100171.

43. Planas, D., Veyer, D., Baidaliuk, A., Staropoli, I., Guivel-Benhassine, F., Rajah, M.M., Planchais, C., Porrot, F., Robillard, N., Puech, J., et al. (2021). Reduced sensitivity of SARS-CoV-2 variant Delta to antibody neutralization. Nature *596*, 276-280. 10.1038/s41586-021-03777-9.

44. Graham, B.S. (2020). Rapid COVID-19 vaccine development. Science *368*, 945-946. 10.1126/science.abb8923.

45. Stephenson, E., Reynolds, G., Botting, R.A., Calero-Nieto, F.J., Morgan, M.D., Tuong, Z.K., Bach, K., Sungnak, W., Worlock, K.B., Yoshida, M., et al. (2021). Single-cell multi-omics analysis of the immune response in COVID-19. Nat Med *27*, 904-916. 10.1038/s41591-021-01329-2.

46. Zhang, J.Y., Wang, X.M., Xing, X., Xu, Z., Zhang, C., Song, J.W., Fan, X., Xia, P., Fu, J.L., Wang, S.Y., et al. (2020). Single-cell landscape of immunological responses in patients with COVID-19. Nat Immunol *21*, 1107-1118. 10.1038/s41590-020-0762-x.

47. Schultheiss, C., Paschold, L., Simnica, D., Mohme, M., Willscher, E., von Wenserski, L., Scholz, R., Wieters, I., Dahlke, C., Tolosa, E., et al. (2020). Next-Generation Sequencing of T and B Cell Receptor Repertoires from COVID-19 Patients Showed Signatures Associated with Severity of Disease. Immunity *53*, 442-455 e444. 10.1016/j.immuni.2020.06.024.

48. Schmidt, F., Weisblum, Y., Muecksch, F., Hoffmann, H.H., Michailidis, E., Lorenzi, J.C.C., Mendoza, P., Rutkowska, M., Bednarski, E., Gaebler, C., et al. (2020). Measuring SARS-CoV-2 neutralizing antibody activity using pseudotyped and chimeric viruses. bioRxiv. 10.1101/2020.06.08.140871.

49. Polack, F.P., Thomas, S.J., Kitchin, N., Absalon, J., Gurtman, A., Lockhart, S., Perez, J.L., Perez Marc, G., Moreira, E.D., Zerbini, C., et al. (2020). Safety and Efficacy of the BNT162b2 mRNA Covid-19 Vaccine. N Engl J Med *383*, 2603-2615. 10.1056/NEJMoa2034577.

50. Satija, R., Farrell, J.A., Gennert, D., Schier, A.F., and Regev, A. (2015). Spatial reconstruction of single-cell gene expression data. Nat Biotechnol *33*, 495-502. 10.1038/nbt.3192.

51. Stuart, T., Butler, A., Hoffman, P., Hafemeister, C., Papalexi, E., Mauck, W.M., Hao, Y., Stoeckius, M., Smibert, P., and Satija, R. (2019). Comprehensive Integration of Single-Cell Data. Cell *177*, 1888-1902.e1821. 10.1016/j.cell.2019.05.031.

52. Becht, E., McInnes, L., Healy, J., Dutertre, C.A., Kwok, I.W.H., Ng, L.G., Ginhoux, F., and Newell, E.W. (2018). Dimensionality reduction for visualizing single-cell data using UMAP. Nat Biotechnol. 10.1038/nbt.4314.

53. Lun, A.T., Chen, Y., and Smyth, G.K. (2016). It's DE-licious: A Recipe for Differential Expression Analyses of RNA-seq Experiments Using Quasi-Likelihood Methods in edgeR. Methods Mol Biol *1418*, 391-416. 10.1007/978-1-4939-3578-9_19.

1 54. Soneson, C., and Robinson, M.D. (2018). Bias, robustness and scalability in single-cell differential expression
2   analysis. Nat Methods *15*, 255-261. 10.1038/nmeth.4612.

3 55. Ahlmann-Eltze, C., and Huber, W. (2021). glmGamPoi: fitting Gamma-Poisson generalized linear models on
4   single cell count data. Bioinformatics *36*, 5701-5702. 10.1093/bioinformatics/btaa1009.

5 56. Kolberg, L., Kerimov, N., Peterson, H., and Alasoo, K. (2020). Co-expression analysis reveals interpretable
6   gene modules controlled by. Elife *9*. 10.7554/eLife.58705.

7 57. Raudvere, U., Kolberg, L., Kuzmin, I., Arak, T., Adler, P., Peterson, H., and Vilo, J. (2019). g:Profiler: a web
8   server for functional enrichment analysis and conversions of gene lists (2019 update). Nucleic Acids Res *47*,
9   W191-W198. 10.1093/nar/gkz369.

10 58. Bolger, A.M., Lohse, M., and Usadel, B. (2014). Trimmomatic: a flexible trimmer for Illumina sequence data.
11   Bioinformatics *30*, 2114-2120. 10.1093/bioinformatics/btu170.

12 59. Bolotin, D.A., Poslavsky, S., Mitrophanov, I., Shugay, M., Mamedov, I.Z., Putintseva, E.V., and Chudakov,
13   D.M. (2015). MiXCR: software for comprehensive adaptive immunity profiling. Nat Methods *12*, 380-381.
14   10.1038/nmeth.3364.
15

Figure 1

Figure 2

Figure 3

Fig

A

B

	WA-1 virus	Beta virus	Delta virus
PBS	5 mice	6 mice	5 mice
WT-mRNA-LNP	5 mice	5 mice	6 mice
B.1.351-mRNA-LNP	6 mice	6 mice	5 mice
B.1.617-mRNA-LNP	5 mice	5 mice	5 mice

C

D

Fig

A

Vaccine

- PBS
- WA-1
- B.1.351
- B.1.617

Concentration

- 0ug
- 10ug
- 1ug

Cluster

B

C

D

E

F

B cell sub-clusters

T cell sub-clusters

G

B cell populations

T cell populations
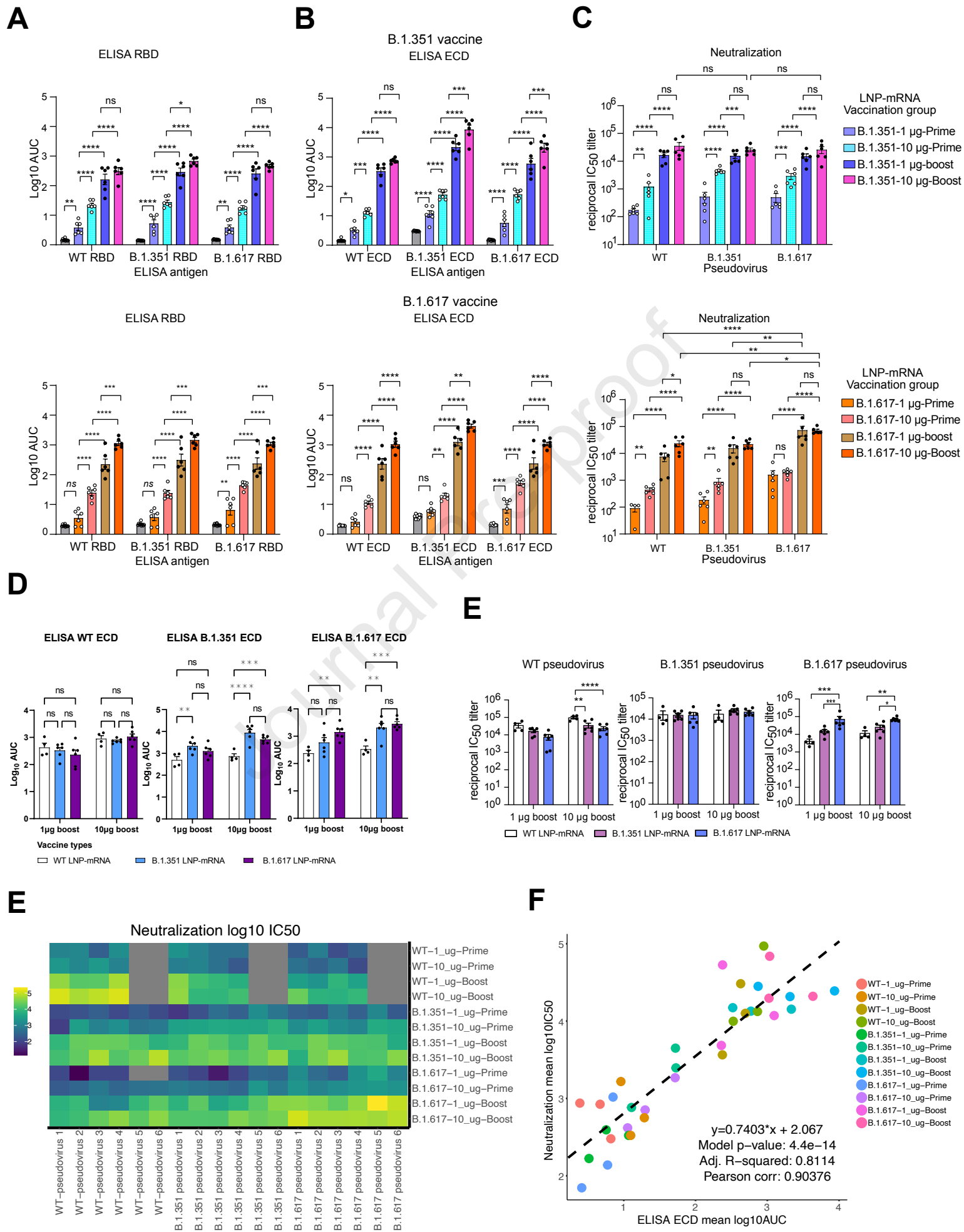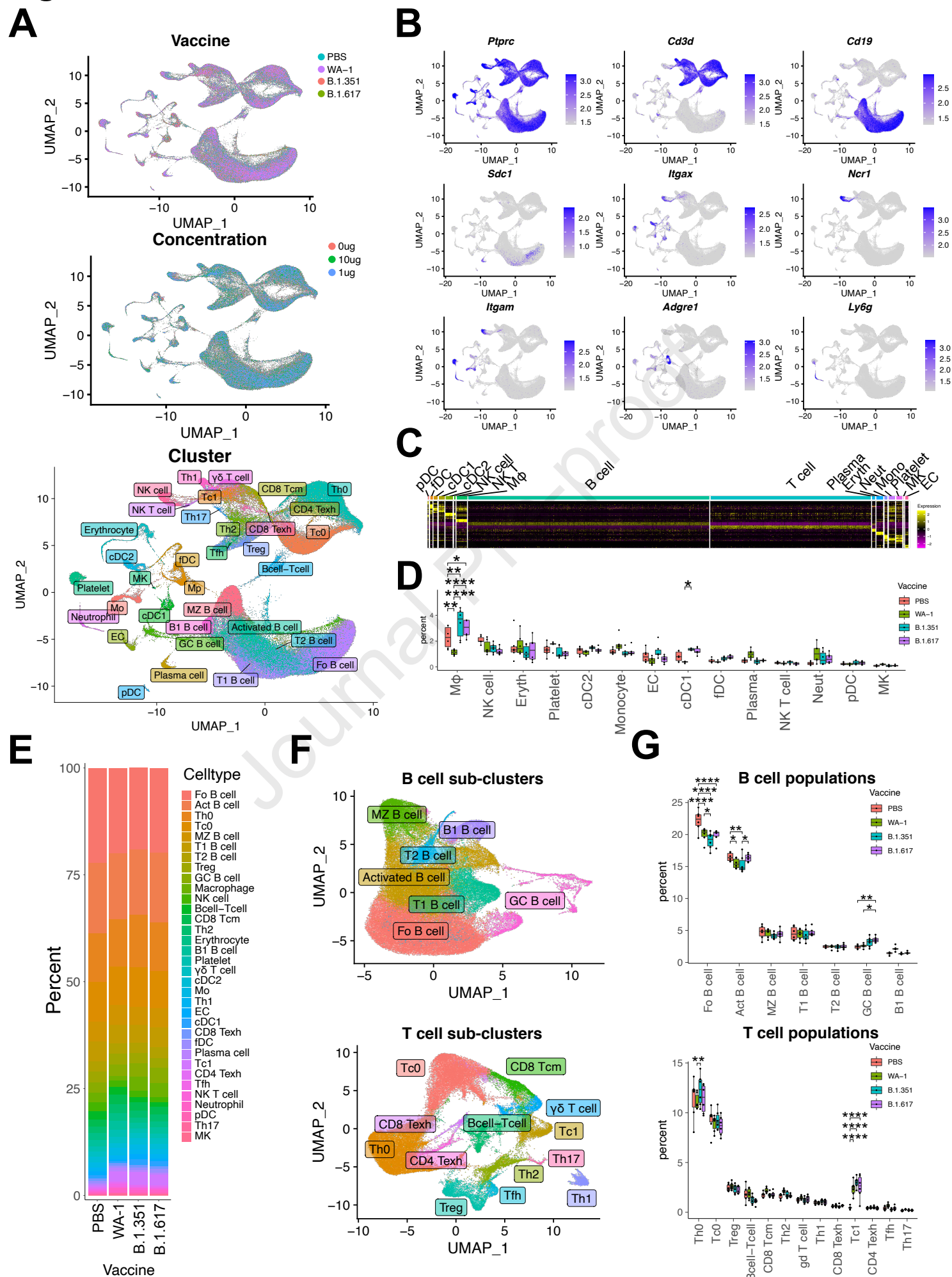
Figure 6

A

Activated B cells

Diff. Expression
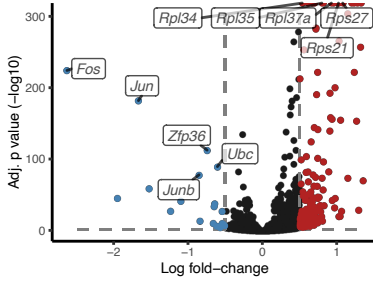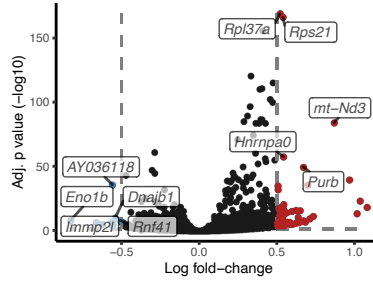
WA-1 vs PBS | B.1.351 vs PBS | B.1.617 vs PBS
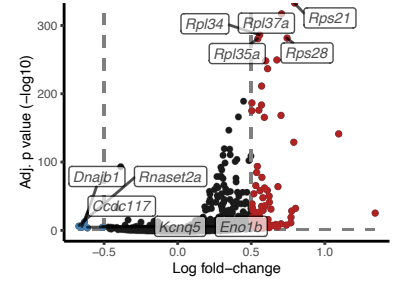
B

Upreg. pathways
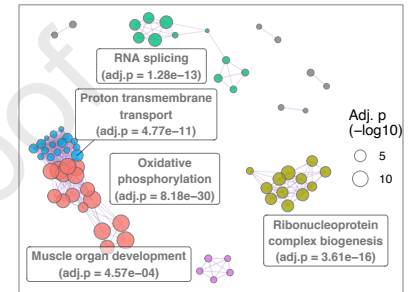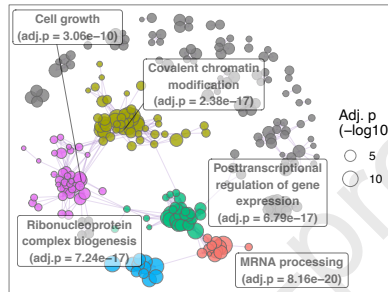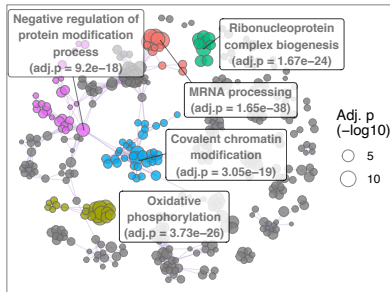
C

D
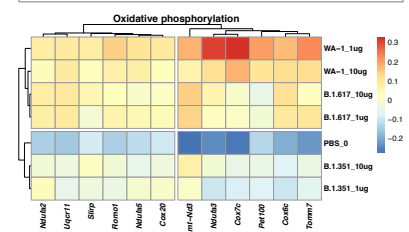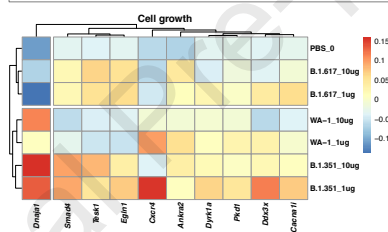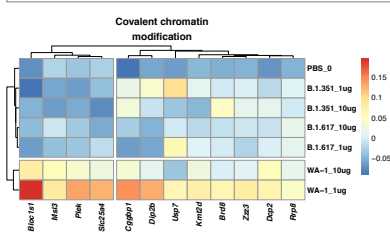
Activated CD8 T cells

Diff. Expression
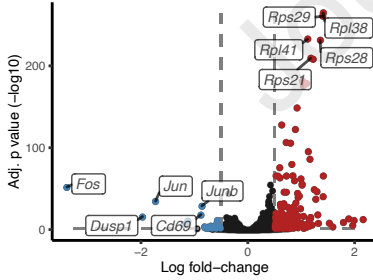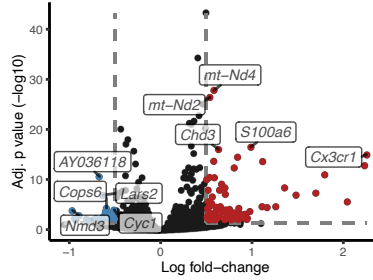
WA-1 vs PBS | B.1.351 vs PBS | B.1.617 vs PBS
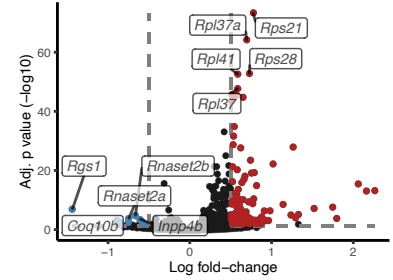
E

Upreg. pathways
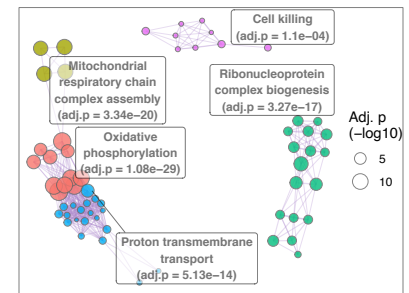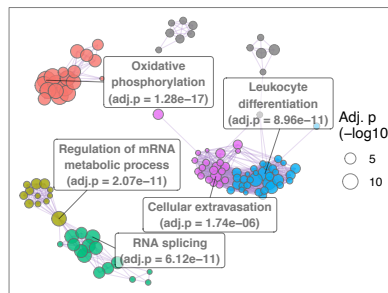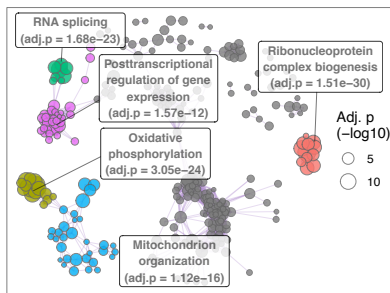
F
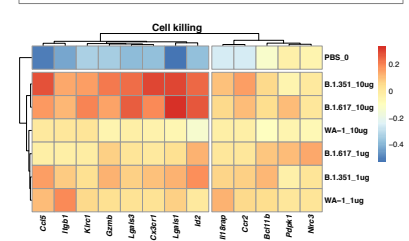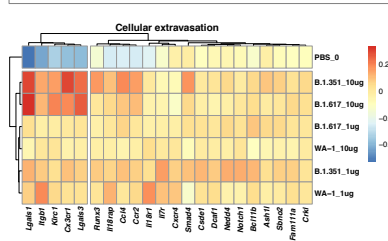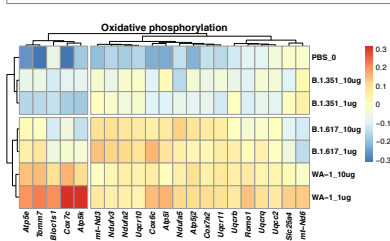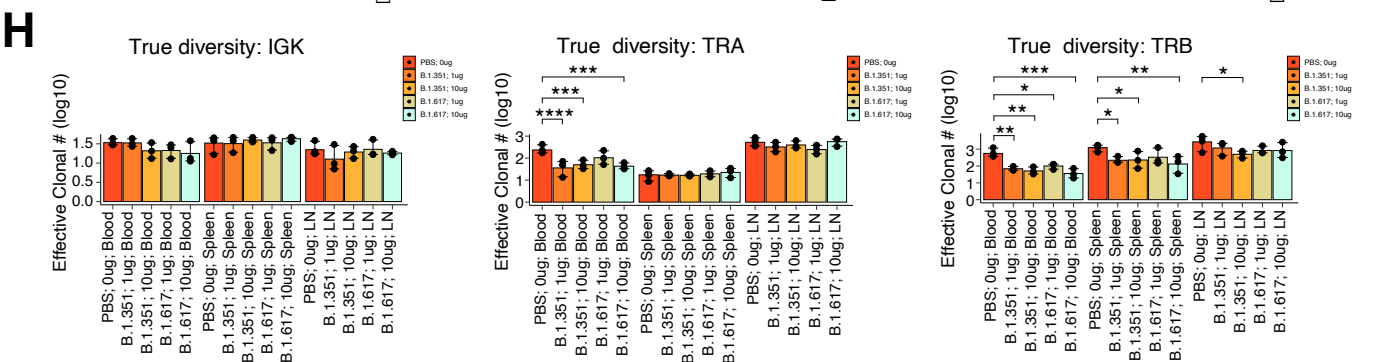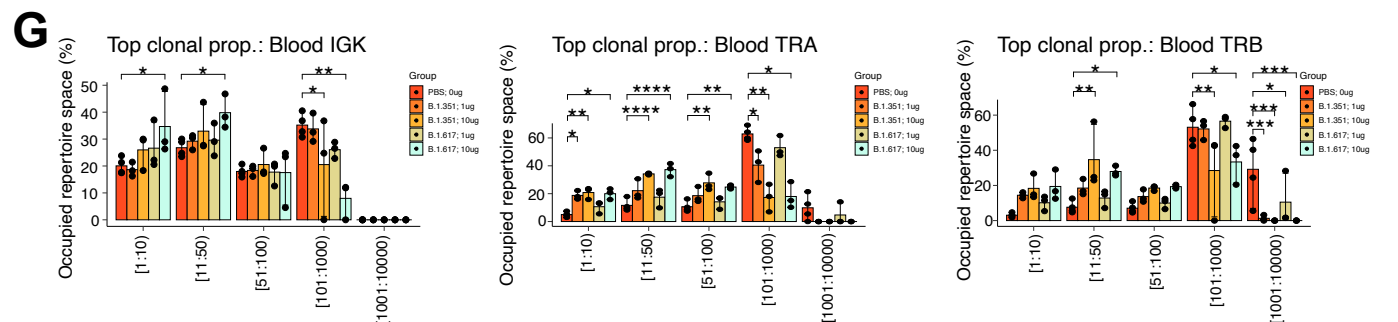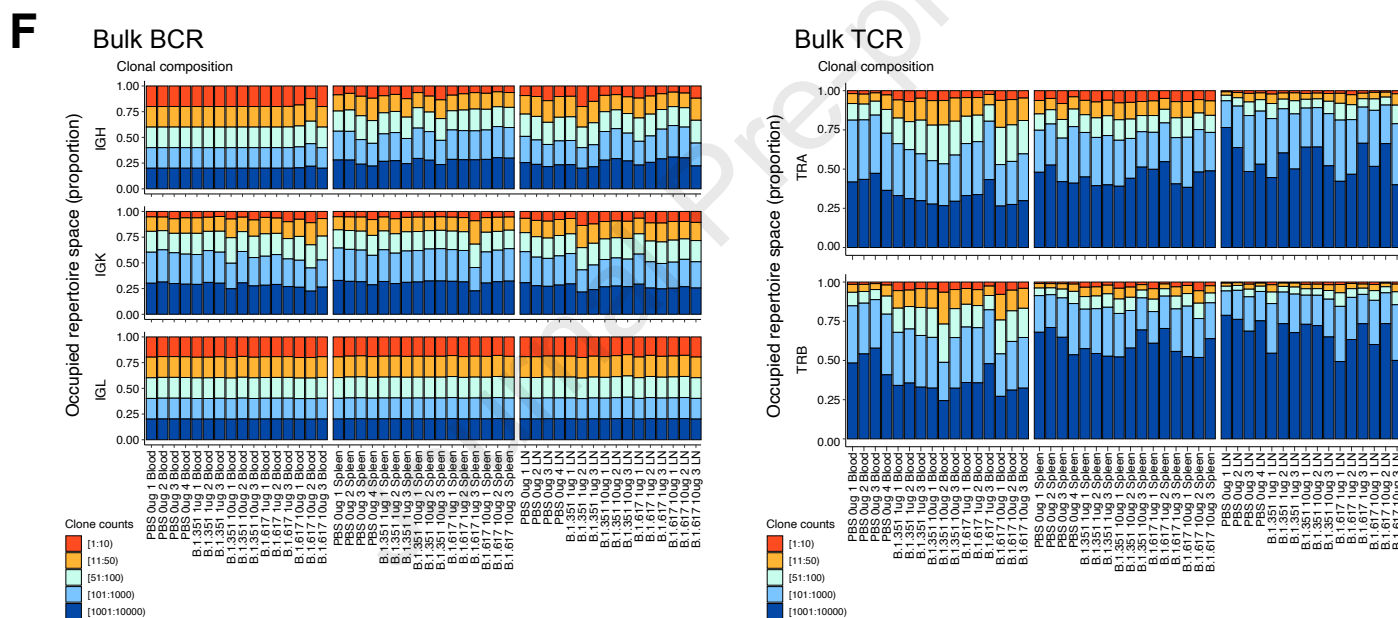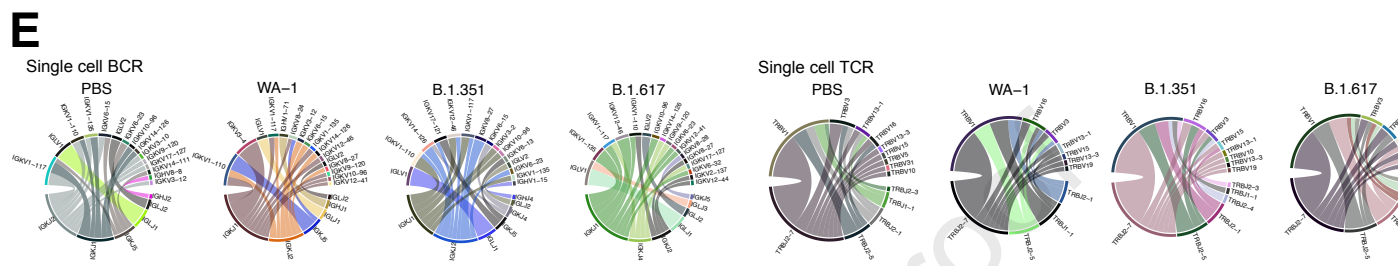
Highlights

- WT LNP-mRNA shows reduced neutralization to the B.1.351 and B.1.617 variants

- B.1.617 LNP-mRNA elicits B.1.617-neutralizing activity stronger than WT LNP-mRNA

- WT, B.1.351 and B.1.617 LNP-mRNA protect against WA-1, Beta and Delta VoC challenges

- Single cell and BCR/TCR-seq reveal systems immune profiles of vaccinated animals

eTOC

Peng et. al. characterize the B cell and T cell responses elicited by WT, B.1.351 and B.1.617 mRNA vaccine candidates. All three LNP-mRNA protect against WA-1, Beta and Delta variants-of-concern challenges. Single cell, BCR and TCR sequencing reveals systems immune profiles of variant-specific LNP-mRNA vaccinated animals.

KEY RESOURCES TABLE

REAGENT or RESOURCE	SOURCE	IDENTIFIER
Antibody		
Anti-mouse secondary antibody	Fisher Scientific	Cat#31439
PE–anti-human FC antibody	Biolegend	Cat#M1310G05
Anti-mouse CD28 antibody Clone 37.51	Biolegend	Cat#102116
CD3 PE/Cy7 Clone 17A2	Biolegend	Cat#100320
CD8a BV421 Clone QA17A07	Biolegend	Cat#155010
CD4 FITC Clone GK1.5	Biolegend	Cat#100406
IFN-γ PE Clone W18272D	Biolegend	Cat#163503
TNF Percp-Cy5.5 Clone MP6-XT22	Biolegend	Cat#506322
IL2 BV510 Clone JES6-5H4	Biolegend	Cat#503833
IL4 BV605 Clone 11B11	Biolegend	Cat#504126
IL5 APC Clone TRFK5	Biolegend	Cat#504306
Bacterial and Virus Strains		
SARS-CoV-2 WT pseudovirus	This study	This study
B.1.351 variant pseudovirus	This study	This study
B.1.617 variant pseudovirus	This study	This study
Biological Samples		
Chemicals, Peptides, and Recombinant Proteins		
DPBS	Kline	Cat#14190144
RPMI 1640 Medium	Gibco	Cat#11875-093
Fetal Bovine Serum	Sigma Aldrich	Cat#F4135-500ML
DMEM	Kline	Cat#11995065
Penicillin-Streptomycin (10,000 U/mL)	Gibco	Cat#15140122
Glutamax	Med School	Cat#35050061
2-mercaptoethonal	Sigma	M6250
Brefeldin A	Biolegend	Cat#420601
TWEEN-20	Sigma-Aldrich	Cat# P1379
50TS microplate washer	Fisher Scientific	Cat#BT50TS16
Neon™ Transfection System 10 µL Kit	ThermoFisher	Cat# MPK1025
BD Cytofix/Cytoperm fixation/permeabilization solution kit	Fisher Scientific	Cat#BDB554714
ACK Lysing Buffer	Lonza	Cat#BP10-548E
ACE2–Fc chimera	Genescript	Cat#Z03484
Gibson Assembly Master Mix - 50 rxn	NEB	Cat#E2611L
HiscribeTM T7 ARCA mRNA Kit (with tailing)	NEB	Cat#E2060S
Phusion Flash High-Fidelity PCR Master Mix	ThermoFisher	Cat#F548L
E-Gel™ Low Range Quantitative DNA Ladder	ThermoFisher	Cat#12373031
QIAquick Gel Extraction Kit	Qiagen	Cat#28706
QIAamp Fast DNA Tissue Kit	Qiagen	Cat#51404
EndoFree® Plasmid Maxi Kit	Qiagen	Cat#12362
Quant-iT™ RiboGreen™ RNA Assay Kit	ThermoFisher	Cat#R11490
Tetramethylbenzidine substrate	Biolegend	Cat#421101

SMARTer Mouse BCR IgG H/K/L Profiling Kit	Takara	Cat#634424
SMARTer Mouse TCR a/b profiling kit	Takara	Cat#634404
RNeasy® Plus Mini Kit	Qiagen	Cat#74134
Glow-discharged formvar/carbon-coated copper grid	Electron Microscopy Sciences	FCF400-Cu-50
2% (w/v) uranyl formate	Electron Microscopy Sciences	Cat#22450
Library Construction Kit, 16 rxns	10X Genomics	Cat#1000190
Live/Dead aqua fixable stain	Thermofisher	Cat#L34976
GenVoy-ILM T Cell Kit for mRNA with Spark Cartridges	Precision Nanosystems	Cat#1000683
GenVoy-ILM	Precision Nanosystems	Cat#NWW0042
BSA	Fisher Scientific	BP1600-100
100 µm cell strainer	Corning	Cat#352360
40 µm cell strainer	Corning	Cat#352340
BbSI	Kline	Cat#R3539L
Bovine Serum Albumin	Sigma Aldrich	Cat#A9418-100G
EDTA	Kline	Cat#AB00502-01000
Macron™ 2796-05 Phosphoric Acid, 85%	Avantor	Cat#MK-2796-05
Polyethylenimine HCl MAX, Linear, Mw 40,000 (PEI MAX 40000)	POLYSCIENCES INC	Cat#24765-1
Tris-Cl pH 7.5	Boston Bioproducts	Cat#IBB-594
N1-Methylpseudouridine-5'-Triphosphate - (N-1081)	TriLink (NC)	Cat#N-1081-1
Sucrose	Thomas	Cat#C987K85 (EA/1)
Tetramethylbenzidine	Biolegend	Cat#421101
PepTivator SARS-CoV-2 Prot_S Complete, research grade	Miltenyi Biotec	Cat#130-127-951
SARS-CoV-2 (2019-nCoV) Spike S1+S2 ECD-His Recombinant Protein	SINO	Cat#40589-V08B1
SARS-CoV-2 (2019-nCoV) Spike RBD	Quote UQ7100	Cat#40592-V08B
SARS-CoV-2 Spike RBD (L452R,T478K)	SINO	Cat#40592-V08H90
SARS-CoV-2 Spike S1+S2 (E154K, L452R, E484Q, D614G, P681R, E1072K, K1073R) Protein (ECD, His Tag)	SINO	Cat#40589-V08B12
SARS-CoV-2 (2019-nCoV) Spike RBD (L452R, E484Q) Protein (His Tag)	SINO	Cat#40592-V08H88
SARS-CoV-2 (2019-nCoV) Spike S1+S2 (L18F, D80A, D215G, LAL242-244 deletion, R246I, K417N, E484K, N501Y, D614G, A701V) Protein (ECD, His Tag)	SINO	Cat#40589-V08B07
SARS-CoV-2 (2019-nCoV) Spike RBD(N501Y)-His Recombinant Protein	SINO	Cat#40592-V08H82
SARS-CoV-2 (2019-nCoV) Spike RBD(K417N, E484K, N501Y)-His Recombinant Protein	SINO	Cat#40592-V08H85
Chromium Next GEM Single Cell 5' Kit v2, 16 rxns PN-1000263	10X Genomics	Cat#PN-1000263
Chromium Next GEM Chip K Single Cell Kit, 16 rxns PN-1000287	10X Genomics	Cat#PN-1000287
Dual Index Kit TT Set A, 96 rxns PN-1000215	10X Genomics	Cat#PN-1000215
Mouse BCR Amplification Kit, 16 rxns PN-1000255	10X Genomics	Cat#PN-1000255
SPRIselect - 60 mL	Beckman Coulter	Cat#B23318
Chromium Single Cell Mouse TCR Amplification Kit, 16 rxns	10X Genomics	Cat#PN-1000254

Critical commercial assays		
Deposited data		
Single cell RNA-seq data of Vaccinated animals	GEO/SRA	GEO/SRA
Single cell VDJ-seq data of Vaccinated animals	GEO/SRA	GEO/SRA
Bulk VDJ-seq data of Vaccinated animals	GEO/SRA	GEO/SRA
Flow cytometry data of Vaccinated animals	Mendeley Data	DOI: 10.17632/2m6hvhhmr4.2
Experimental models: Cell lines		
HEK293FT	ThermoFisher	Catalog Number: R70007
HKE293T-hACE2	Schmidt et al., 2020	Gift from Dr Bieniasz' lab
Vero-E6	ATCC	Catalog Number: CRL-1586™
Experimental Models: Organisms/Strains		
C57BL/6Ncr	Charles River	strain #556
B6.Cg-Tg(K18-ACE2)2Prlmn/J	Jackson Laboratory	strain #034860
Oligonucleotides		
gBlocks	IDT	Custom, sequence specific, various
primers	IDT	Custom, sequence specific, various
Recombinant DNA		
pcDNA3.1	Addgene	Cat# V790-20
pHIVNLGagPol	Schmidt et al., 2020	Gift from Dr Bieniasz' lab
pCCNanoLuc2AEGFP	Schmidt et al., 2020	Gift from Dr Bieniasz' lab
pSARS-CoV-2 SΔ19	Schmidt et al., 2022	Gift from Dr Bieniasz' lab
pVP22b (B.1351 variant (6P))	This study	This study
pVP29b (B.1.617 variant (6P))	This study	This study
pVP31b (WT spike (6P)	This study	This study
pCCNanoLuc2AEGFP plasmid	Schmidt et al.	Gift from Dr Bieniasz' lab
Polyethylenimine	POLYSCIENCES INC	Cat#24765-1
(HIV-1/NanoLuc2AEGFP)-SARS-CoV-2 plasmid	This study	This study
(HIV-1/NanoLuc2AEGFP)-B.1.351 variant plasmid	This study	This study
(HIV-1/NanoLuc2AEGFP)-B.1.617 variant plasmid	This study	This study
Software and Algorithms		
FlowJo software 9.9.6	FlowJo, LLC	https://www.flowjo.com
GraphPad Prism 8.0	GraphPad Software Inc	https://www.graphpad.com/scientific-software/prism/
Pymol	Schrödinger	http://www.pymol.org/
Cell Ranger v3.1.0	10X Genomics	https://support.10xgenomics.com/single-cell-gene-expression/software/pipelines/latest/installation

Loupe V(D)J Browser	10X Genomics	https://support.10xgenomics.com/single-cell-vdj/software/visualization/latest/installation
Trimmomatic	Bolger et al., Bioinformatics, 2014	https://github.com/timflutre/trimmomatic
mixcr	Bolotin et al., Nat Methods, 2015	https://github.com/milaboratory/mixcr
R	R project	https://www.r-project.org
Seurat R package	Satija et al., Nat Biotechnol 2015	https://satijalab.org/seurat/index.html
plyr R package	Wickham. (2011). Journal of Statistical Software	http://www.jstatsoft.org/v40/i01/
dplyr R package	Wickham et al., (2021). dplyr: A Grammar of Data Manipulation. R package version 1.0.7	https://CRAN.R-project.org/package=dplyr
patchwork R package	Pedersen (2020). patchwork: The Composer of Plots. R package version 1.1.1	https://CRAN.R-project.org/package=patchwork
ggplot2 R package	Wickham. (2016). ggplot2: Elegant Graphics for Data Analysis. Springer-Verlag New York	https://ggplot2.tidyverse.org
ggrepel R package	Slowikowski (2021). ggrepel: Automatically Position Non-Overlapping Text Labels with 'ggplot2'. R package version 0.9.1	https://CRAN.R-project.org/package=ggrepel
limma R package	Ritchie et al., (2015). limma powers differential expression analyses for RNA-sequencing and microarray studies. Nucleic Acids Research 43(7), e47	https://git.bioconductor.org/packages/limma
edgeR R package	Robinson et al., Bioinformatics 2010; McCarthy et al., Nucleic Acid Research 2012	https://git.bioconductor.org/packages/edgeR
stringr R package	Hadley Wickham (2019). stringr: Simple, Consistent Wrappers for Common String Operations. R package version 1.4.0	https://CRAN.R-project.org/package=stringr
ggridges R package	Claus O. Wilke (2021). ggridges: Ridgeline Plots in 'ggplot2'. R package version 0.5.3	https://CRAN.R-project.org/package=ggridges
igraph R package	Csardi, G., & Nepusz, T. (2006). The Igraph Software Package for Complex Network Research. InterJournal	https://igraph.org

	2006, Complex Systems, 1695.	
network R package	Butts C. (2008). network: a Package for Managing Relational Data in R. Journal of Statistical Software, 24 (2)	https://CRAN.R-project.org/package=network
sna R package	Carter T. Butts (2020). sna: Tools for Social Network Analysis. R package version 2.6	https://CRAN.R-project.org/package=sna
Immunarch R package	ImmunoMind Team, Zenodo, 2019	https://github.com/immunomind/immunarch
Circlize R package	Gu et al., Bioinformatics, 2014	https://cran.r-project.org/package=circlize
Pheatmap R package	Kolde, 2019	https://cran.r-project.org/package=pheatmap
Future R package	Bengtsson, 2021	https://cran.r-project.org/package=future
SeuratWrappers R package	Satija et al., 2020	https://github.com/satijalab/seurat-wrappers
glmGamPoi R package	Ahlmann-Eltze and Huber, Bioinformatics, 2021	https://github.com/const-ae/glmGamPoi
Other		
SARS-CoV-2 WT-LNP-mRNA vaccine candidate	This study	This study
B.1.351-LNP-mRNA vaccine candidate	This study	This study
B.1.617-LNP-mRNA vaccine candidate	This study	This study

1 **Supplemental Information for**
2
3 **Variant-specific vaccination induces systems immune responses and potent in vivo protection against SARS-CoV-2**

Supplemental Figure 1
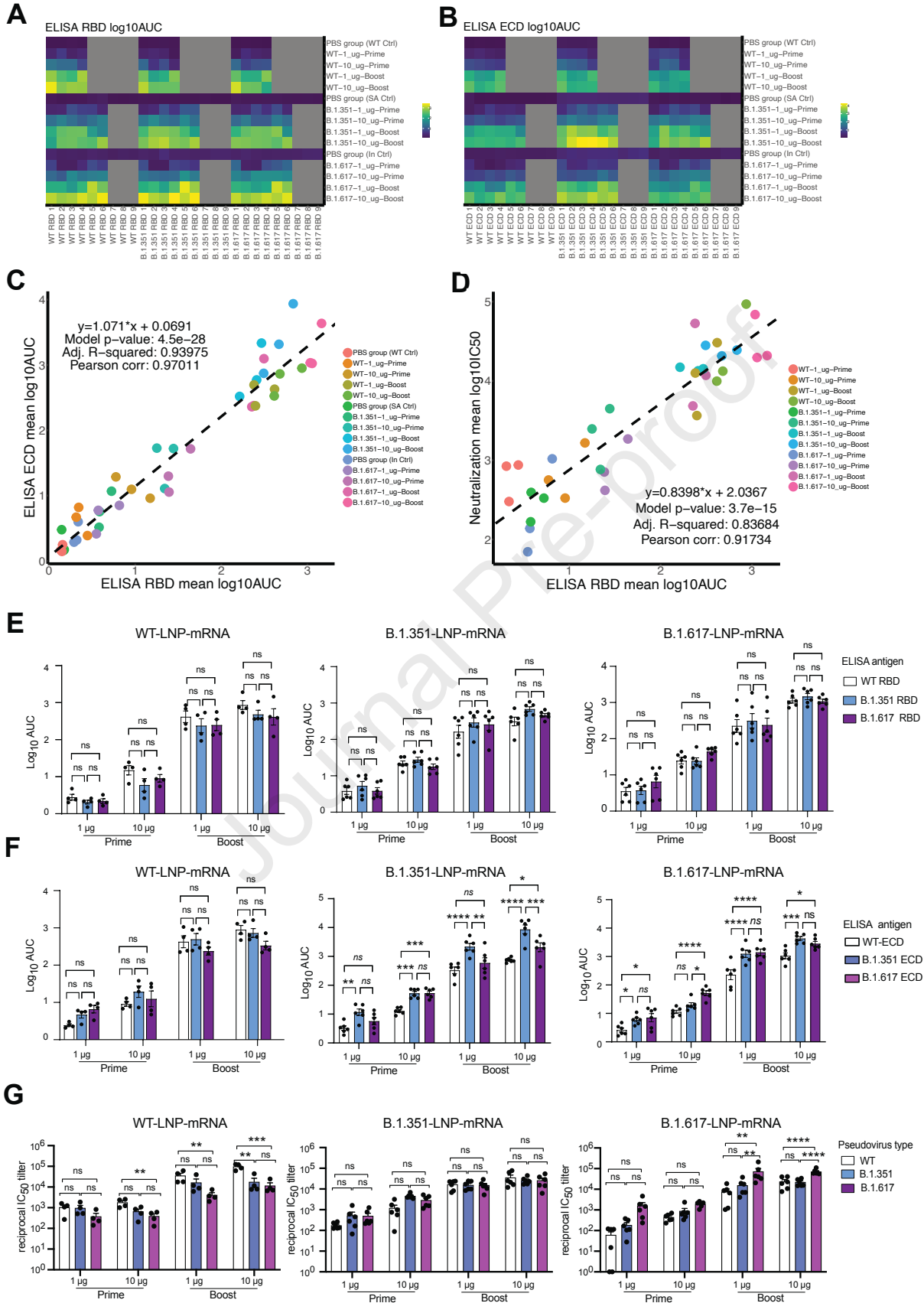
1 **Figure S 1 | Workflow of production and physical characterization of the spike mRNA and lipid nanoparticles used for the**
2 **LNP-mRNA vaccine candidates; and additional data on antibody responses of all three groups of LNP-mRNA vaccinated**
3 **animals**
4 **A**, Heatmap of ELISA titers of animals vaccinated by all three LNP-mRNAs, against the RBDs from three different spikes of
5 SARS-CoV-2.
6 **B**, Heatmap of ELISA titers of animals vaccinated by all three LNP-mRNAs, against the ECDs from three different spikes of
7 SARS-CoV-2.
8 **C**, Correlation X-Y scatterplots of ELISA and neutralization titers between ELISA RBD log10AUC vs ELISA ECD log10AUC
9 for all vaccine groups
0 **D**, Correlation X-Y scatterplots of ELISA and neutralization titers between ELISA RBD log10AUC vs neutralization log10IC50
1 for all vaccine groups.
2 **E-G,** ELISA and neutralization titers of animals vaccinated by WT-LNP-mRNA, B.1.351-LNP-mRNA and B.1.617-LNP-mRNA
3 (same data as in Figures 1-2, plot for visualizing comparisons between antigens.
4 **E,** Serum ELISA titers of vaccinated animals against RBD from three different spikes (WT, B.1.351, and B.1.617) of SARS-CoV-
5 2 (n = 6).
6 **F,** Serum ELISA titers of vaccinated animals against ECD from three different spikes (WT, B.1.351, and B.1.617) of SARS-CoV-
7 2 (n = 6).
8 **G,** Serum neutralization titers of vaccinated animals against three pseudoviruses (WT, B.1.351, and B.1.617) of SARS-CoV-2 (n =
9 6).
0 **Related to: Figure(s) 1, 2**

Supplemental Figure 2
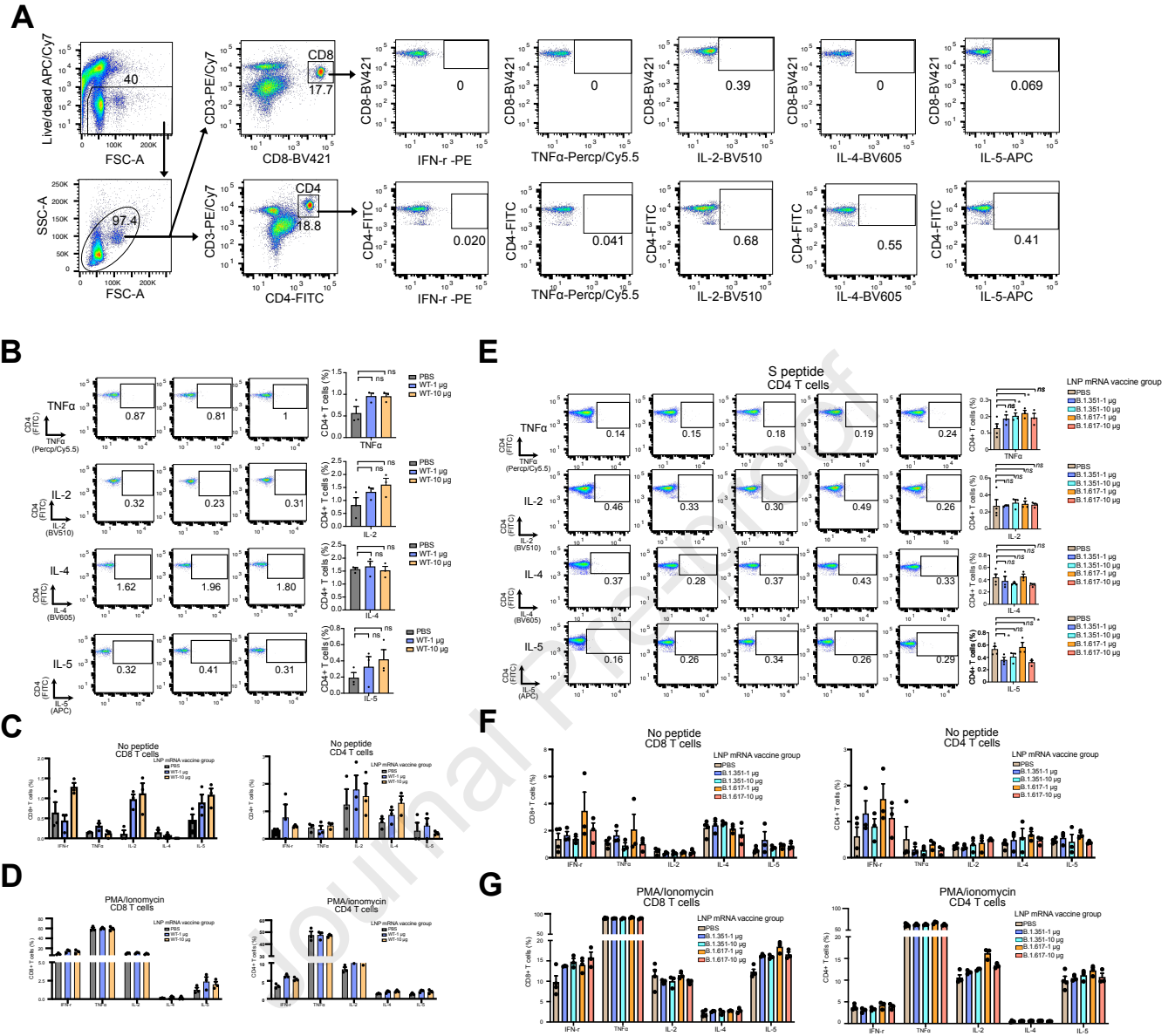
Figure S 2 | Additional flow cytometry analysis of WT-LNP-mRNA, B.1.351-LNP-mRNA and B.1.617-LNP-mRNA induced S protein-specific T cell response

A, Flow cytometry panel and gating strategy to quantify SARS-CoV-2 S-specific T cells in B.1.351-mRNA-LNP and B.1.617-mRNA-LNP vaccinated group and PBS group.

B, Percentage of CD4 T cells expressing TNFα, IL-2, IL4, and IL5 in response to S peptide pools of WT-mRNA-LNP vaccines treated mice and PBS treated control mice.

C-D, Percentage of CD8 T cells (**left**) and CD4 cells (**right**) expressing IFN-γ, TNFα, IL-2, IL-4, and IL-5 of splenocytes from WT-LNP-mRNA vaccinated mice and PBS treated control mice without peptide stimulation (**C**), or in response to PMA/ionomycin stimulation (**D**).

E, Percentage of CD4 T cells expressing TNFα, IL-2, IL4, and IL5 in response to S peptide pools of B.1.351-mRNA-LNP and B.1.617-mRNA-LNP vaccinated group and PBS group.

F-G, Percentage of CD8 T cells (**left**) and CD4 cells (**right**) expressing IFN-γ, TNFα, IL-2, IL-4, and IL-5 of splenocytes from B.1.351-mRNA-LNP and B.1.617-mRNA-LNP vaccinated mice and PBS treated control mice without peptide stimulation (**F**), or in response to PMA/ionomycin stimulation (**G**).

Notes:

In this figure:

Each dot represents data from one mouse.

Statistical significance labels: n.s., not significant; * $p < 0.05$; ** $p < 0.01$; *** $p < 0.001$; **** $p < 0.0001$

Related to: Figure(s) 1, 3

Supplemental Figure 3

A
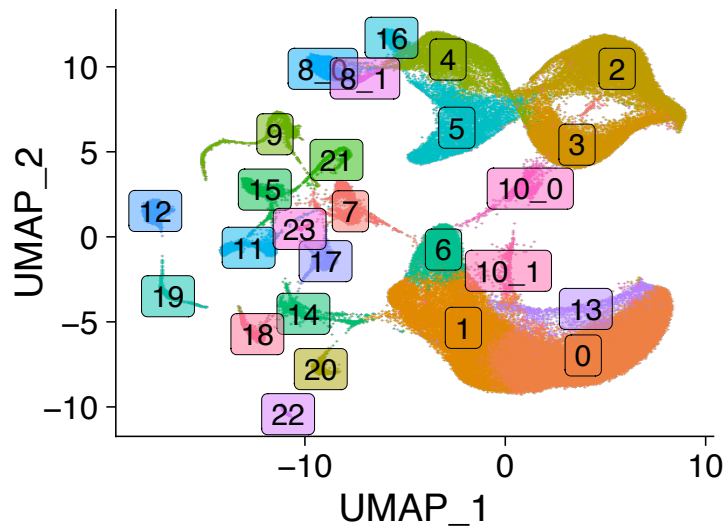
B
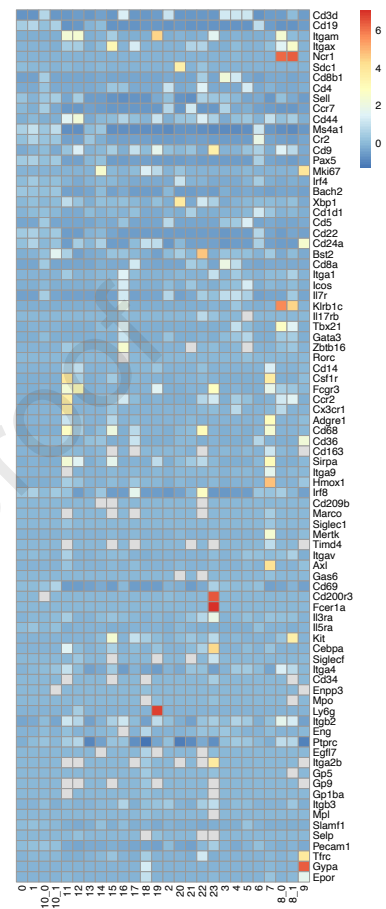
C

Erythrocyte markers
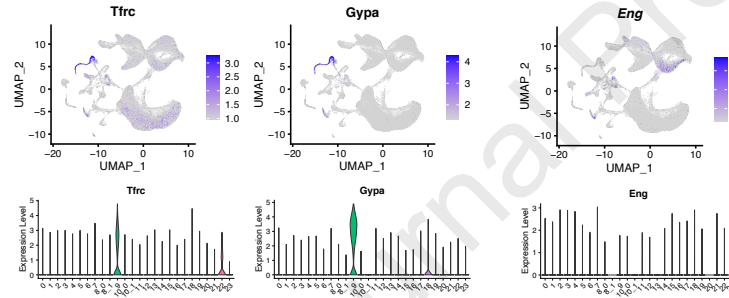
EC markers
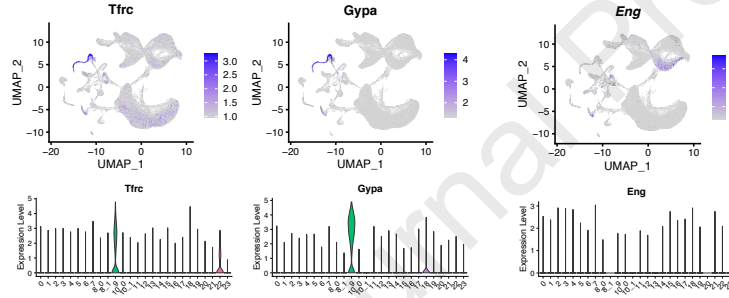
Mono/macro markers
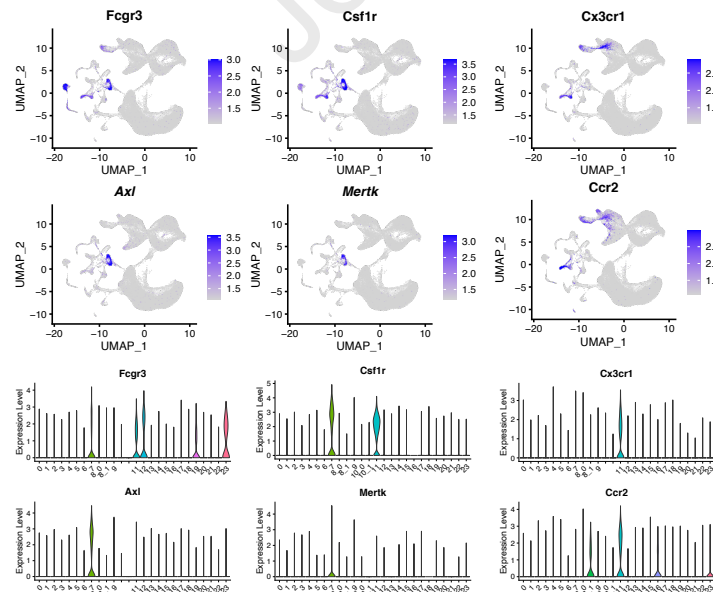
MK/Platelet markers

1
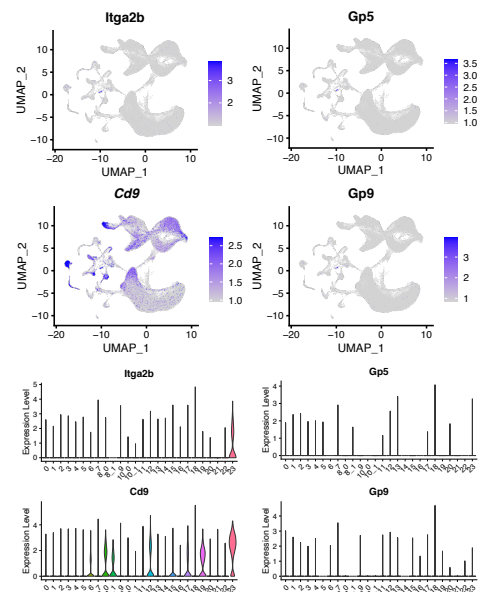
1 **Figure S3 | Additional analysis of single cell transcriptomics and immune repertoire profiling of variant-specific LNP-**
2 **mRNA vaccinated animals**
3 **A,** UMAP visualization of all 141,729 cells pooled across samples and conditions. Cells colored and labelled by cluster.
4 **B,** Heatmap of common immune marker gene expression across indicated clusters. Expression values are scaled across cells and
5 averaged by cluster. NA values were given for < 1% detectable expression amongst a cluster population.
6 **C,** UMAP heatmaps and violin plots of the expression of cell type-specific markers used for assignment of cell identity.
7 Normalized, unscaled expression values used for each plot.
8 **Related to: Figure 5**

Supplemental Figure 4

A

B cell population clustering

B

B cell marker expression

C

Developmental markers

Activation markers

GC B cell markers
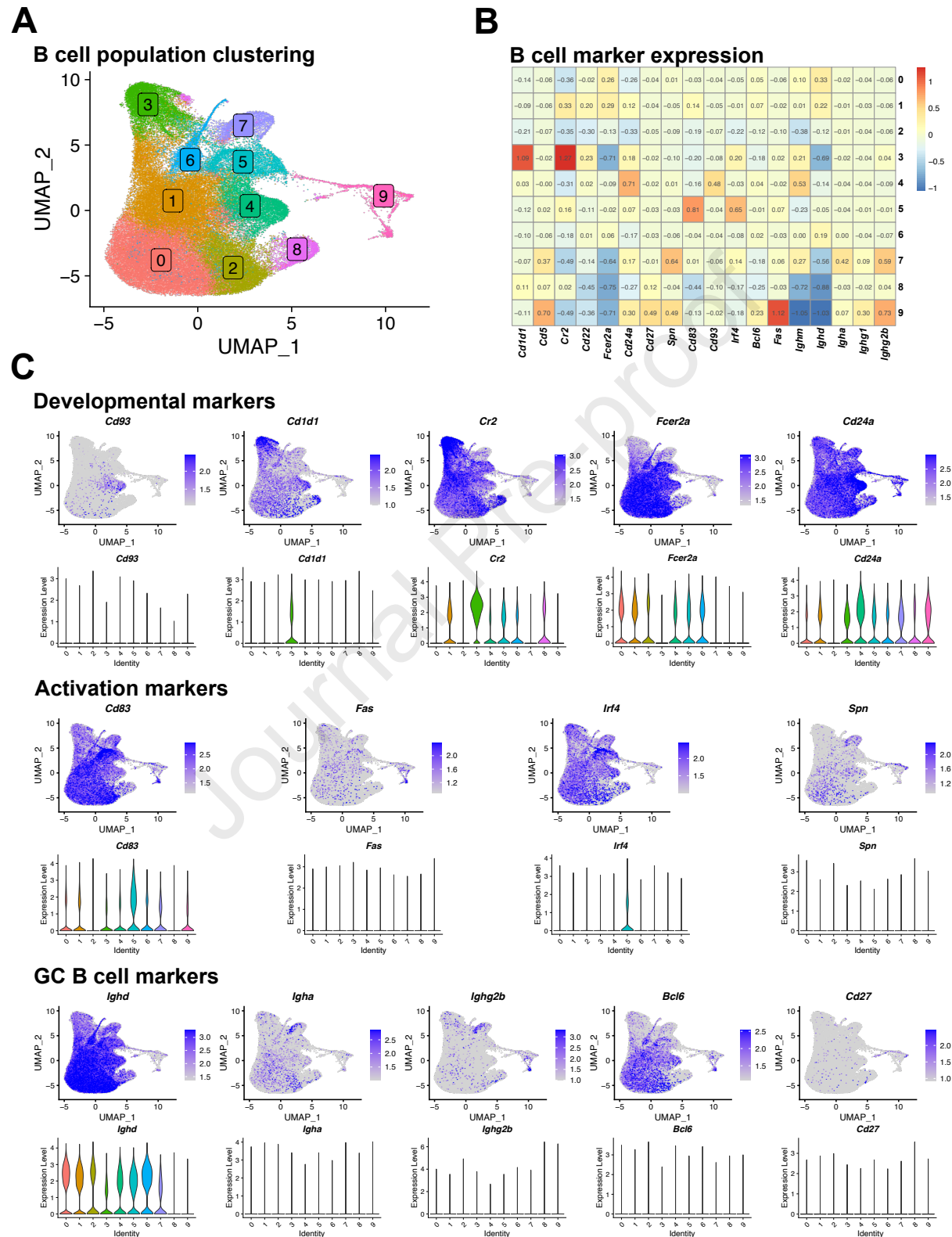
1   **Figure S 4 | Additional analysis of B cell subpopulations in scRNA-seq profiling of variant-specific LNP-mRNA vaccinated**
2   **animals**
3   **A,** UMAP visualization of CD19+ B cell populations pooled across samples and conditions. Cells colored and labelled by cluster.
4   **B,** Heatmap of B cell subset-specific gene expression across indicated clusters. Expression values were scaled across cells and
5   averaged by cluster. NA values were given for < 1% detectable expression amongst a cluster population.
6   **C,** UMAP heatmaps and violin plots of the expression of cell type-specific markers used to assign cell identity. Normalized,
7   unscaled expression values used for each plot.
8   **Related to: Figure 5**

Supplemental Figure 5

A

T cell population clustering

B

T cell marker expression

C

Common T cell markers

Th cell transcription factors

Cytokines and effector molecules

1

10
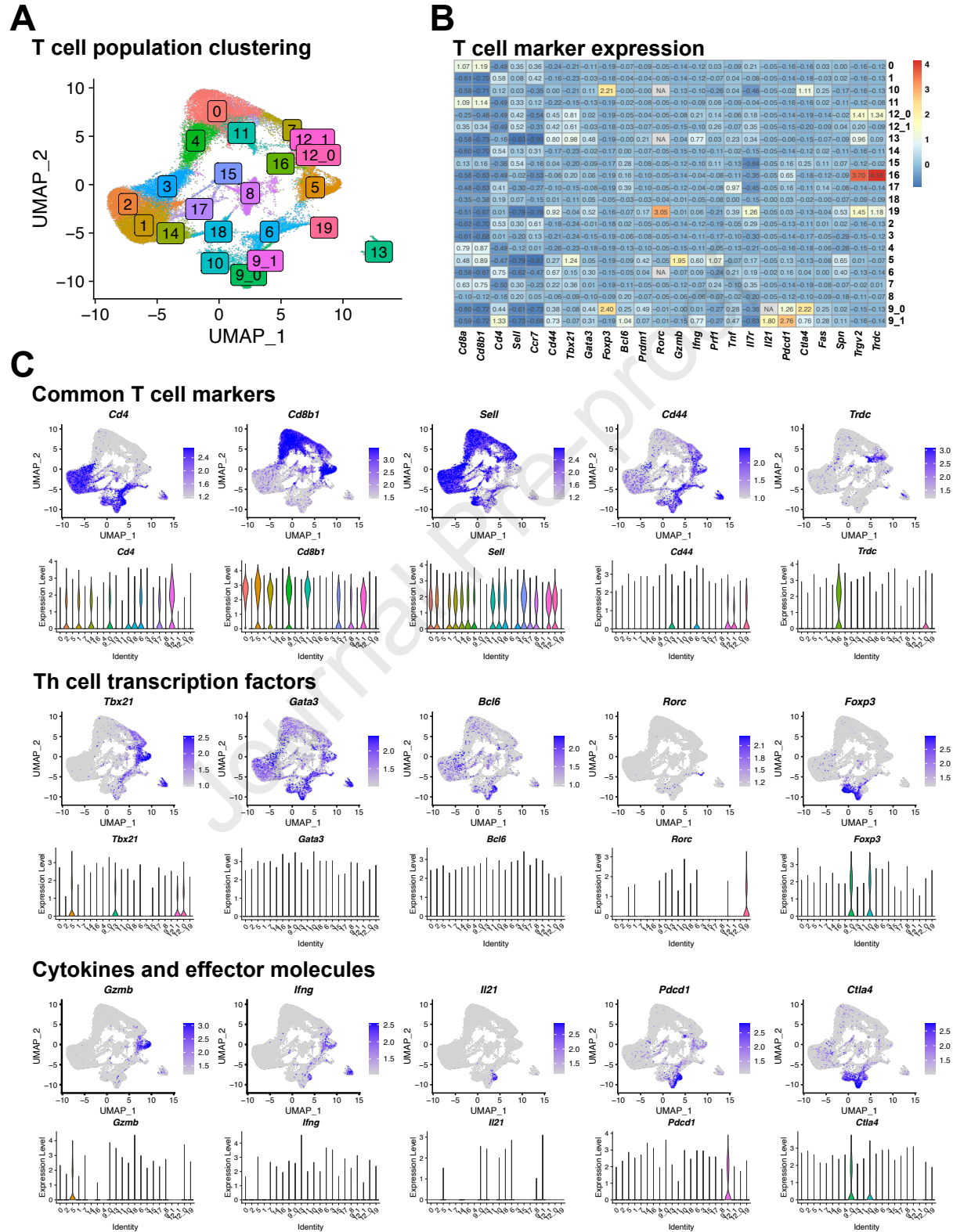
1 **Figure S 5 | Additional analysis of T cell subpopulations in scRNA-seq profiling of variant-specific LNP-mRNA vaccinated**
2 **animals**
3 **A,** UMAP visualization of CD3d+ T cell populations pooled across samples and conditions. Cells colored and labelled by cluster.
4 **B,** Heatmap of T cell subset-specific gene expression across indicated clusters. Expression values are scaled across cells and
5 averaged by cluster. NA values were given for < 1% detectable expression amongst a cluster population.
6 **C,** UMAP heatmaps and violin plots of the expression of cell type-specific markers used to assign cell identity. Normalized,
7 unscaled expression values were used for each plot.
8 **Related to: Figure 5**

Supplemental Figure 6

A

B

C

cDC1 markers

cDC2 markers

pDC markers

fDC markers
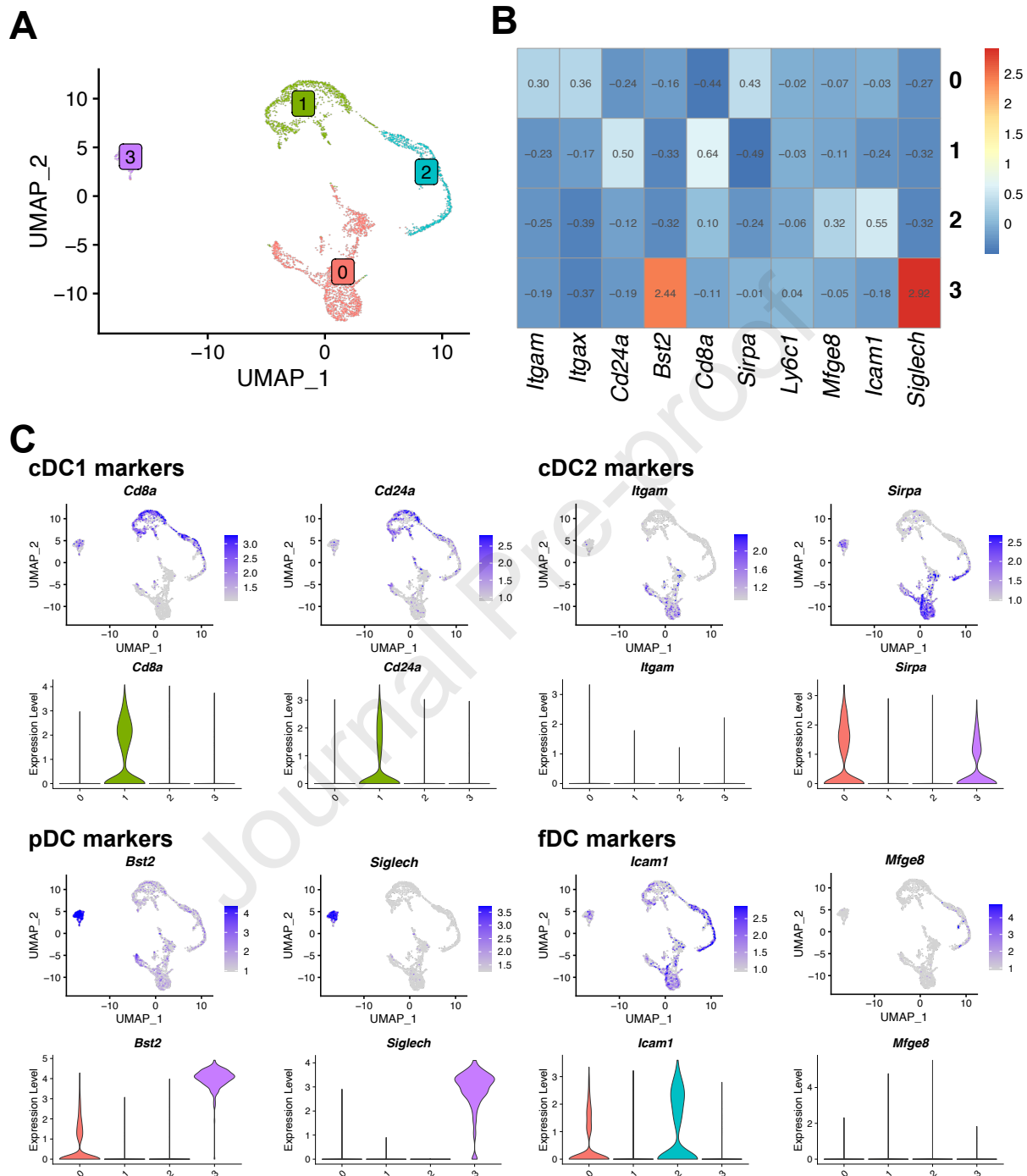
1 **Figure S 6 | Additional analysis of dendritic cell subpopulations in scRNA-seq profiling of variant-specific LNP-mRNA**
2 **vaccinated animals**
3 **A,** UMAP visualization of Itgax (Cd11c) + dendritic cell (DC) populations pooled across samples and conditions. Cells colored
4 and labelled by cluster.
5 **B,** Heatmap of DC cell subset-specific gene expression across indicated clusters. Expression values are scaled across cells and
6 averaged by cluster. NA values were given for < 1% detectable expression amongst a cluster population.
7 **C,** UMAP heatmaps and violin plots of the expression of cell type-specific markers used to assign cell identity. Normalized,
8 unscaled expression values used for each plot.
9 **Related to: Figure 5**

Supplemental Figure 7

Figure S 7 | Additional analysis of differential gene expression in the B and T cell subpopulations of variant-specific LNP-mRNA vaccinated animals

A, D, F, Network plots of clustered terms from pathway analyses of upregulated genes in the indicated cell type and DE comparative analysis. Pathway enrichment analyses were performed by gProfiler2, and significantly enriched pathways were clustered with Leiden algorithm. Pathway clusters (supra-pathways) are labeled by their most significant member term along with its enrichment q value. The top five supra-pathways are shown for each plot.

B, E, G, Expression heatmaps of DE genes from a selected upregulated supra-pathway. Single-cell expression values were scaled then averaged across vaccination groups.
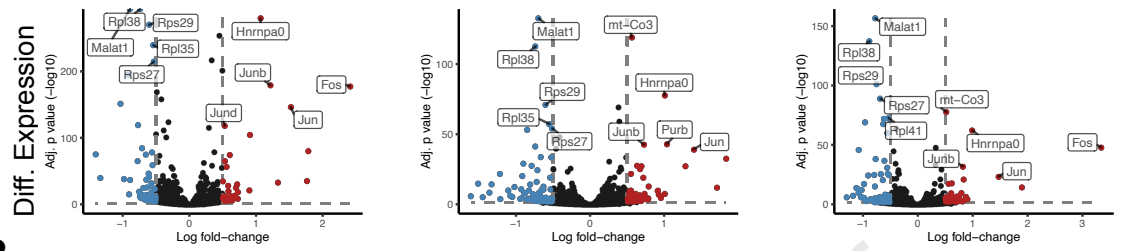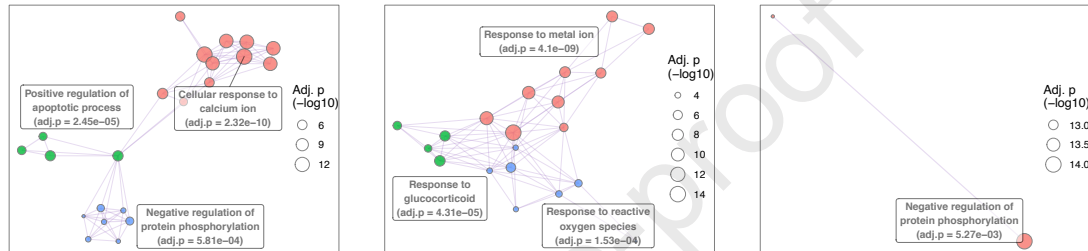
Related to: Figure 6

Supplemental Figure 8
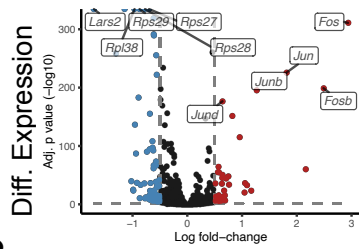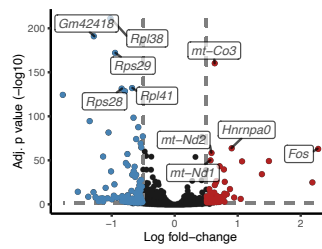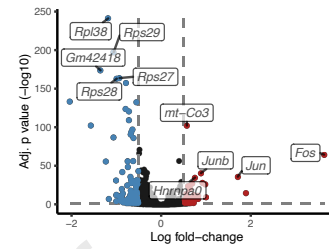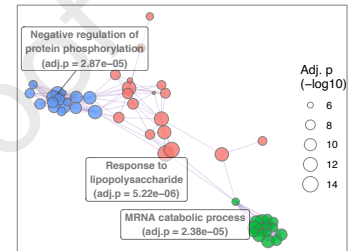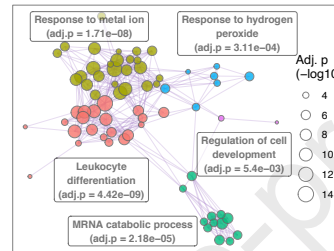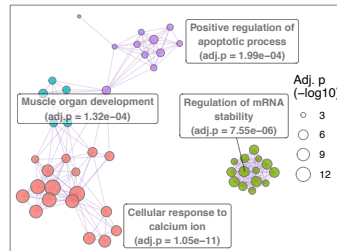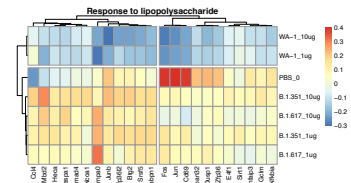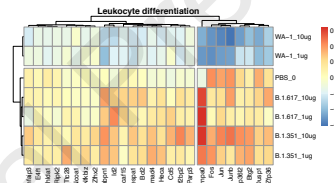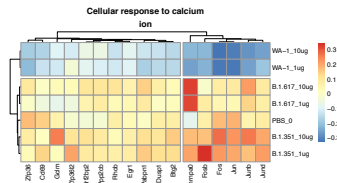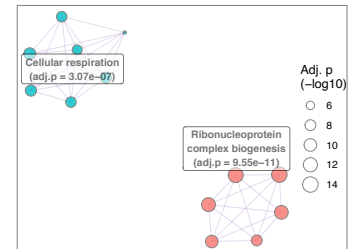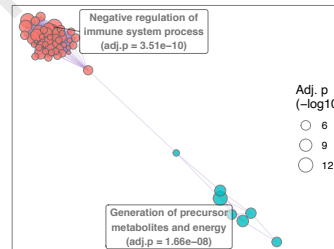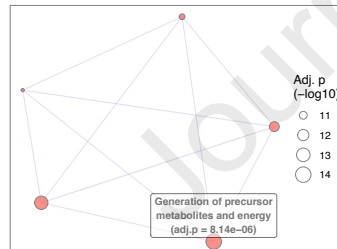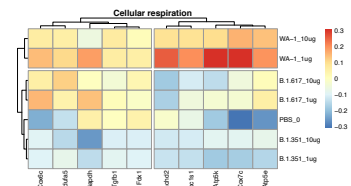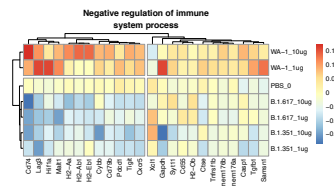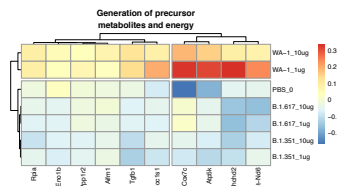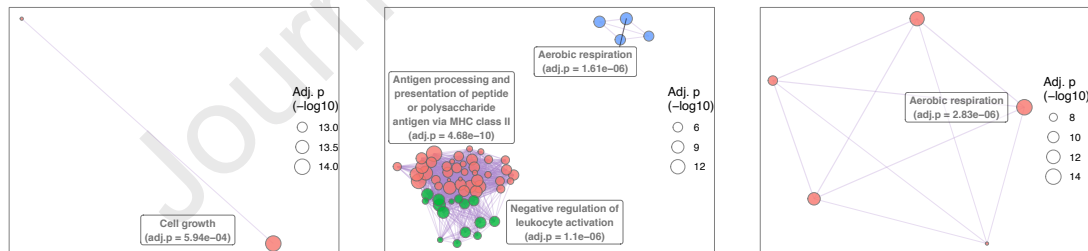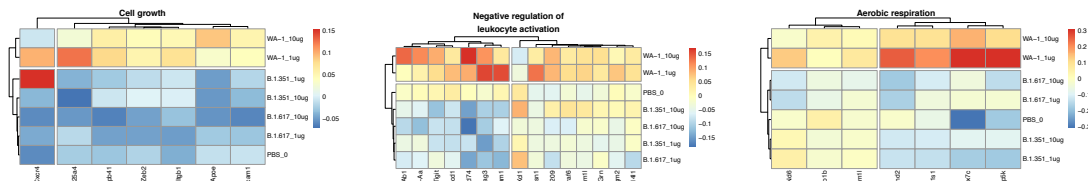
Figure S 8 | Differential expression analysis in the B and T cell subpopulations between B.1.351-LNP-mRNA and WA-1-LNP-mRNA vaccinated animals

A, Volcano plots of differential expression (DE) analyses in B cells or CD8 T cells from B.1.351-LNP-mRNA vs WA-1-LNP-mRNA vaccinated animals. Analyses were performed using quasi-likelihood F tests of scRNA-seq data fitted with gamma-Poisson generalized linear models.

B, D, Network plots of clustered terms from pathway analyses of (**B**) upregulated and (**D**) downregulated genes in the indicated DE comparative analysis. Pathway enrichment analyses were performed by gProfiler2, and significantly enriched pathways were clustered with Leiden algorithm. Pathway clusters (supra-pathways) are labeled by their most significant member term along with its enrichment q value. The top five supra-pathways are shown for each plot.

C,E, Expression heatmaps of DE genes from a selected (**C**) upregulated and (**E**) downregulated supra-pathway. Single-cell expression values were scaled then averaged across vaccination groups.

Related to: Figure 6

Supplemental Figure 9

Figure S 9 | Differential expression analysis in the B and T cell subpopulations between B.1.617-LNP-mRNA and WA-1-LNP-mRNA vaccinated animals

A, Volcano plots of differential expression (DE) analyses in B cells or CD8 T cells from B.1.617-LNP-mRNA vs WA-1-LNP-mRNA vaccinated animals. Analyses were performed using quasi-likelihood F tests of scRNA-seq data fitted with gamma-Poisson generalized linear models.

B, D, Network plots of clustered terms from pathway analyses of (**B**) upregulated and (**D**) downregulated genes in the indicated DE comparative analysis. Pathway enrichment analyses were performed by gProfiler2, and significantly enriched pathways were clustered with Leiden algorithm. Pathway clusters (supra-pathways) are labeled by their most significant member term along with its enrichment q value. The top five supra-pathways are shown for each plot.

C, E, Expression heatmaps of DE genes from a selected (**C**) upregulated and (**E**) downregulated supra-pathway. Single-cell expression values were scaled then averaged across vaccination groups.

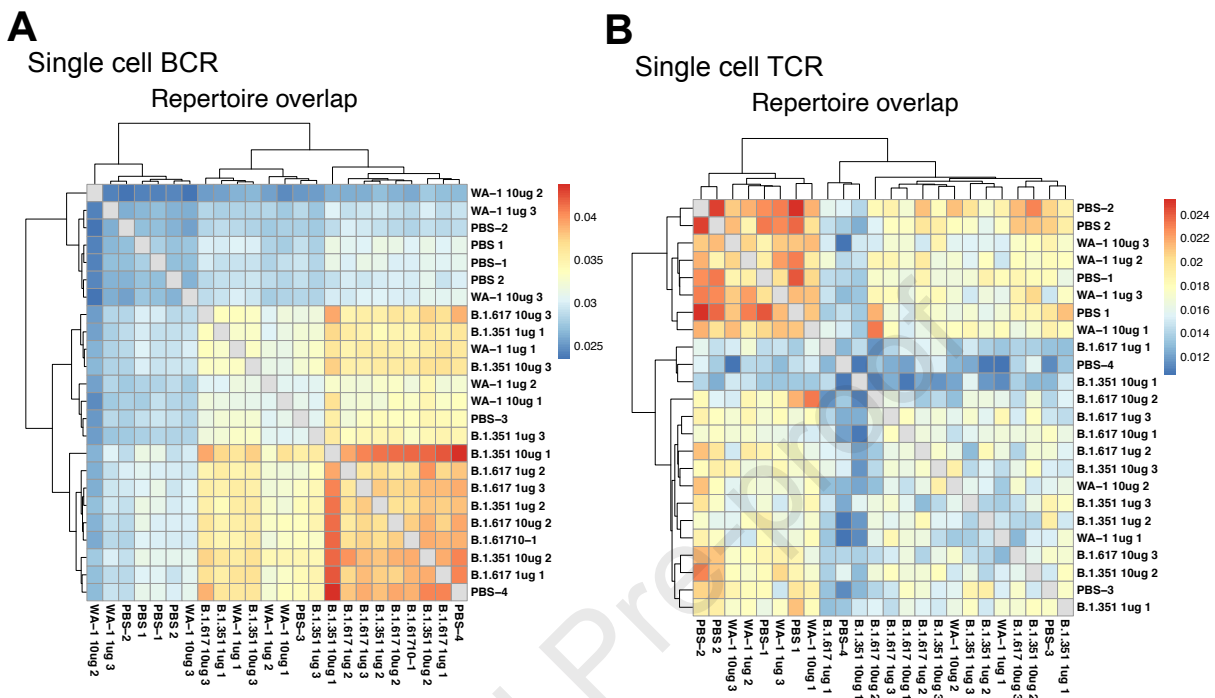**Related to: Figure 6**

Supplemental Figure 10

1 **Figure S 10 | Additional analysis of single cell VDJ BCR-seq and TCR-seq data between variant-specific LNP-mRNA**
2 **vaccinated animals**
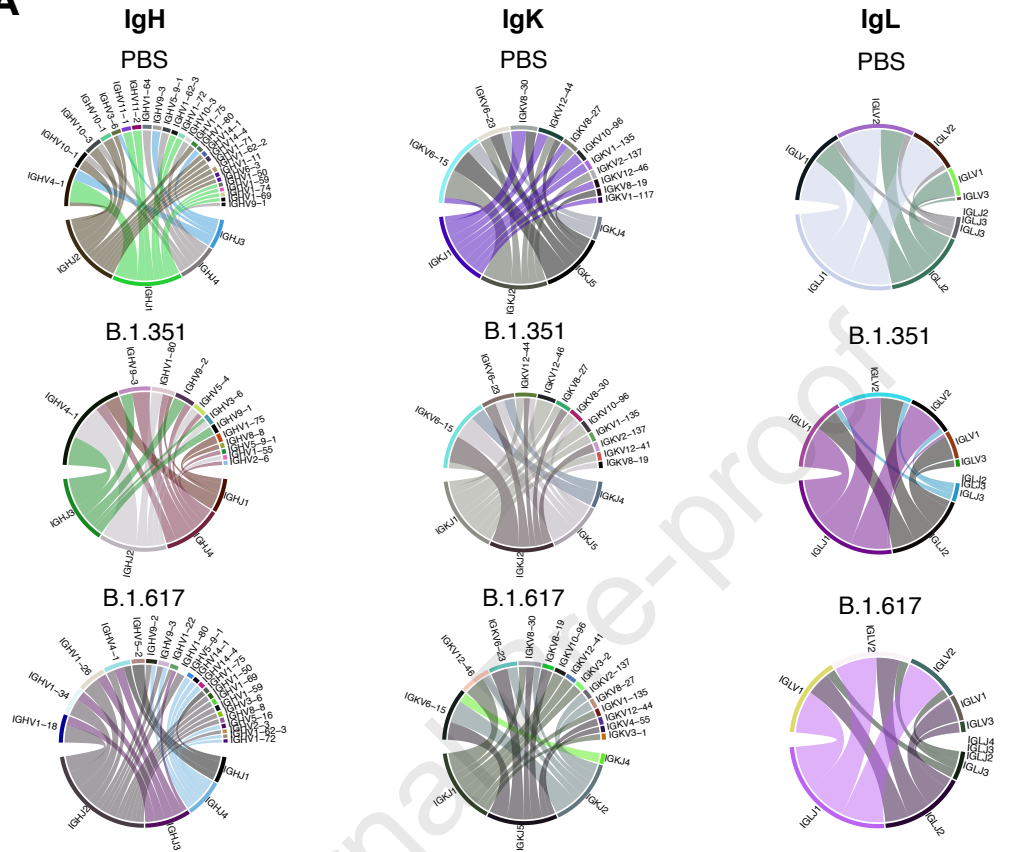3 **A,** Heatmaps of BCR repertoire overlap between single cell BCR-seq datasets, represented by Jaccard indices.
4 **B,** Heatmaps of TCR repertoire overlap between single cell TCR-seq datasets, represented by Jaccard indices.
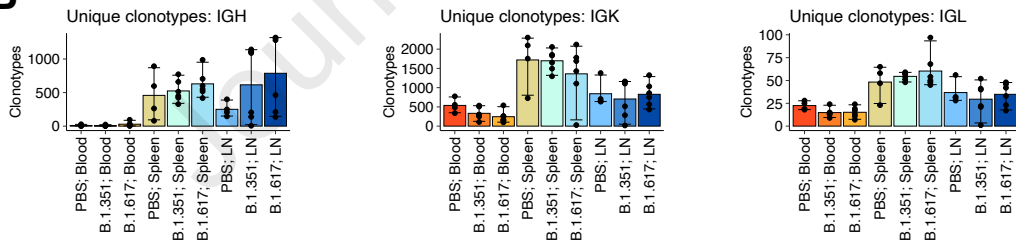5 **Related to: Figure 7**
6
7

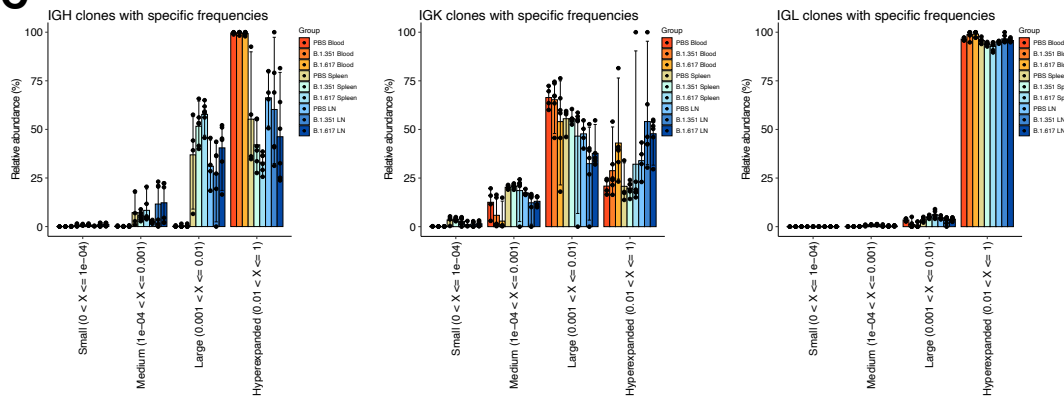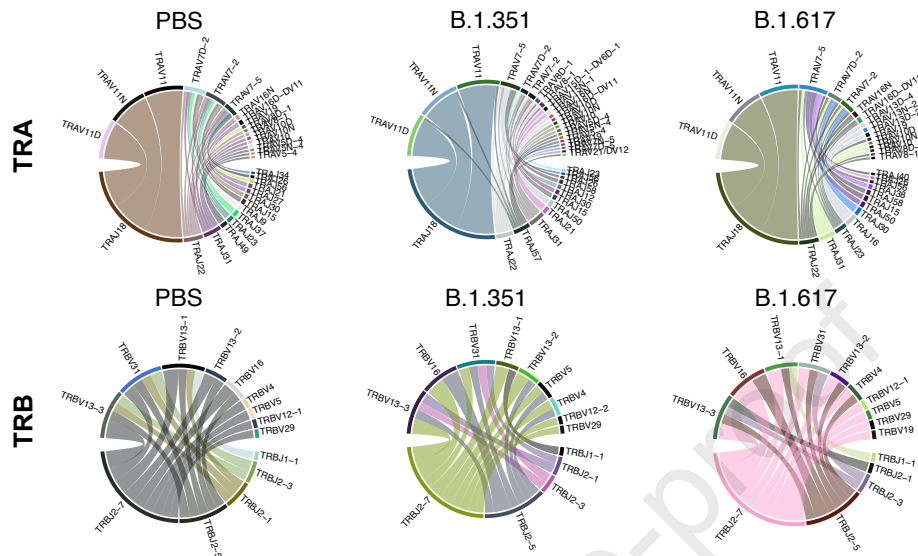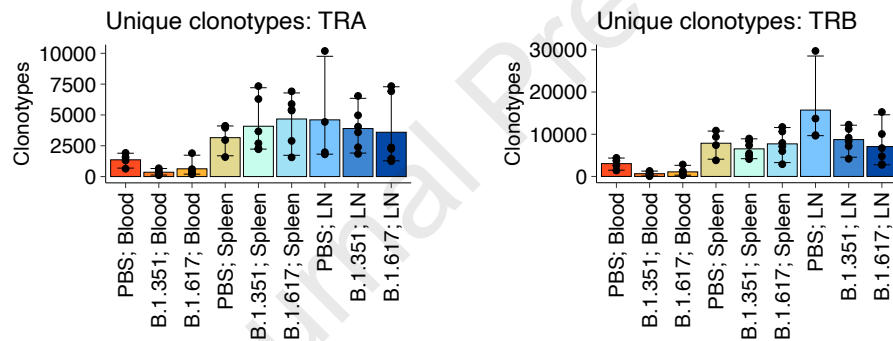# Supplemental Figure 11

1   **Figure S 11 | Additional analysis of bulk VDJ BCR-seq data between variant-specific LNP-mRNA vaccinated animals**

2   **A,** Circos plots of V-J clonotype distribution for IGH, IGK, and IGL BCR-seq datasets. The 20 most abundant V-J combinations

3   are shown for pooled vaccination group.

4   **B,** Bar plots of the unique clonotype numbers among blood, spleen, and lymph node samples from different variant-specific LNP-

5   mRNA vaccinated animals.

6   **C,** Bar plots of the relative abundance of IGH, IGK, and IGL clonotypes from different tissues within specific clonotype frequency

7   ranges.

8   **Notes:** PBS samples: n = 4; B.1.351 and B.1.617 samples: n = 6.

9   **Related to: Figure 7**

Supplemental Figure 12
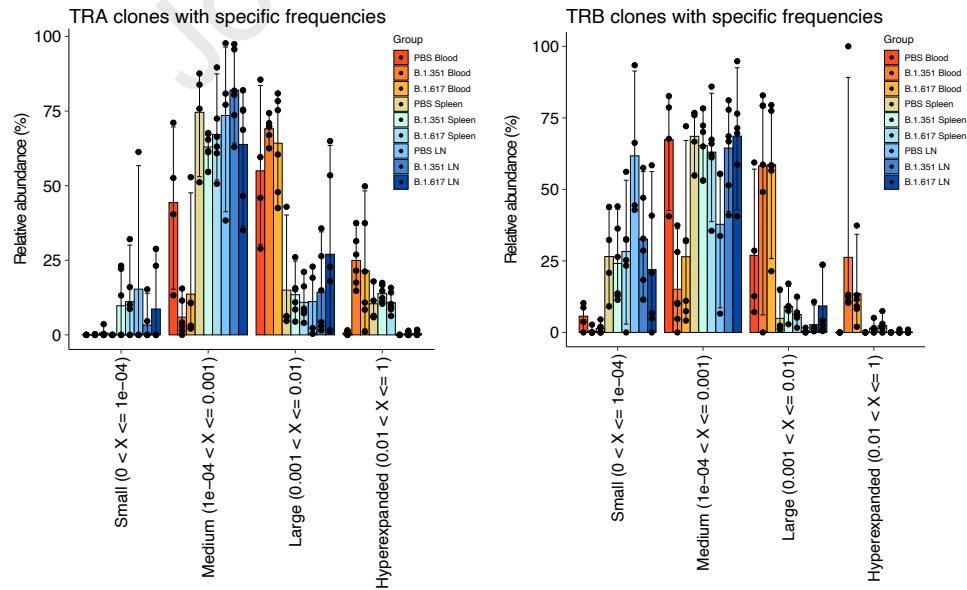
A

B

C

1
2

Figure S 12 | Additional analysis of bulk VDJ TCR-seq data between variant-specific LNP-mRNA vaccinated animals

A, Circos plots of V-J clonotype distribution for TRA, TRB, and TRD TCR-seq datasets. The 20 most abundant V-J combinations are shown for pooled vaccination group.

B, Bar plots of the unique clonotype numbers among blood, spleen, and lymph node samples from different variant-specific LNP-mRNA vaccinated animals.

C, Bar plots of the relative abundance of TRA, TRB, and TRD clonotypes from different tissues within specific clonotype frequency ranges.

Notes: PBS samples: n = 4; B.1.351 and B.1.617 samples: n = 6.

Related to: Figure 7

Other Supplemental Files

Supplemental Source Data and Statistics (non-NGS)
A supplemental excel file contains all original data and statistics for non-high-throughput experiments.

Data S1. Supplemental Dataset (NGS)
A zip file containing five excel files for all NGS processed data, including 5 separate datasets.

Dataset 1 | Single cell GEX of PBS, WA-1-LNP-mRNA, B.1.351-LNP-mRNA, and B.1.617-LNP-mRNA treated animals
Tabs in this dataset:
S01. Metadata of merged single cell GEX dataset. Dataset contains basic statistics, clustering information, cell type assignment, and UMAP embeddings for each cell.
S02. Differentially expressed genes (DEGs) for each cell type compared to all others, using Wilcoxon ranked sum test.
S03. List of 118 immune gene markers for identification of specific cell types.
S04. Assigned cell types and specific markers used for identification.
S05. Cell type proportions for each sample.
S06. Statistics for comparison of cell type proportions between vaccination groups, using a two-way ANOVA test.

Dataset 2 | T cell and B cell specific analyses of single cell GEX of PBS, WA-1-LNP-mRNA, B.1.351-LNP-mRNA, and B.1.617-LNP-mRNA treated animals
Tabs in this dataset:
S07. Design matrices for DE analyses.
S08. DE results of WA-1 vaccination effect in different activated immune cell types, using a Quasi-likelihood F (QLF) test for WA-1 vaccination as the coefficient equal to zero in a generalized linear model (GLM).
S09. DE results of B.1.351 vaccination effect in different activated immune cell types, using a QLF test for B.1.351 as the GLM coefficient equal to zero.
S10. DE results of B.1.617 vaccination effect in different activated immune cell types, using a QLF test for B.1.617 as the GLM coefficient equal to zero.
S11. DE results of B.1.351 vs WA-1 vaccination in different activated immune cell types, using a QLF test for B.1.351 – WA-1 as the GLM contrast equal to zero.
S12. DE results of B.1.617 vs WA-1 vaccination in different activated immune cell types, using a QLF test for B.1.617 – WA-1 as the GLM contrast equal to zero.
S13. Pathway network analysis results for WA-1 DE analysis in B cells.
S14. Pathway network analysis results for WA-1 DE analysis in CD8 T cells.
S15. Pathway network analysis results for WA-1 DE analysis in CD4 T cells.
S16. Pathway network analysis results for B.1.351 DE analysis in B cells.
S17. Pathway network analysis results for B.1.351 DE analysis in CD8 T cells.
S18. Pathway network analysis results for B.1.351 DE analysis in CD4 T cells.
S19. Pathway network analysis results for B.1.617 DE analysis in B cells.
S20. Pathway network analysis results for B.1.617 DE analysis in CD8 T cells.
S21. Pathway network analysis results for B.1.617 DE analysis in CD4 T cells.
S22. Pathway network analysis results for B.1.351 – WA-1 DE analysis in B cells.
S23. Pathway network analysis results for B.1.351 – WA-1 DE analysis in CD8 T cells.
S24. Pathway network analysis results for B.1.351 – WA-1 DE analysis in CD4 T cells.
S25. Pathway network analysis results for B.1.617 – WA-1 DE analysis in B cells.
S26. Pathway network analysis results for B.1.617 – WA-1 DE analysis in CD8 T cells.
S27. Pathway network analysis results for B.1.617 – WA-1 DE analysis in CD4 T cells.

Dataset 3 | Single cell BCR-seq and TCR-seq of PBS, WA-1-LNP-mRNA, B.1.351-LNP-mRNA, and B.1.617-LNP-mRNA treated animals
Tabs in this dataset:
S28. BCR clonotype counts.
S29. BCR clonotype statistics, including relative clone abundance and top clone proportions across different ranges.
S30. Diversity statistics for BCR clonotypes, including data for Chao1, true diversity and Gini-Simpson methods.
S31. BCR clonotype counts.
S32. BCR clonotype statistics, including relative clone abundance and top clone proportions across different ranges.
S33. Diversity statistics for BCR clonotypes, including data for Chao1, true diversity and Gini-Simpson methods.

Dataset 4 | Bulk BCR-seq PBS, WA-1-LNP-mRNA, B.1.351-LNP-mRNA, and B.1.617-LNP-mRNA treated animals

Tabs in this dataset:

S34. IGH clonotype counts.

S35. IGH clonotype statistics, including relative clone abundance and top clone proportions across different ranges.

S36. Diversity statistics for IGH clonotypes, including data for Chao1, true diversity and Gini-Simpson methods.

S37. IGK clonotype counts.

S38. IGK clonotype statistics, including relative clone abundance and top clone proportions across different ranges.

S39. Diversity statistics for IGK clonotypes, including data for Chao1, true diversity and Gini-Simpson methods. Details of the two-way ANOVA test for true diversity are included.

S40. IGL clonotype counts.

S41. IGL clonotype statistics, including relative clone abundance and top clone proportions across different ranges.

S42. Diversity statistics for IGL clonotypes, including data for Chao1, true diversity and Gini-Simpson methods.

Dataset 5 | Bulk TCR-seq PBS, WA-1-LNP-mRNA, B.1.351-LNP-mRNA, and B.1.617-LNP-mRNA treated animals

Tabs in this dataset:

S43. TRA clonotype counts.

S44. TRA clonotype statistics, including relative clone abundance and top clone proportions across different ranges.

S45. Diversity statistics for TRA clonotypes, including data for Chao1, true diversity and Gini-Simpson methods. Details of the two-way ANOVA test for true diversity are included.

S46. TRB clonotype counts.

S47. TRB clonotype statistics, including relative clone abundance and top clone proportions across different ranges.

S48. Diversity statistics for TRB clonotypes, including data for Chao1, true diversity and Gini-Simpson methods. Details of the two-way ANOVA test for true diversity are included.

S49. TRD clonotype counts.

S50. TRD clonotype statistics, including relative clone abundance and top clone proportions across different ranges.

S51. Diversity statistics for TRD clonotypes, including data for Chao1, true diversity and Gini-Simpson methods. Details of the two-way ANOVA test for true diversity are included.